Multilevel organisation of hybrid materials based on zeolite L crystals for Light Emitting Devices applications

Thesis by

Varun VOHRA

Engineer in Polymer Science from the European School for Chemistry, Polymer and Materials (ECPM, Strasbourg)
Master's degree in Material Science from the University Louis Pasteur (Strasbourg)

For the Degree of Doctor of Philosophy in Material Science
(University of Milano Bicocca)

Tutor: Professor Riccardo Tubino

Research conducted under the supervision of Dr. Chiara Botta at the Istituto per lo Studio delle Macromolecole (ISMac-CNR) in the framework of the European RTN "Nanomatch" Contract No.MRTN-CT-2006-035884

Acknowledgements

First of all, I would like to acknowledge my family and particularly my parents, Mr. Ramesh Chander Vohra and Mrs. Meena Vohra, who have been very supportive both morally and financially throughout all my studies and without whom, not only would I not be part of this world, but I definitely would not have been where I am right now. My parents have been the most supportive but my sister, Mrs. Sandrine Vohra Purushotaman, and my brother in law, Mr. Bijoy Purushotaman, have also been there for me whenever I needed them and I would like to thank my future niece for sharing the time they should have dedicated to her with me.

My PhD research work was conducted at the Istituto per lo Studio delle Macromolecole (ISMac) under the supervision of Dr. Chiara Botta. Through her wise advices and interesting discussions, she helped me become scientifically more mature and broaden my interests giving me enough freedom to achieve some of the most important results of my PhD work. I am also very grateful to the laboratory director, Dr. Alberto Bolognesi for giving me the opportunity to work in his laboratory and for the constant interest and enthusiasm he has shown me concerning my work which was very motivating. Everybody at ISMac should be acknowledged for their support, for the nice atmosphere that resides there which allows one to work in good conditions.

More specifically, I thank Dr. Umberto Giovanella and Dr. Mariacecilia Pasini for the great advices they gave me respectively on the physical and chemical aspects of my work, Dr. Elisa Salmoiraghi (even though her name is hard to spell) for her crazyness and for being a good friend, Dr. Mauro Parini and Dr. Paolo Betti for making my break times even more enjoyable and for the crazy night outs we have done together (to decompress from the stress of work), Dr. Francesco Galeotti for being my tennis partner, Dr. Antonella Manca, Dr. Sara Bursomanno and Dr. Clelia Cogliati for broadening my knowledge of the fun people who work at the CNR and again, all the people who worked with me.

As this work was supported by the European Commission through the Human Potential Program (Marie-Curie RTN 'Nanomatch' Contract No.MRTN-CT-2006-035884 Website: www.nanomatch.eu), I want to thank the coordinators and all the people involved in the project. Through the meetings and workshop I have attended, I met great people who are both scientifically interesting and socially enjoyable, especially the young researchers. I particularly enjoyed the company of Fabio (the little Sicilian guy), Alicja, Agnieszka (Polski girls), Arantxa (the crazy Spanish one), Jan (and his snowboard and beer expertise), Mark (and his addiction for coca cola), Krisztina (and her funny laugh) and Lucas (the Brasilian playboy) with whom I built a real friendship as well as some collaborations and Le-Quyenh Dieu for her wise advices on all the topics we discuss. Professor Gion Calzaferri has been the inspiration for most of my PhD work and I'm therefore regardful to him.

Last but not least, I would like to thank my friends for all over the world, the ones I met during my life in France, the ones I met here in Milano and the ones I met through my travels around the world. To quote just a few, my thoughts go particularly to Terry Saracino for the wonderful time we have spent together, Sophie Martial for always being my little Hitchette, the Matthieuz (Miler and Baert) for being faithful friends, Pitch for co-finding the "fils du Gmouton et de la Gbrebis" with me, Neha "auntie" for being always transparently present, Jana and Anna who, although they are far away, are always in my heart, Mélanie, Anne-sophie for giving me the lectures I had missed when we were in Polymer speciality in Strasbourg and Kati Larionova for the many supportive kalli.

And I would finally like to thank everybody that read these acknowledgements until the end (hopefully, you will also read the thesis until the end; it's much more interesting).

Table of Contents:

I. Introduction and basic principles

A. Introduction

"Technology is a way of **organizing** the universe so that man doesn't have to experience it." When Mother Theresa said that, she didn't realize that she was describing the concept of nanotechnologies focusing on two important ideas in this field: organization and things that you don't see or feel. The universe today is full of so-called nanotechnologies but if you ask someone in the street if he knows what nanotechnologies are he would probably answer "it's something like my Nano Ipod©" and that person would actually be really close to the truth: something useful and that you can't see. Even though nanotechnologies are seen as a relatively recent subject, they have been present forever in nature. The superhydrophobicity of the Lotus leaf or the highly efficient light harvesting system in plants wouldn't exist if there was no nanostructuration lying underneath.

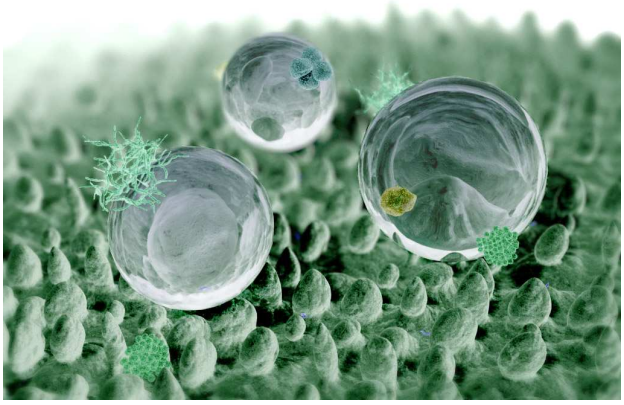

Fig I-1: Superhydrophobicity on the Lotus leaf as a result of the multilevel structures of the leaf surface

In 1946 Theodor Förster described how molecules like chlorophylls can transfer electronic excitation energy by means of induced dipole-dipole interaction. However, for electronic excitation energy transfer to take place between pigments, several conditions must

be met. The pigments must be kept in a well defined orientation, highly organised with a short inter-molecular distance and they must be prevented from building dimers. Such organization can be achieved in zeolite L crystals, a crystalline porous aluminosilicate by introducing specifically tuned organic dyes within the hexagonally arranged zeolite L channels. These loaded zeolite crystals can then be manipulated in a way that they further organize. One of the major challenges in the case of zeolites is to find a way to address (electrically or optically) the dye included.

The present doctoral thesis aims to contribute to the advances in structuration and organization of organic molecules in order to built thin films and nanofibers which could then be used in devices such as Light Emitting Devices (LED) or hybrid solar cells. Conjugated polymers, such as the ones synthesized by Alan Heeger, Alan MacDiarmid and Hideki Shirakawa (Nobel prize in chemistry in 2000) exhibit electroluminescent properties thus being a material that can be used in Organic LED (OLED). Since their work, vast research has been conducted in the field of polymer LED aiming to improve their properties and to tune their emission spectra. In OLED there are many colour mixing techniques all characterized by having multiple emitters in a single device. Some of the most common techniques are multi-layer structures of green, red, and blue emitters; energy transfer blends comprised of a blue donor and red/orange acceptor; bimolecular complex emitters which produce exciplex and excimer states to broaden the emission; microcavity structures which tune the final emission via deconstructive interference; multi-pixel structures which combine multiple emissive regions in to a single structure; and doping of a single emission layer with multiple emitters. This work will mainly concentrate on the two first techniques reported above.

Another type of organization of polymer chains consists in the electrospinning technique which allows obtaining fibers of polymeric materials with diameters down to a few hundreds of nanometers using a high voltage supply. Such structures present many

advantages as we will see later on but more specifically they are flexible and confined in space which could lead to very interesting applications in the field of biotechnologies to specifically excite a cell for example. The same idea lays behind the inclusion of zeolite L crystals to the external world. The many advantages of the zeolite nanochannels which will be described in Chapter II have to be linked in some way to the external world in order to create and develop new technologies such as nanosensing and nanolasing. Conjugated polymers will be therefore used as a medium to link the macroworld of devices to the peculiar properties of the nanoworld. The work presented here is a proof of concept but could be the base of many functional devices obtained with low costs techniques and allowing to obtain functional devices where the organization and the confinement of the different mechanisms which take place will open very interesting perspectives in most of the opto electronic related fields.

B. Basic principles of photophysics

1. The complex nature of light

Many of the observable properties of light can be understood if it is regarded as a wave which travels with a finite speed *c* (3 x 10^8 m/s). In 1864, James Clerk Maxwell could show that equations which he had derived to describe the behaviour of time-varying electric and magnetic fields (**Eq. 1**) predicted the existence of propagating waves and his theory yields precisely the speed of light (known from measurements) as their velocity.[1,2]

$$\oint \mathbf{E} \cdot d\mathbf{A} = q / \varepsilon_0$$

$$\oint \mathbf{B} \cdot d\mathbf{A} = 0$$

$$\oint \mathbf{E} \cdot d\mathbf{S} = -d\Phi_{\mathbf{B}} / dt$$

$$\oint \mathbf{B} \cdot d\mathbf{S} = \mu_0 i + \mu_0 \varepsilon_0 d\Phi_{\mathbf{E}} / dt$$

Eq. 1 : Maxwell's equations

Figure I-2 displays a schematic representation of such an electromagnetic wave: The red and blue arrows symbolize the electric and magnetic fields respectively, which are perpendicular to one another and perpendicular to the direction the wave is travelling. If the wave moves in *z*-direction, and the electric field oscillates in the *x*-direction, then the magnetic field oscillates in the *y*-direction.

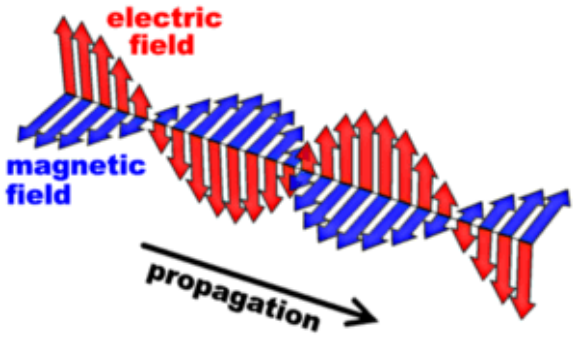

Figure I-2: schematic representation of an electromagnetic wave

The amplitude of these fields varies along the propagation path; this is indicated by the lengths of the arrows. Both these fields also vary in time and this leads to the propagation of the wave. Two important parameters to characterize an electromagnetic wave are its wavelength λ and its frequency ν. The wavelength λ is the shortest distance between two points along the propagation path at which the electric field amplitude is the same at any given moment (**Figure I-3**).

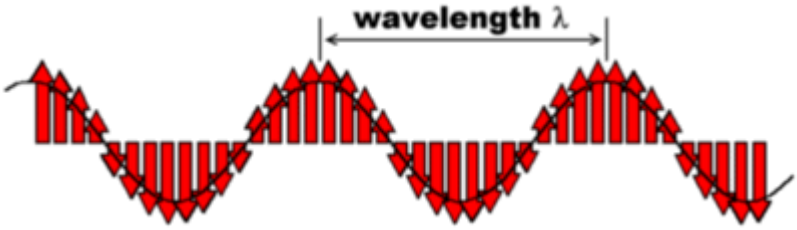

Figure I-3: sideview of an electromagnetic wave

The frequency of the electromagnetic radiation is a measure for how fast the electric and the magnetic field oscillate (the number of times per second they change their direction for any point along the propagation path). Visible light corresponds to wavelengths between 380 and 720 nm (**Figure I-1**).

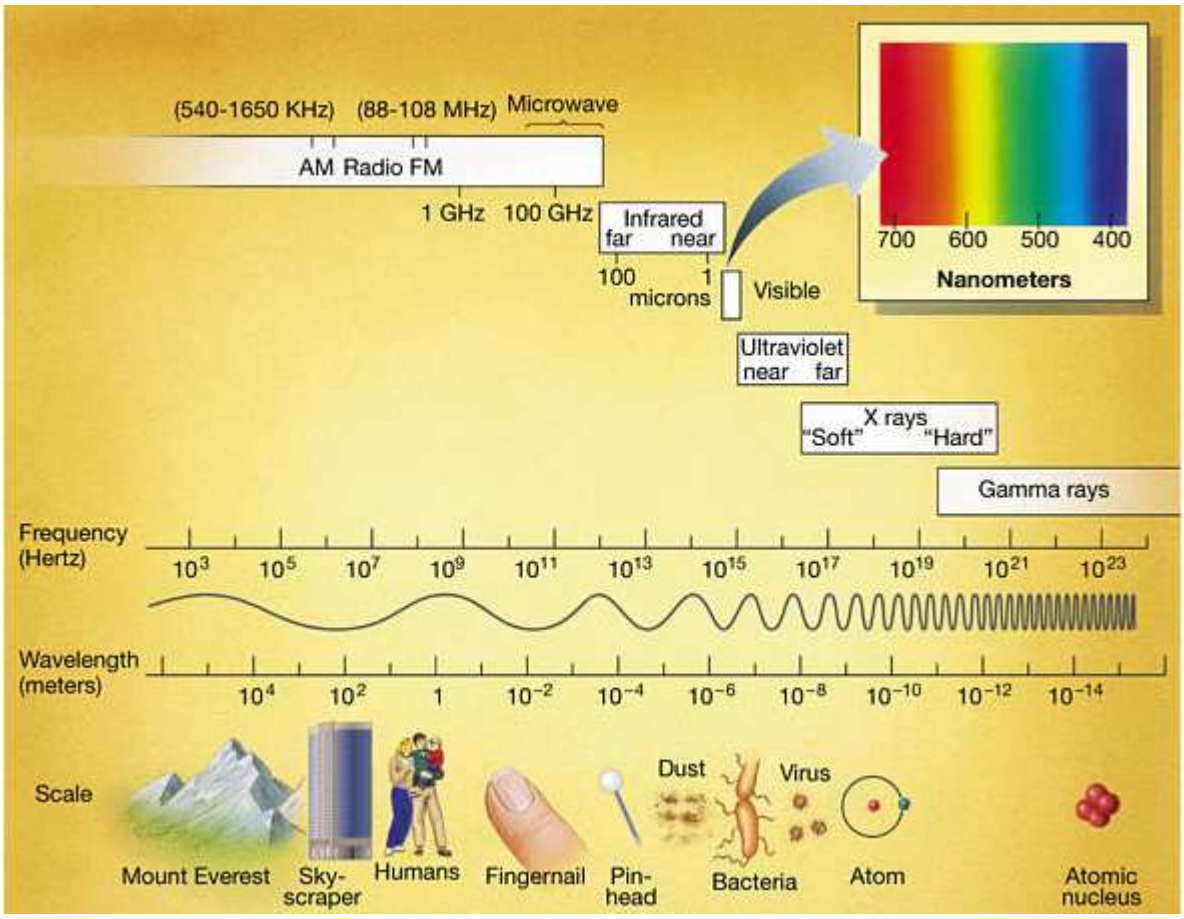

Figure I-4: the electromagnetic spectrum

Even though the Maxwell's electrodynamic theory is very successful in explaining the properties of light, it cannot account for all experimental observations and the idea that the energy in a radiation field is quantized in discrete steps, which is a contradiction to the model of "smooth" electromagnetic waves, has to be introduced. These "grains" of energy are called photons.[3,4] Light can therefore be described in two opposite ways and the right “nature” of light to be taken in account will depend on the experiment and whether light will show either its wave character or its photon character as it will never be both at the same time. This notion is called the principle of complementarity. [5] The photon picture is often very convenient to describe the interaction of light with molecules: the energy of a photon is proportional to the frequency of the radiation (and inversely proportional to its wavelength). When a photon

"hits" a molecule, if it carries enough energy to access one of the allowed excited states of the molecule, it can change the molecule's state in various ways.

2. Interactions of light with molecules

When the electronic cloud of a molecule is excited (after the absorption of one photon), the π-electron density is changed, which means that the geometry of the molecule, in particular the distances between the carbon atoms, is slightly changed. This leads to coupling of the electronic excitation with vibrations. Therefore, absorption leads to an electronic transition accompanied by a series of vibronic bands where 0, 1, 2, etc. vibration quanta are created along with the electronic excitation.

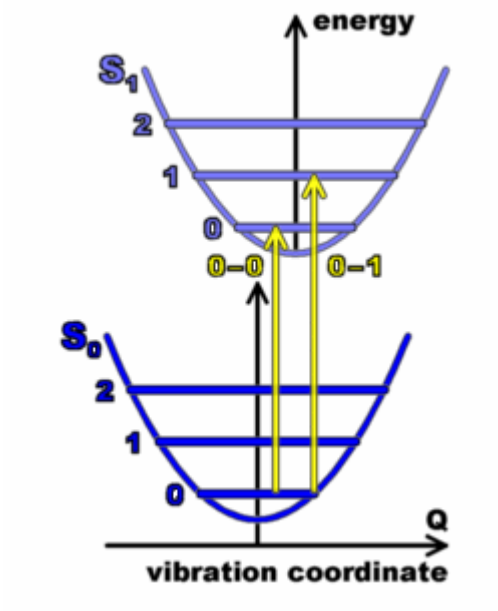

Figure I-5: potential energy curves and absorption mechanism

The **Figure I-5** shows potential energy curves for this vibration of the atoms in the ground and first excited state of the electron cloud, as functions of a vibration coordinate. Absorption induces transitions between levels, as indicated by the arrows.

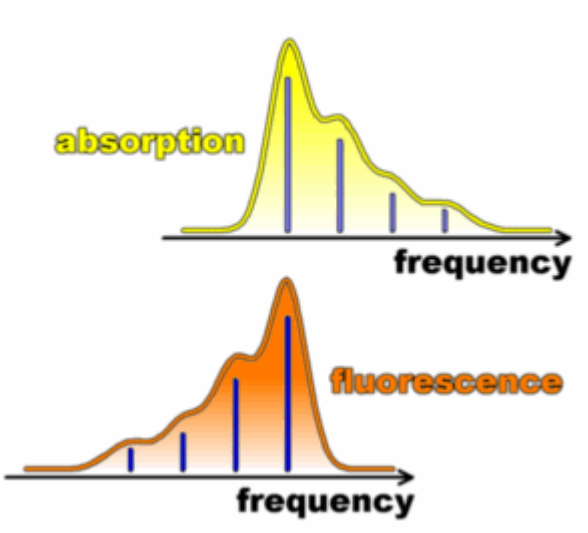

Figure I-6: schematic representation of the absorption and the fluorescence spectrum of a molecule

In the conjugated fluorescence process, one photon is emitted from the relaxed excited state (0 vibrations) to vibrational levels of the ground state. Vibronic coupling will give rise to side-bands at energies higher than the 0-0 transition in the case of absorption, and lower energies in the case of fluorescence. For purely harmonic vibrations, this leads to symmetry (mirror image) between normalized absorption and fluorescence spectra as a function of energy. A schematic representation of the absorption and the fluorescence spectrum of a molecule as a function of the frequency is shown in **Figure I-6** . Each transition is represented by sticks, or by very sharp lines at low temperatures. At room temperature, all lines are broadened (smooth contours).

It is important to consider how strongly a molecular transition is coupled to radiation. The quantity describing the strength of this coupling is called oscillator strength. It is proportional to the square of the transition dipole moment, a vector homogeneous to an electric dipole and with a constant orientation with respect to the molecular axis. Being conjugated processes, absorption and fluorescence strengths are related (as long as the geometry of the molecule does not change too much between absorption and emission). The inverse of the radiative lifetime of the molecule is proportional to the integral of its absorption

coefficient over the spectrum. However, other relaxation processes than the radiative ones can be accessible from the excited state of the molecule, thus decreasing the fluorescence intensity. The ratio of the radiative rate over the sum of the radiative and the nonradiative rate is called the fluorescence quantum yield. Molecules with high radiative rates will therefore tend to be better emitters. This is the case of many laser dyes, which are also good fluorescent probes.

(1) the Jablonski diagram

The non-radiative processes are mainly governed by radiation-less transitions to lower-lying electronic states,[6,7] in particular the ground state, and to a lesser extent the metastable triplet state (**Figure I-7**). Planar rigid molecules tend to exhibit a lower quantity of non radiative processes. As a rule, therefore, good fluorophores have to be planar, rigid and sufficiently stable chemically to sustain many excitation-emission cycles in such reactive environments as air or water.

A schematic level scheme of an organic molecule which includes the three main electronic states involved in absorption, fluorescence, and intersystem crossing is shown below. Such a scheme is called a Jablonski diagram.[7] When light energy is absorbed, it can be converted to thermal energy, kinetic energy or chemical energy (no matter what conversion process takes place, the initial absorption always creates an excited state of the absorbing molecule). The fate of the excited state is determined by a number of factors, which control whether the atom or molecule loses the energy by emission of a photon (fluorescence or phosphorescence), heat, or some photochemical process. (Intermediate states can also occur if the atom or molecule undergoes intersystem crossing or internal conversion).

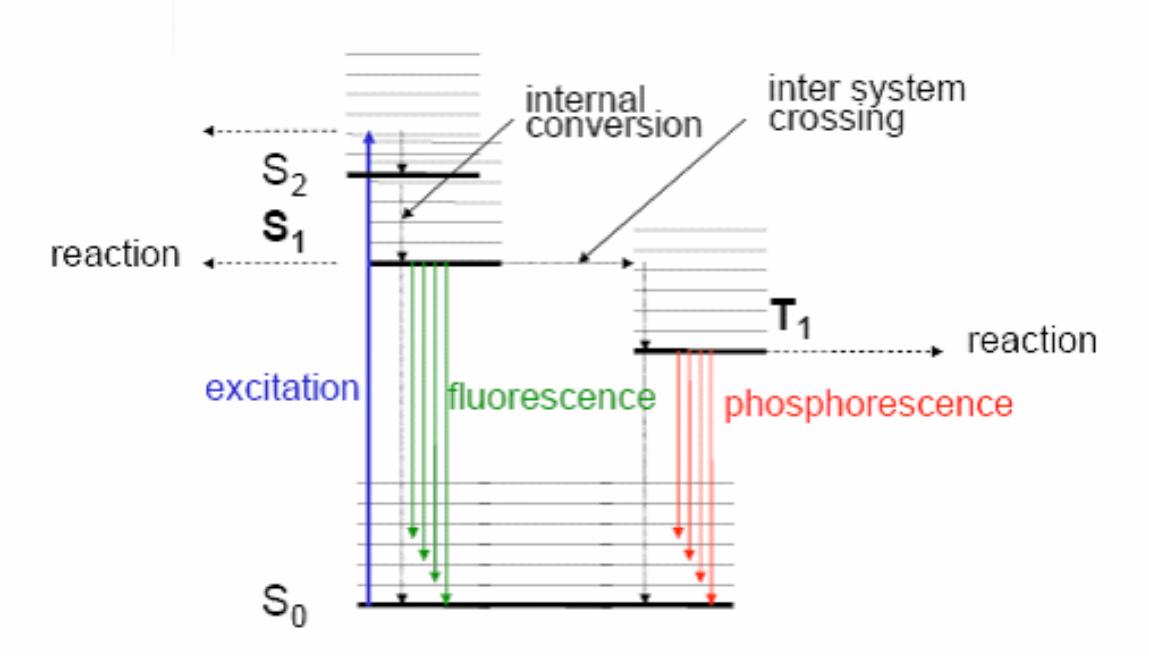

Figure I-7: the Jablonski diagram

In the diagram as drawn, the molecule may be in a singlet or a triplet state. This is the multiplicity of a species, and describes how that species interacts with a magnetic field. Transitions between states are allowed if they are of the same multiplicity (from one singlet state to another or from one triplet state to another), and formally forbidden if a change of multiplicity occurs (from singlet to triplet or vice versa). Formally forbidden transitions are sometimes called relatively forbidden because they occur, but are often less frequent (take a longer time) than transitions that are not forbidden. The ground state of a large majority of fluorescent molecules is a singlet state, which means that their electrons are paired into a zero spin state. The ground state is therefore called S_0. The first excited singlet state S_1 is the one reached after absorption of a photon. Because magnetic field effects are weak, a photon cannot flip spins which is why the first excited state is also a singlet. Although, because of exchange interactions, another excited state at lower energy exists: it is the triplet state T_1, with total spin of 1. It therefore has three spin sublevels (usually undistinguishable at room temperature). Transitions between singlet and triplet states are called intersystem crossing (ISC). ISC is spin-forbidden, therefore caused only by weak interactions such as spin-orbit

coupling. ISC transition rates are rather low and the lifetime of the triplet state is rather long (often microseconds to seconds). However, the triplet states play a central role in the photodynamics of the molecule, because they limit the number of resonant absorptions and fluorescence per unit time that a molecule can perform. The thickly drawn lines in this diagram represent the lowest vibrational level of each state. The thinner lines are higher vibrational levels of that state. Absorption of a photon occurs within 10^{-15} second. The energy of the photon must match the energy of the transition. If there is not a transition of the same energy in a molecule then absorption cannot occur. Jagged lines in the diagram represent radiationless transitions; that is, photons are neither absorbed nor emitted. The first excited singlet state typically has a lifetime of nanoseconds. Should intersystem crossing occur to the triplet state, which can happen with high efficiency under certain circumstances, then the triplet state may live for milliseconds or even longer.

(2) What happens after the absorption of a photon?

Fluorescence

The emission of light is a random spontaneous process. The emission lifetime is a measure of the probability of a certain percentage of the excited states decaying within that time. It is a reasonable approximation that electronic transitions originate from the lowest vibrational level of a given state. Frequently the highest energy fluorescence band is of lower energy than the lowest energy absorption band. The energy difference observed between these two bands is called the Stokes shift.[9-12] A Stokes shift is generally defined as the energy difference between the maximum absorption and the maximum fluorescence.

Internal Conversion

The radiationless transitions described above that don't involve a change of multiplicity are referred to as internal conversions. Energy is released in the form of heat when internal conversion occurs. Internal conversion can be a very rapid process and is responsible for the prompt loss of vibrational energy to the lowest vibrational level for each electronic state. This is the reason that fluorescence is assumed to occur from the lowest vibrational level of any state. No matter what level is initially populated by light absorption, internal conversion will rapidly release (10^{-12} sec) vibrational energy until the lowest vibrational level is reached, long before fluorescence occurs.

Intersystem Crossing

Radiationless transitions between two states of different multiplicity are termed intersystem crossings. Like internal conversion, these transitions result in a loss of energy as heat, but because they are formally forbidden, they require a longer time to occur. The electronic configuration of some molecules favours intersystem crossing from singlet states produced by light absorption to a triplet state of similar energy. These transitions are very important in photobiology, because the excited triplet state can have a relatively long lifetime allowing ample time for the excited state molecule to use the absorbed energy in a reaction with another molecule nearby. Intersystem crossing is also the typical precursor event to phosphorescence.

Phosphorescence

Phosphorescence is the emission of a photon involving a change of multiplicity, while fluorescence does not involve a change. Because the change in multiplicity is formally forbidden, phosphorescence lifetimes are significantly longer than fluorescence lifetimes. Phosphorescence is commonly observed from T_1 to S_o. Because the lifetime of phosphorescence is so long, molecules in T_1 may lose their energy by other transitions that are more efficient, or by chemical reaction. Common methods of deactivation include solvent interactions and energy transfer to oxygen.

Quantum yield

We can predict how much of the absorbed light energy will follow each of the possible deactivation pathways or photophysical processes if we know the rates of the various transitions. The efficiency of a photophysical process is normally expressed in terms of a quantum yield. The quantum yield is given the symbol $\phi$and is defined as the number of products formed per photon absorbed. For example the quantum yield for photoionization, ϕ_I can be expressed as

$$\phi_I = \frac{\text{Number of electrons produced}}{\text{Number of photons absorbed}}$$

The quantum yield of fluorescence F may be written:

$$\phi_F = \frac{\text{Number of photons emitted}}{\text{Number of photons absorbed}}$$

The quantum yield may also be written as a fraction of species that take one route compared to species that take all routes:

$$\phi_F = \frac{k_r}{k_r + k_{nr} + k_{isc} + k_c}$$

where k_r is the radiative rate constant, k_{nr} is the non radiative rate constant, k_{isc} is the rate constant for intersystem crossing, and k_c is the rate constant for chemical reaction. The quantum yield for generation of S_1 is unity, since for every photon absorbed the molecule will be promoted to S_1.

3. Optical spectroscopy

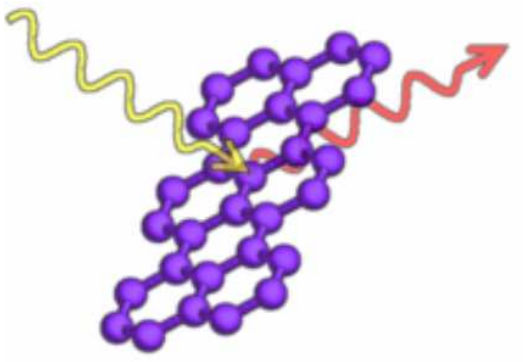

Figure I-8: schematic representation of the interactions between a photon and a molecule

An incident photon can be absorbed by a molecule. The photon energy is then converted into an excitation of that molecule's electron cloud. This type of interaction is sensitive to the internal structure of the molecule, since the laws of quantum mechanics only allow the existence of a limited number of excited states of the electron cloud of any given chemical species. Each of these excited states has a defined energy; the absorption of the photon has to bridge the energy gap between the ground state (lowest energy state) and an allowed excited state of the electron cloud. Molecules can therefore be identified by their

absorption spectrum: Their wavelength-dependent capacity for absorbing photons depends on the energy spacing of the states of their electron cloud. This is, for example, the reason why astronomers use absorption lines to determine the composition of a star. Molecules which strongly absorb visible light appear coloured to the human eye and are therefore called "chromophores" ("carriers of colour").

From this state the molecule can relax to the electronic ground state by transforming the excess energy into vibrations of the nuclei or by transferring it through a non radiative mechanism to the molecule's surroundings, but it can of course also simply re-emit a photon. This re-emission of the absorbed energy is called fluorescence and some single-molecule chromophores can have fluorescence yields of more than 90% (they are sometimes called fluorophores). However, when a photon is emitted it does not always carry the full excess energy of the electronically excited state; the difference corresponds to what goes to the nuclei and the environment. Due to this partial energy loss a significant portion of the fluorescence emission occurs at wavelengths above the one that corresponds to the energy gap between ground and lowest excited state. Our excitation on the other hand will naturally operate at or below that wavelength, since it has to provide a flux of photons which have sufficient energy to bring the chromophore to the excited state.

(1) Beer-Lambert law: base of absorption spectroscopy

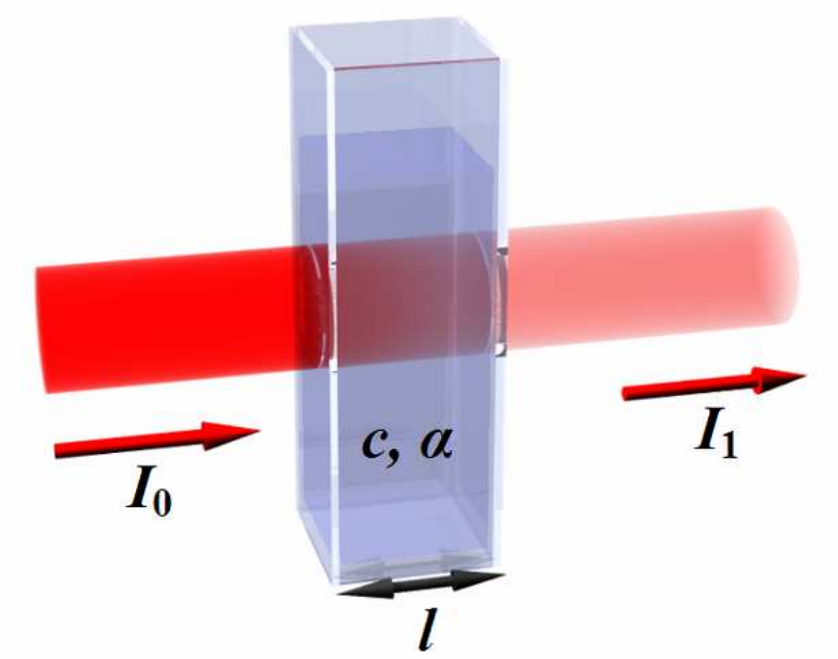

Figure I-9: inside UV-visible absorption

The Beer-Lambert law describes the absorption of light in a transparent material. Lambert's law states that the proportion of light absorbed by a material is independent of the intensity of the incident radiation.[13,14] Beer's law states that the absorption is proportional to the concentration of the sample. The combination of these two laws gives the expression:

$$A = \varepsilon \cdot C \cdot \ell$$

where **A** is the absorbance, ε is the molar absorption coefficient, **C** is the concentration and ℓ is the pathlength. The absorbance is measured experimentally and is given by:

$$A = \log \frac{I_o}{I_t}$$

where I_o is the intensity of the incident light and I_t is the intensity of the light transmitted through the sample. It is sometimes more convenient to express the molar absorption coefficient as an absorption cross section σ:

$$\ln \frac{I_o}{I_t} = \sigma \cdot N \cdot \ell$$

where **N** is the number of absorbing species per unit volume.

There is a common confusion with absorbance that arises from terminology. It must be made clear that absorbance is the log of the ratio of incident and transmitted light. The absorbed light is the number of photons absorbed. The number of photons absorbed, I_a, can be calculated by rearranging the Beer-Lambert equation given above:

$$I_a = I_o \cdot (1 - 10^{-\varepsilon c \ell})$$

The Beer-Lambert law is the base of the UV-visible absorption spectroscopy allowing one to obtain the absorption spectrum of a given molecule in solution.

(2) The potentials of fluorescence spectroscopy

All fluorescence instruments contain three basic items: a source of light, a sample holder and a detector. In addition, to be of analytical use, the wavelength of incident radiation needs to be selectable and the detector signal capable of precise manipulation and presentation. In sophisticated instruments, monochromators are provided for both the selection of exciting light and the analysis of sample emission. Such instruments are also capable of measuring the variation of emission intensity with exciting wavelength, the fluorescence excitation spectrum.

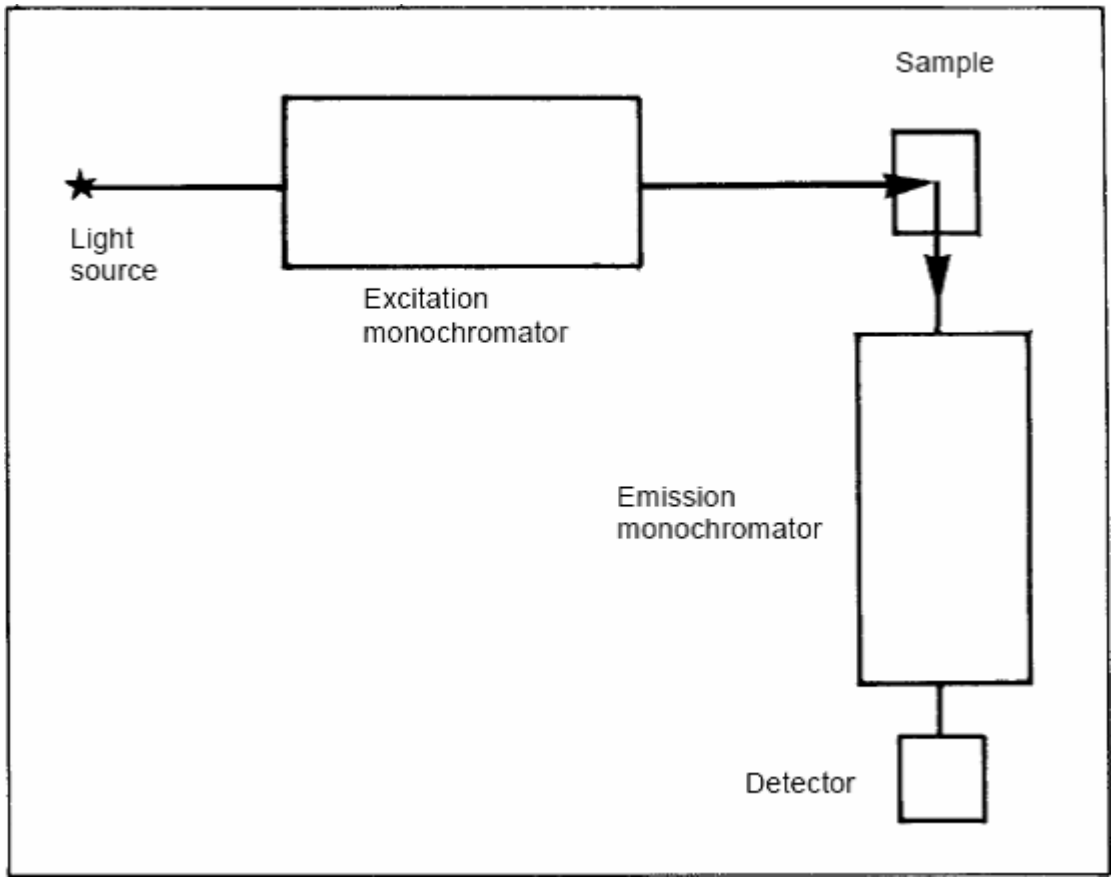

Figure I-20: schematic representation of the luminescence spectrometer

Commonly employed sources in fluorescence spectrometry have spectral outputs either as a continuum of energy over a wide range or as a series of discrete lines. Although in many cases the output from a line source will be adequate, it is rare that an available line will exactly coincide with the optimum excitation wavelength of the sample. It is therefore advantageous to employ a source whose output is a continuum and the most commonly employed type is the xenon arc. The output is essentially a continuum on which are superimposed a number of sharp lines, allowing any wavelength throughout the UV-visible region of the spectrum to be selected.

Most modern instruments of this type employ diffraction grating monochromators to select both the excitation and emission wavelengths. Such a fluorescence spectrometer is capable of

recording both excitation and emission spectra and therefore makes full use of the analytical potential of the technique.

All commercial fluorescence instruments use photomultiplier tubes as detectors and a wide variety of types are available. The material from which the photocathode is made determines the spectral range of the photomultiplier. The limit of sensitivity of a photomultiplier is normally governed by the level of dark current (which is the signal derived from the tube with no light falling on it). The dark current is caused by thermal activation and can usually be reduced by cooling the photomultiplier. Our measurements PL continuous-wave measurements were obtained with an SPEX 270 M monochromator equipped with an N2-cooled CCD and a monochromated Xe lamp. The spectra were corrected for the instrument response.

The spectral response of all photomultipliers varies with wavelength, but it is sometimes necessary to determine the actual quantum intensity of the incident radiation and a detector insensitive to changes in wavelength is required. A suitable quantum counter can be made from a concentrated solution of Rhodamine B in ethylene glycol which has the property of emitting the same number of quanta of light as it absorbs, but over a very wide wavelength range. Thus, by measuring the output of the quantum counter at one wavelength, the number of incident quanta over a wide wavelength range can be measured. This is, in particular, necessary for excitation profile measurements.

(a) Excitation profiles

The excitation profiles measurements are very useful to study energy transfer processes which will be introduced in the next chapter. Fluorescence spectra are recorded with a wide range of excitation wavelengths. The fluorescence of the studied molecules will be integrated for each excitation wavelength. Consequently, those integrations will be plotted

with respect to the excitation wavelength to give rise to the uncorrected excitation profile. As the name suggests, this first spectrum needs to be corrected because of the changes in the lamp intensity throughout the wavelength range that will be considered. We therefore use quantum counters (usually Rhodamine B) to correct the lamp intensity. The correction spectrum corresponds to the integration of the emission from the quantum counter at each of the excitation wavelengths plotted with respect to these excitation wavelengths. The uncorrected excitation profile should be divided by the correction spectra in order to obtain the effective excitation profiles.

In order to study energy transfer from one donor to the acceptor, making the excitation profiles of the acceptor alone and the acceptor in the presence of the donor is an alternative to the lifetime measurements (which will not be introduced). Both excitation profiles should be obtained by integration of the fluorescence from the acceptor only. In the case of an energy transfer, the resulting spectra (**Figure I-11**) will be different and the difference will correspond to the excitation profile (or absorption spectrum) of the donor: the donor is excited and transfer's energy to the acceptor which then emits although it is not excited directly. On the other hand, if no energy transfer occurs, the two excitation profiles will be identical.

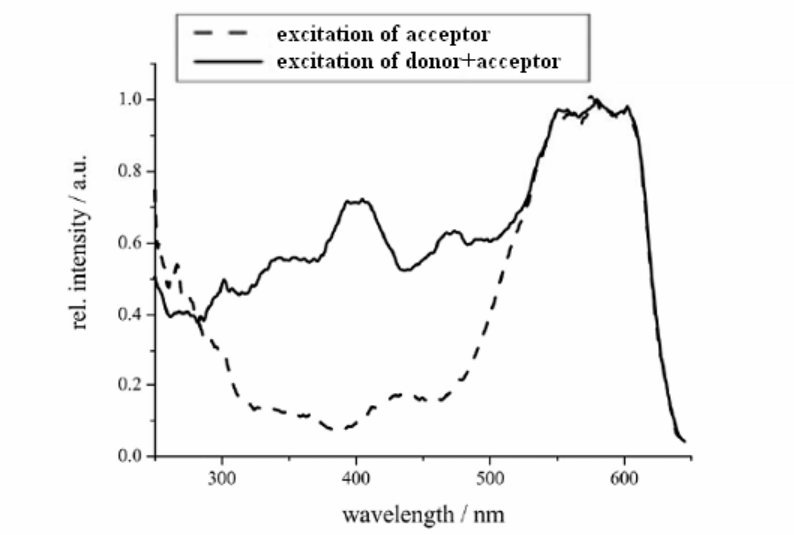

Figure I-11: excitation profiles of an example of donor-acceptor system

(b) Solid state quantum yield measurements

The quantum yield of a fluorescent material gives us important information about the material. The quantum yield depends on many external parameters, e.g. if the molecule is in solid state or in solution. In solution, the measurements will be done by comparing the fluorescence intensity of the molecule with the intensity of a quantum counter. Solution measurements do not require any particular instrument and can be done with the fluorescence spectrometer introduced previously. On the other hand, the solid state measurements require an integrating sphere such as the one presented in **Figure I-12**.

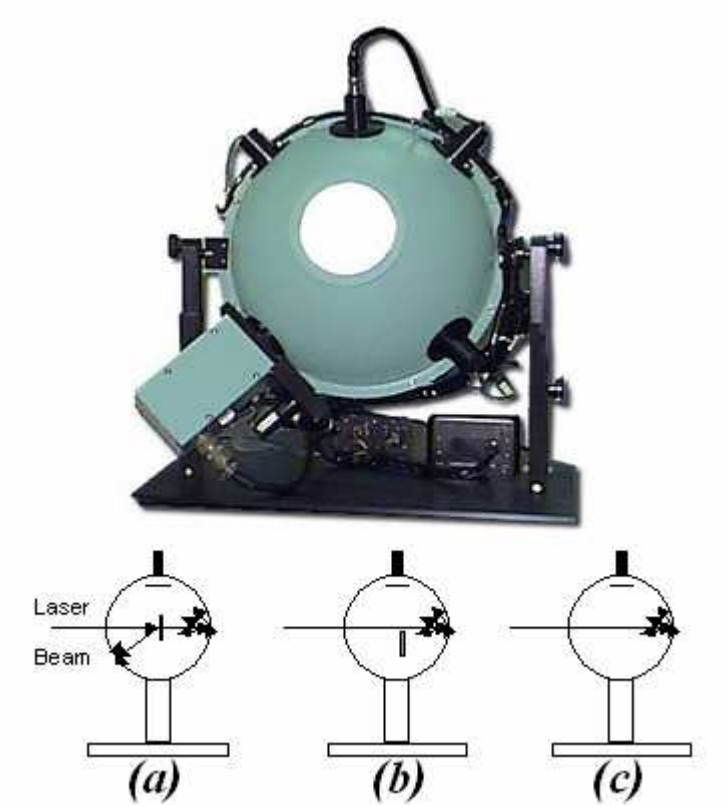

Figure I-12: picture of an integrating sphere (top) and schematic representation of the three measurements (bottom) in which the laser strikes the sample directly (a), after impinging the sphere (b) and where no sample is present in the sphere (c)

The PL QY on solid-state materials was obtained by using a home-made integrating sphere[15,16] and correcting the spectra of the low-emissive materials for the background of the exciting lamp, according to the following equations:

$$QY = \frac{P_c^* - (1 - A)P_b^*}{AL_a}$$

$$P_{c/b}^* = P_{c/b} - \frac{L_{c/b}}{L_a} P_a$$

where P and L are the integrated intensity of the PL spectra and the exciting lamp, respectively; index c refers to the measurement with the laser impinging the sample, and b and a refer to the measurements with the lamp impinging the sphere with the sample inside and outside, respectively.

4. The use of fluorescence in microscopy

The emission of light through the fluorescence process is nearly simultaneous with the absorption of the excitation light due to a relatively short time delay between photon absorption and emission, ranging usually less than a microsecond in duration. Fluorescence microscopy takes advantage of this phenomenon and consists in the irradiation of the sample with a desired and specific band of wavelengths, and in the separation of the much weaker emitted fluorescence from the excitation light. In a properly configured microscope, only the emission light should reach the eye or detector so that the resulting fluorescent structures are superimposed with high contrast against a very dark (or black) background. The limits of detection are generally governed by the darkness of the background, and the excitation light is typically several hundred thousand to a million times brighter than the emitted fluorescence.

There are two types of fluorescence microscopies: the wide field fluorescent optical microscopy and the confocal microscopy. A wide-field fluorescence microscope uses a lamp, e.g. a Mercury arc lamp, to illuminate and excite the specimen. This is a fast and economical way to obtain fluorescent images, which can be viewed directly with your eyes through the ocular or captured with a camera. This is any microscope whereby image formation takes place by the optic without scanning. The lens directly forms an image, which can be projected on a camera or observed through the oculars.

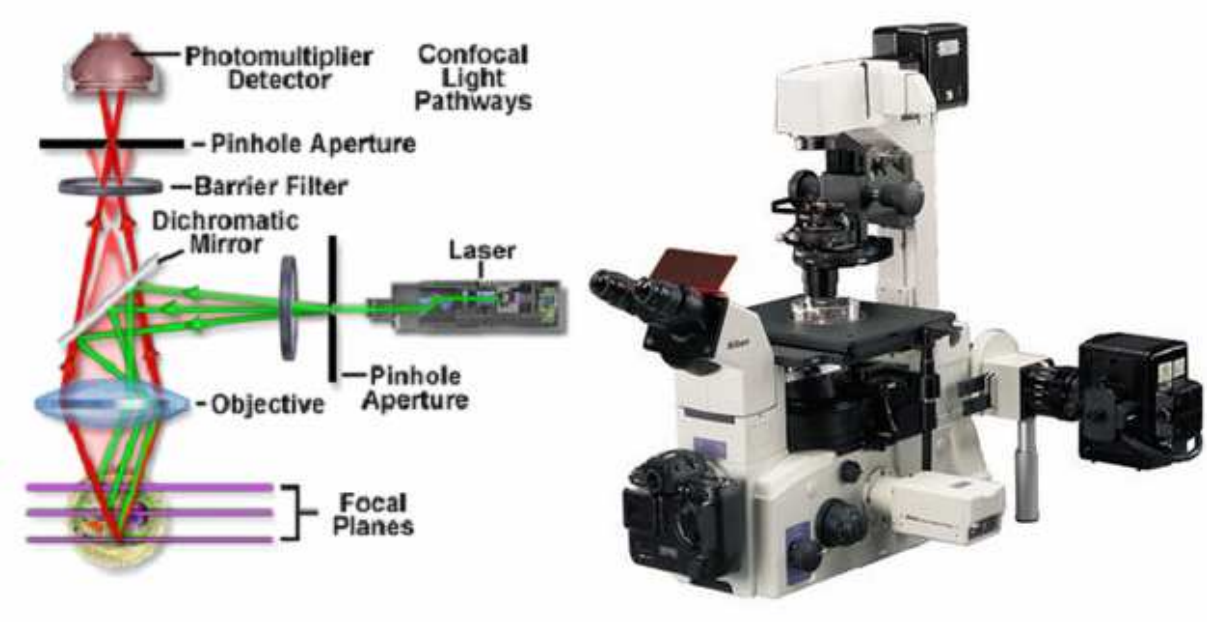

Figure I-13: schematic representation of the confocal microscope (left) and picture of the Nikon TE-2000U inverted confocal microscope (right)

Confocal microscopy[17-19] offers several distinct advantages over traditional widefield fluorescence microscopy,[20-22] including the ability to control depth of field, elimination or reduction of background information away from the focal plane (that leads to image degradation), and the capability to collect serial optical sections (from different focal plans) from thick samples. The basic key to the confocal approach is the use of spatial filtering

techniques to eliminate out-of-focus light or glare in samples whose thickness exceeds the dimensions of the focal plane.

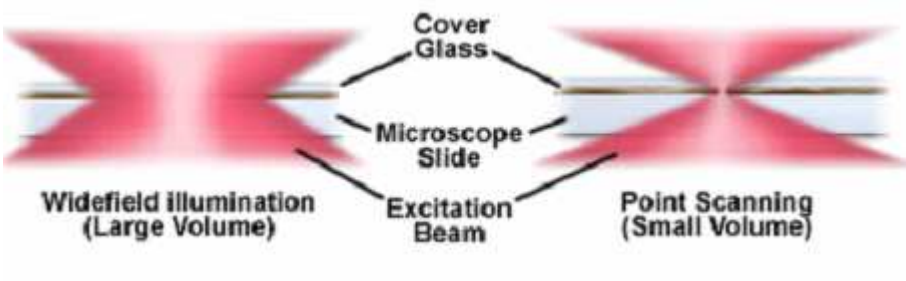

Figure I-14: comparaison between wide field and confocal fluorescence microscope

In a conventional widefield optical fluorescence microscope, secondary fluorescence emitted by the sample often occurs through the excited volume and obscures resolution of features that lie in the objective focal plane. The problem is especially important with thicker samples (greater than 2 micrometers), which usually exhibit such a high degree of fluorescence emission that most of the fine detail is lost. Confocal microscopy provides only a marginal improvement in both axial (**z**; along the optical axis) and lateral (**x** and **y**; in the sample plane) optical resolution, but is able to exclude secondary fluorescence in areas removed from the focal plane from resulting images. Even though resolution is somewhat enhanced with confocal microscopy over conventional widefield techniques, it is still considerably less than that of the transmission electron microscope. In this regard, confocal microscopy can be considered a bridge between these two classical methodologies. **L**aser scanning confocal microscopy represents one of the most significant advances in optical microscopy ever developed, primarily because the technique enables visualization deep within the sample and affords the ability to collect sharply defined optical sections from which three-dimensional renderings can be created. The basic concept of confocal microscopy was originally developed by Marvin Minsky in the mid-1950s (patented in 1961) when he was a postdoctoral student at Harvard University. Minsky wanted to image neural networks in

unstained preparations of brain tissue and was driven by the desire to image biological events as they occur in living systems. Modern confocal microscopes can be considered as completely integrated electronic systems where the optical microscope plays a central role in a configuration that consists of one or more electronic detectors, a computer (for image display, processing, output, and storage), and several laser systems combined with wavelength selection devices and a beam scanning assembly. Coherent light emitted by the laser system (excitation source) passes through a pinhole aperture that is situated in a conjugate plane (confocal) with a scanning point on the specimen and a second pinhole aperture positioned in front of the detector (a photomultiplier tube). As the laser is reflected by a dichromatic mirror and scanned across the specimen in a defined focal plane, secondary fluorescence emitted from points on the specimen (in the same focal plane) pass back through the dichromatic mirror and are focused as a confocal point at the detector pinhole aperture. The significant amount of fluorescence emission that occurs at points above and below the objective focal plane is not confocal with the pinhole. Because only a small fraction of the out-of-focus fluorescence emission is delivered through the pinhole aperture, most of this extraneous light is not detected by the photomultiplier and does not contribute to the resulting image. Refocusing the objective in a confocal microscope shifts the excitation and emission points on a specimen to a new plane that becomes confocal with the pinhole apertures of the light source and detector.

II. First level of organization: Hybrid organic/inorganic assembly based on zeolite L crystals

The concept of using materials of different chemical nature, assembling them to obtain a new one which exhibits enhanced properties can be applied to many different fields.[23] Although, to obtain interesting properties, a simple mixture of organic and inorganic materials is not enough, one has to organize them in a specific way. Some of the most significative examples of such hybrid systems can be found in nature and more specifically in the human body. If we take a closer look at our bones, we understand that nature has been able to design a material with extremely high mechanical properties by combining organic and inorganic materials arranged in the appropriate architecture.[24] In this chapter will be presented one of the concepts which allow us to obtain enhanced fluorescent properties through supramolecular assembly of dye molecules in monodirectional channels of an inorganic guest. The idea of having such supramolecular assembly is not limited to hybrid organic-inorganic assemblies. The formation of organic crystals embedding organized fluorescent dye molecules can also lead to enhanced fluorescence properties[25] but the inorganic crystals present a major advantage with respect to those all organic inclusion compounds: the hybrid materials can be manipulated and processed using organic solvents and can be heated at high temperatures without destroying the crystal.

A. The zeolite L crystal

Zeolites are microporous crystalline solids containing holes and channels within their well-defined structures. Generally zeolite frameworks consist of silicon, aluminium and oxygen and their pores contain cations, water or other molecules. So far over 60 different species of naturally occurring zeolites have been discovered and described.[26,27] Zeolites are widely used in industry due to both their ion-exchange properties and large availability at low cost.[28-31] The interesting characteristics of zeolites motivated industries to synthesise them.

The history of synthetic zeolites started in 1950 when Union Carbide managed the synthesis of pure zeolite A and zeolite X. Since then, a lot of research has been done on this topic. To date, over 100 zeolite framework topologies are synthetically available.

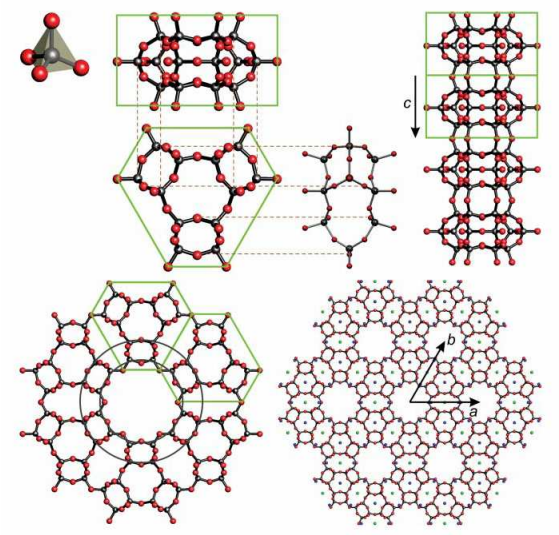

Figure II-1: the zeolite L crystal structure

In the 1950s, the scientists of the Linde Company, a division of Union Carbide Corporations, were the first to synthesize zeolite Linde type L, or short, zeolite L.[32,33] Zeolite L has a cylindrical shape with hexagonal symmetry. The stoichiometry of zeolite L with M+ as charge compensating cation is equal to |M9(H2O)21| [Al9Si27O72] in a fully hydrated crystal. Zeolite L has been found to be an ideal host for supramolecular organization of dyes. **Figure II-1** presents the crystalline structure of zeolite L. The primary building units are TO_4 tetrahedra where T can be an Al or a Si atom. The SiO4 tetrahedra are electrically neutral whereas the AlO4 entities have a negative charge, leading to an overall anionic zeolite framework. This negative charge is compensated by cations which are located at specific positions within the framework. The cations can participate in ion-exchange processes. The secondary building unit, the cancranite cage, is obtained by linking the primary units through oxygen bridges. The cancranite cages are stacked into columns along the c-axis. The channels consist of 7.5 Å long unit cells (u.c.). They have a free open diameter of 7.1 Å and are 12.6 Å

wide at the largest place. The centre-to-centre distance between two neighbouring main channels is 18.4 Å. The resulting monodirectional channels along the c-axis of the crystal can therefore be filled by cationic exchange with the counter which can lead to supramolecular organization inside the channels.

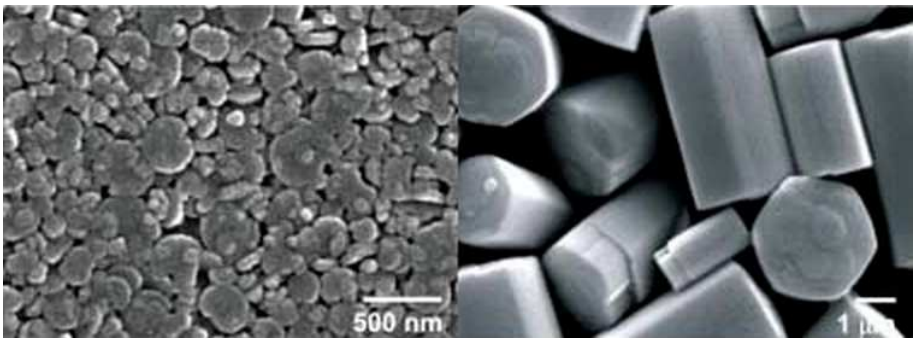

Figure II-2: SEM images of different sizes of zeolite L crystals: nanodisc shaped (left) and long cylindrical microcrystals (right)

As one can see from **Figure II-2,** zeolite L crystals have different sizes and shapes. Some of them are small nanometric disc shaped crystals and others are micro objects with a long tube like morphology.

B. Supramolecular organization of organic dyes inside the zeolite L channels

1. Organic guest molecules

(1) Cationic exchange

Insertion of dyes into the channels of zeolite L can be realized in different ways: by cation exchange for cationic dyes, or from the gas phase for neutral dyes.[34,35] A typical procedure for the insertion of neutral molecules is to dry the zeolite under vacuum and then to sublime the dye, again under vacuum. Cation exchange can be carried out from different solvents. Choice of the right solvent and temperature may be critical. It is important to choose a solvent which doesn't dissolve the dye too much so that the insertion inside the zeolite channels is favoured. In this section, we will focus on the simple solution based cationic

exchange of monovalent cationic dyes. Such dyes are known to occupy two unit cells in zeolite L. Therefore, a loading of 100% of the zeolite crystal would correspond to a ratio between number of unit cells and dye molecules of 2:1.

(2) Oxonine

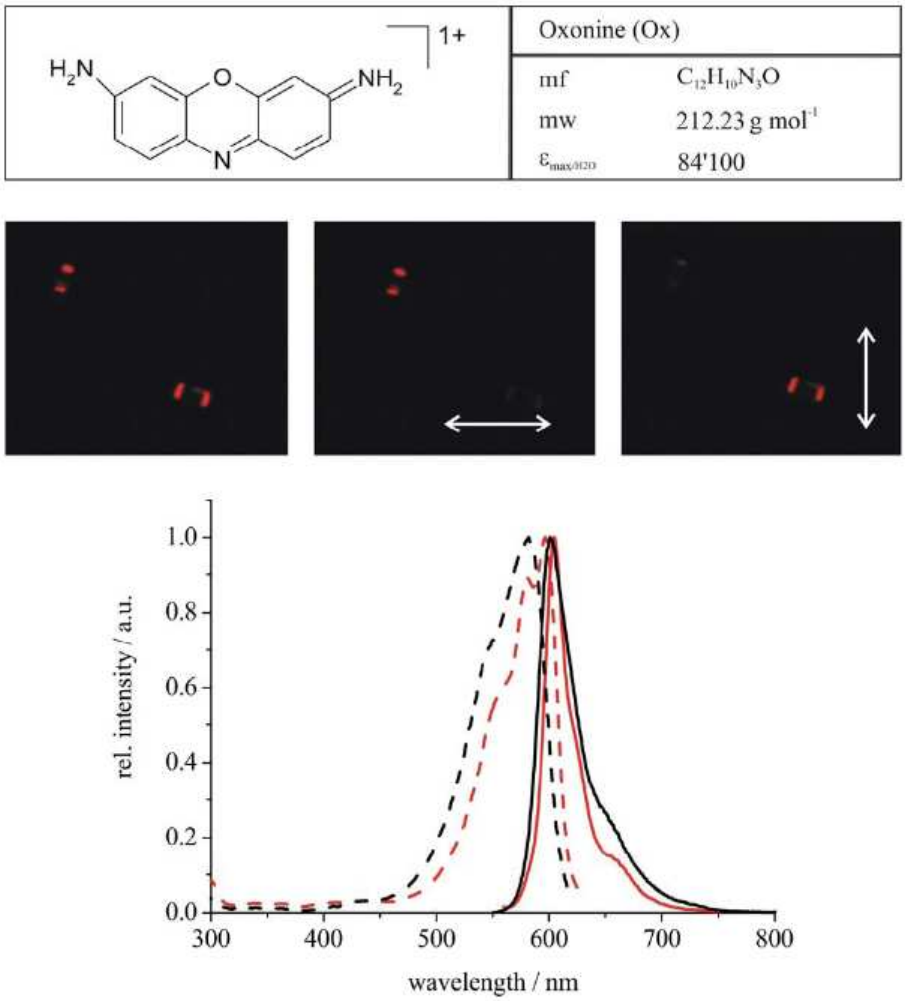

Figure II-3: Top: Structure, molecular formula (mf), molecular weight (mw) and extinction coefficient (ε_{max}) of oxonine. Middle: Polarised fluorescence microscope image of two Ox-zeolite crystals. Bottom: Excitation (dashed) and emission (solid) spectra of oxonine in zeolite (red) and in water (black).

Oxonine[36] is a cationic dye which has Cl as a counter ion. **Figure II-3** displays the formula as well as the chemical structure of the oxonine molecule. The molecule is well soluble in water and can easily be inserted into the zeolite channels from water solutions. Typically, the desired amount of oxonine molecules is added to a suspension of zeolite

crystals in water and kept at 80°C under stirring for at least five hours. One oxonine molecule occupies two unit cells of the zeolite structure and it makes an angle of 72° with respect to the c-axis of the zeolite crystal.[37] **Figure II-3** displays the excitation and emission spectra of the dye loaded zeolite crystals as well as the absorption and emission spectra of the dye in solution. A polarized emission from the loaded zeolite crystals can also be seen which confirms the positioning of the dye molecules almost perpendicular to the channel axis.

(3) Oxazine 1

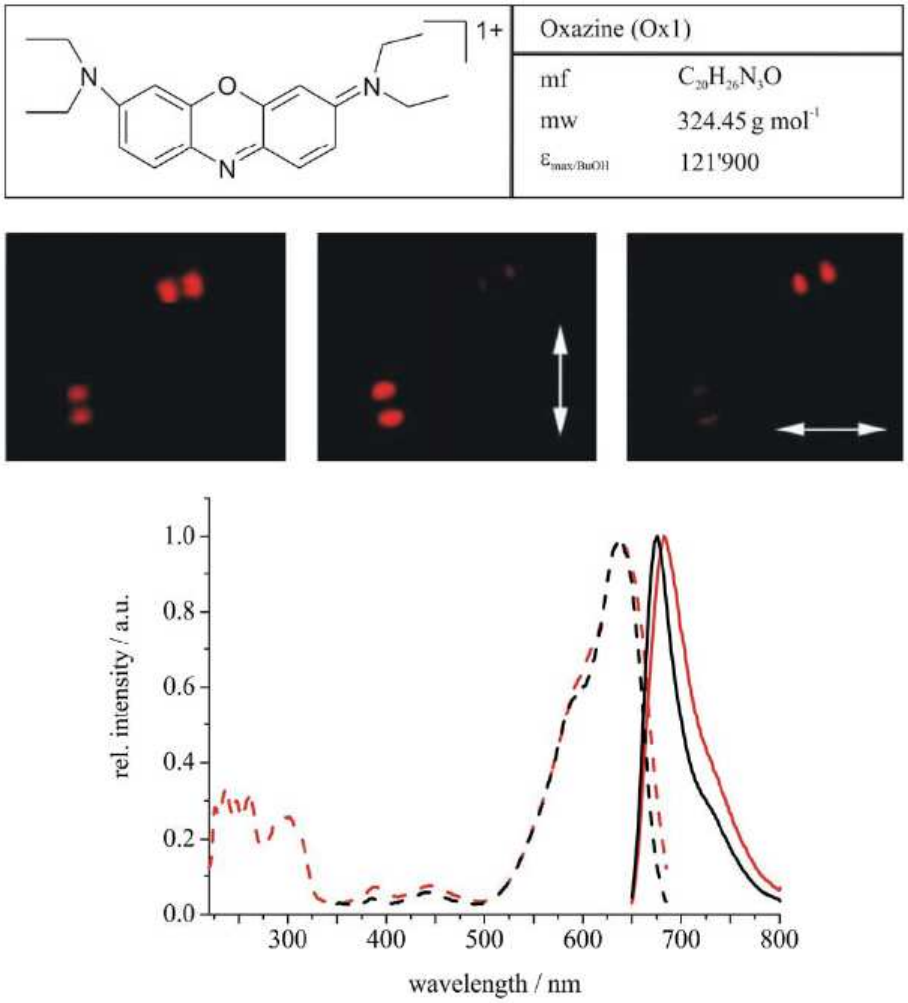

Figure II-4: Top: Structure, molecular formula (mf), molecular weight (mw) and extinction coefficient (ε_{max}) of oxazine 1. Middle: Polarised fluorescence microscope image of two Ox1-zeolite crystals. Bottom: Excitation (dashed) and emission (solid) spectra of oxazine 1 in zeolite (red) and in methanol (black).

Oxazine 1 (Ox1) is a cationic dye which has Cl as a counter ion. **Figure II-4** displays the formula as well as the chemical structure of the Ox1 molecule. Unlike the previous

cationic dye, the Ox1 loading procedure is not from aqueous solutions. Ox1 is soluble in toluene at low concentrations. One Ox1 molecule occupies two unit cells of the zeolite structure and unlike oxonine, it stays parallel to the c-axis of the zeolite crystal. **Figure II-4** displays the excitation and emission spectra of the dye loaded zeolite crystals as well as the absorption and emission spectra of the dye in solution. A polarized emission from the loaded zeolite crystals can also be seen which confirms the positioning of the dye molecules almost parallel to the channel axis.

2. Advantages of the supramolecular assembly

Organic dye molecules tend to form aggregates, which are known to cause fast thermal relaxation of the electronically excited states. They are usually unstable under irradiation, especially when present as monomers. Protection against bimolecular reactions but also unwanted isomerization reactions is possible by encapsulating them in an appropriate host such as a zeolite. Furthermore, such encapsulation provides a protection from the environment and avoids quenching of the photoluminescence due to photo oxidation for example.

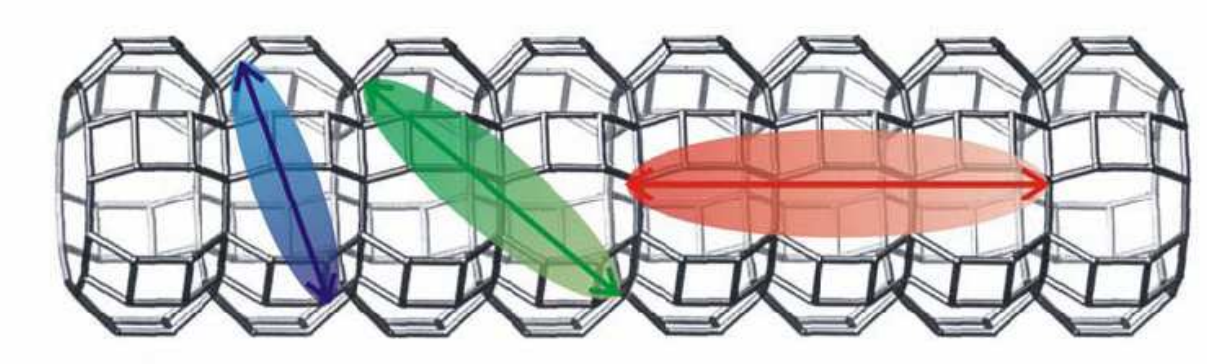

Figure II-5: influence of size on the position of the dye molecule relative to the channel axis of the zeolite crystal

Dye/zeolite composites sometimes represent a supramolecular organization with new material properties. Playing on the size and shape of the guest molecule, one can obtain different situations going from the one where the molecule stays parallel to the channel axis to the opposite one where it is almost perpendicular.[38-40]

As we will see in the following part, in order to have fast and efficient energy transport, it is necessary that the donor and acceptor molecules stay close to each others and that their dipole moments are as parallel as possible. These conditions are necessary for both the homo energy transfer and when the donor and the acceptor molecules are different species. Through the supramolecular assembly in the zeolite framework, optimal conditions for such an efficient energy transfer and a fast energy transport can be achieved by inserting the right molecules into the channels.

C. How can we inject energy inside the zeolite channels?

1. Förster Resonant Energy Transfer (FRET)

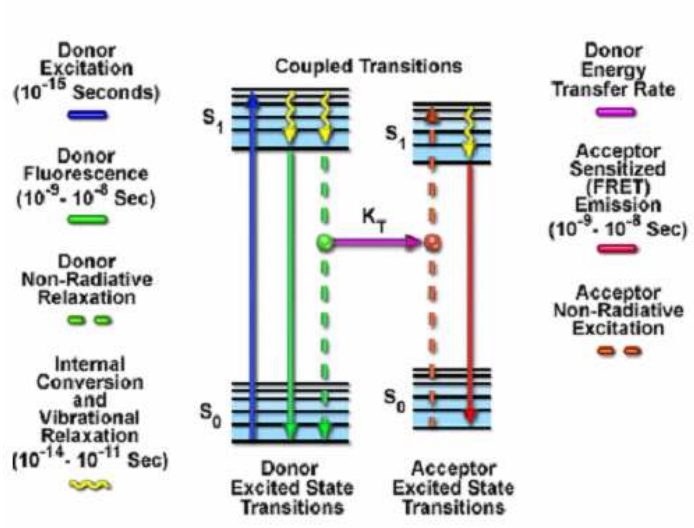

Figure II-6: energy diagram of the FRET process

The fundamental mechanism of FRET involves a donor fluorophore in an excited electronic state, which may transfer its excitation energy to a nearby acceptor fluorophore (or chromophore) in a non-radiative fashion through long-range dipole-dipole interactions.[41-45] The theory supporting energy transfer is based on the concept of treating an excited fluorophore as an oscillating dipole that can undergo an energy exchange with a second dipole having a similar resonance frequency. In this regard, resonance energy transfer is analogous to

the behavior of coupled oscillators, such as a pair of tuning forks vibrating at the same frequency or a radio antenna.

There are only certain pairs of fluorophores suitable for **FRET** since, besides other prerequisites (e.g. dipole orientation, sufficient fluorescence lifetime), the donor emission spectrum has to overlap the excitation spectrum of the acceptor (**Figure II-7**). The overlap integral, $\mathbf{J_{DA}(\lambda)}$, is the region of overlap between the two spectra.

$$J_{DA}(\lambda) = \int F_D(\lambda) \times E_A(\lambda) \times \lambda^4 d\lambda$$

The other parameters that can affect FRET are the quantum yield of the donor and the extinction coefficient of the acceptor. Thus, in order to maximize the FRET, one must choose the highest quantum yield donor, the highest absorbing acceptor, and fluorophores having significant overlap in their spectral profiles. On the other hand, these parameters can also allow one to tune the quantity of energy transferred knowing that it could result in the simultaneous emission of both species.

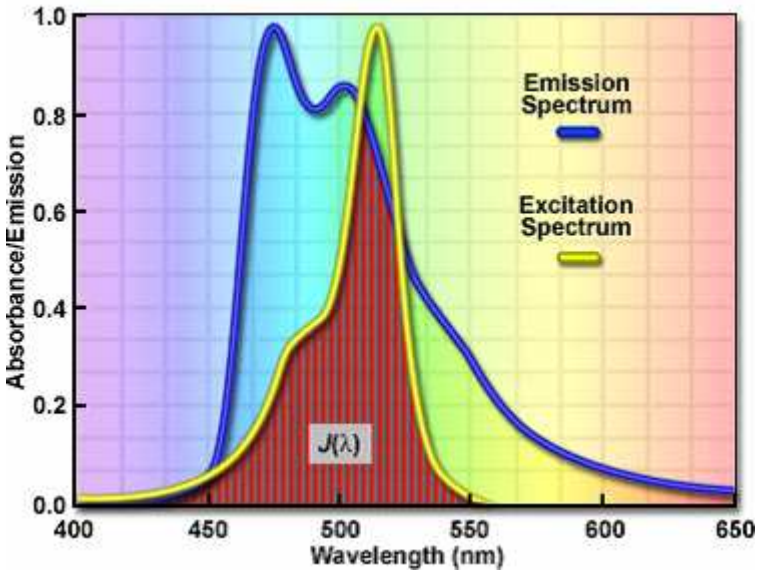

Figure II-7: an example of overlap between the donor's emission and acceptor's excitation spectra

The phenomenon of FRET is not mediated by photon emission, and furthermore, does not even require the acceptor chromophore to be fluorescent. In most applications, however, both donor and acceptor are fluorescent, and the occurrence of energy transfer manifests itself through quenching of donor fluorescence and a reduction of the fluorescence lifetime, accompanied also by an increase in acceptor fluorescence emission. The theory of resonance energy transfer was originally developed by Theodor Förster and, in honor of his contribution, has recently been named after him. The Förster theory shows that FRET efficiency ($\mathbf{E_{FRET}}$) varies as the inverse sixth power of the distance between the two molecules ($\mathbf{r_{DA}}$):

$$E_{FRET} = \frac{1}{1 + \left(\frac{r_{DA}}{R_0} \right)^6}$$

$\mathbf{R_0}$ is the characteristic distance where the FRET efficiency is 50 percent, which can be calculated for any pair of fluorescent molecules (this variable is also termed the **Förster radius**. The FRET efficiency of a theoretical fluorophore pair therefore depends on the distance between the donor and the acceptor as shown in **Figure II-8**.

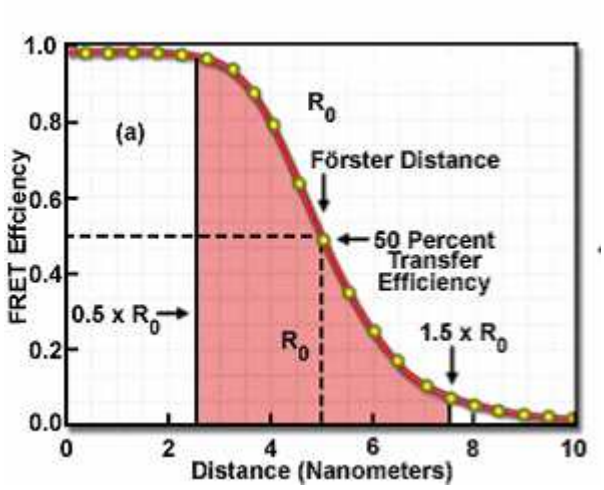

Figure II-8: FRET efficiency vs Distance for an example where R_0 is considered to be 5 nm

Because of the inverse sixth power dependence on the distance between the two molecules, the curve has a very sharp decline. For distances less than $\mathbf{R_0}$, the FRET efficiency is close to maximal, whereas for distances greater than $\mathbf{R_0}$, the efficiency rapidly approaches zero. The useful range for observing FRET is indicated by the red shaded region in **Figure II-8** with values of **r** between 0,5 and 1,5 times $\mathbf{R_0}$.

$\mathbf{R_0}$ can be calculated for any pair of fluorescent molecules using the equation with the well-established input parameters:

$$R_0 = \sqrt[6]{J_{DA}\ \frac{9\ln(10)\,\phi_D\,\kappa^2}{128\,\pi^5 n^4\,N_A}}$$

where J_{DA} is the previously introduced overlap integral between the emission spectrum of the donor and the excitation spectrum of the acceptor, ϕ_D is the fluorescence quantum yield of the donor and the parameter κ^2 describes the relative orientation of the transition dipole moments of the donor and the acceptor (**Figure II-9**).

$$\kappa^2 = (\cos\theta_T - 3\cos\theta_D \cos\theta_A)^2$$

$$\kappa^2 = (\sin\theta_D \sin\theta_A \cos\phi - 2\cos\theta_D \cos\theta_A)^2$$

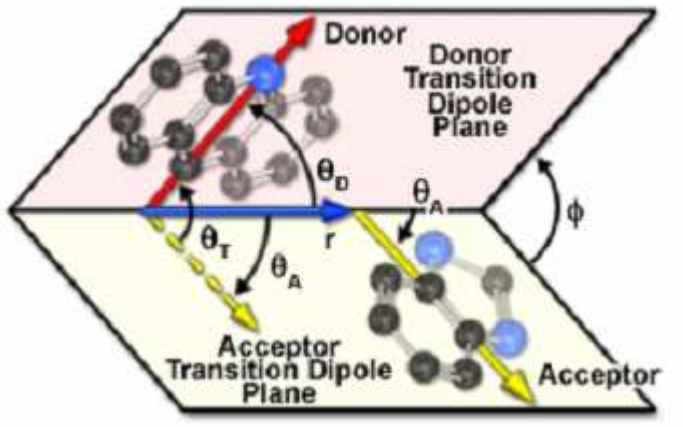

Figure II-9: relative orientation of the donor and the acceptor's dipole moments and calculation of the orientation factor

The orientation angle variable κ^2 simply indicates that the FRET coupling depends on the angle between the two fluorophores in much the same manner as the position of a radio antenna can affect its reception. If the donor and acceptor are aligned parallel to each other, the FRET efficiency will be higher than if they are oriented perpendicular. This degree of alignment defines κ^2. Although κ^2 can vary between zero and 4, it is usually assumed to be 2/3, which is the average value integrated over all possible angles.

2. The stopcock principle

The stopcock principle is based on the design of a particular dye which will allow one to inject energy to the dye inside the zeolite channels. The stopcock molecule is designed in such a way that it stays at the channel entrances and it therefore provides a link between the environment of the zeolite and the dye inside the channels.[46-48] The stopcock molecules are composed of two parts which are covalently bound to each others. Depending on the application and the processes used to address the molecules inside the channel through the stopcock, it will be designed in different ways. A cationic dye or label is linked to a part that is too big to enter the zeolite channels. This second blocking part avoids the complete entrance of the molecule in the zeolite channels which stays at the channel entrance.

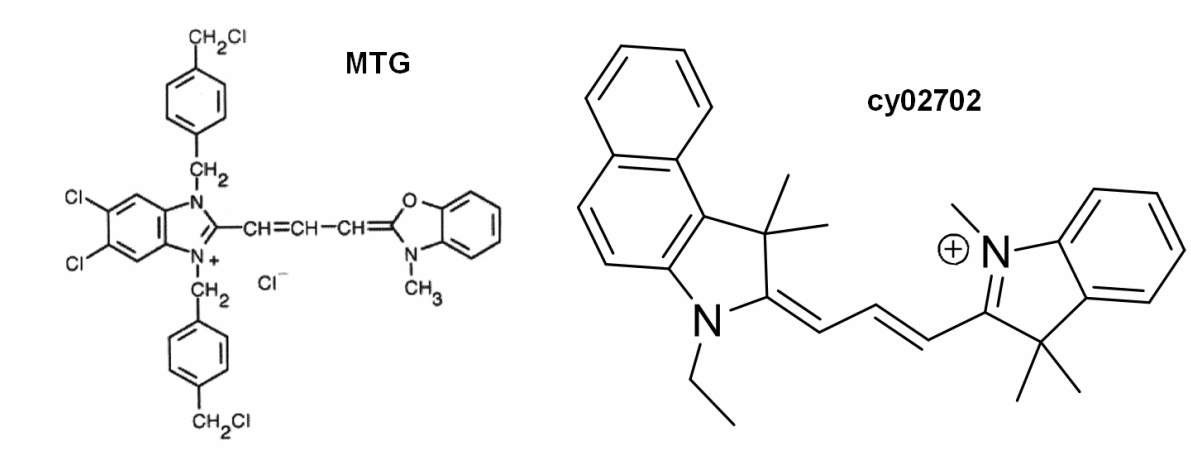

Figure II-10: two examples of fluorescent stopcock molecules (left) MTG and (right) Cy02702

Figure II-10 displays the chemical structures of the two stopcock molecules that were used in this study. The Cy02702 molecule displays a cation on its tail which will be easily introduced inside the zeolite channels. On the other hand, the cation on MTG is on the head and therefore the conditions to have the zeolite/stopcock assembly in this case will be harder to obtain and is much more unstable. When MTG loaded zeolites L are put again in a solvent or blended in a polymer, the risk of having MTG coming out of the zeolite channels is relatively high.

3. Functionalization of the external surface

In order to graft molecules on the external surface of the zeolites, one has to start by functionalizing them with a silicate derivative.[49,50] The choice of the silicate derivative depends on the functions present on the molecule which will be consequently grafted. One of the molecules used for the first functionalization step of the surface of the crystals is the Aminopropyltriethoxy Silane (APTES). The silanol groups present on the external surface (coat and base) of the zeolite react with the aminosilicate forming Si-O-Si bridges. The modified zeolite surface therefore displays amine groups that can be further used for grafting an organic dye with carboxylic acid or aldehyde functions for example. Unlike the stopcock principle, in the case of grafted molecule, the donors for an energy transfer to the dye molecules inside the channels are covalently bound to the zeolite crystals using trivial chemical reactions. The zeolite crystal can also be used as a support for a very efficient energy transfer between two molecules grafted on the surface as it provides a cylindrical substrate where molecules can be grafted close to another (one molecule can be grafted on each of the –OH groups present on the zeolite surface). As the molecules in this case are covalently bound to the surface, the resulting system is much more stable than the one based

on the stopcock molecules. In the case of dye grafted on the external surface, zeolite crystals can be further processed in solution or blended with polymers.

4. Comparative study of the advantages and the drawbacks of each system

Unlike the zeolite crystals loaded with stopcock molecules, in the case of the dye molecule grafted on the external surface, energy transfer occurs not only from the base but also from the coat of the zeolite crystals. Let us have a closer look at the case of the nanozeolites which are 25nm x 25 nm of dimension loaded at 20% of the maximum loading of the zeolite. This corresponds to a ratio dye molecule to repeating unit of the zeolite crystals of 1:10.

The total number of channels in a 25 nm particle is 167 and therefore, the total number of channel openings is 334. The length of the vector c in the zeolite L crystal structure is 0,75 nm. Taking this parameter, the fact that one dye occupies two unit cells, and a Förster's radius of around 5 nm into account, we estimate that the energy is transferred from the grafted dye present on the base to two dye molecules present close to each of the channel entrances. Assuming that the dye molecules are homogeneously dispersed (with a loading of 20%) in the zeolite channels, an average of 134 molecules per crystal can be an acceptor for an energy transfer from the bases. This same number of molecules would also be potential acceptors for an energy transfer if stopcock molecules are used. But in the case of transfer from molecules grafted on the external surface, the energy transfer also occurs from the coat and not only from the bases.

The length of the vectors a and b of the crystal structure of the zeolite L is 1,84 nm, therefore we estimate that energy is transferred from the molecule on the coat of the zeolite to the dye molecules present into the two outermost channels of the zeolite crystals. The number of the two outermost channels of a single crystal is 82 (43 outermost + 39 second outermost).

Thus, the number of dye molecules that can be excited through energy transfer from the coat is 82 x 4 = 328 molecules.

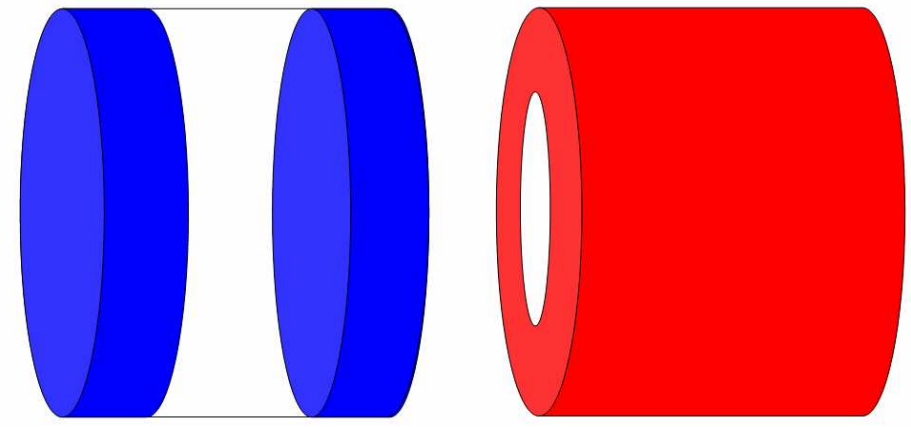

Figure II-11: schematic representation of the positions of the dyes which can be an acceptor for energy transfer: (left) acceptor molecules for both stopcock and functionalisation approaches and (right) for functionalisation but not for energy transfer from stopcocks

Using both the energy transfer processes from the base and the coat simultaneously, we strongly increase the probability of addressing a large number of dye molecules included in the nanosized inorganic crystal. Therefore, the co-occurring energy transfers from the dye grafted on the bases and the coat of the zeolite crystals lead to a far more efficient process than the systems based on stopcock molecules.

III.Second level of organization: Zeolite L crystals assembled in polymeric materials

As we saw in the previous chapter, the dye inside the zeolite channels can be addressed through energy transfer from a dye which is somehow linked to the zeolite (stopcock molecule or dye molecule grafted on the external surface) but now a strategy to properly address the zeolite crystals is needed. As the aim of this study is to build functional opto electronic devices, it is important to provide a medium to contact the zeolite crystals. In order to do that, the approach we will be focusing on is to embed or assemble the zeolite crystals in a conjugated polymer. Conjugated polymers present many advantages and can be the base of low cost production of highly efficient opto electronic devices.[51-55] Conjugated polymers are now widely used in opto electronic devices such as OLED because of their intrinsic optical and electronical properties, but also because they can be processed and structured much more easily then inorganic materials. The genesis of the field can be traced back to the mid 1970s when the first polymer capable of conducting electricity polyacetylene was prepared by accident by Shirakawa.[56] The subsequent discovery by Heeger and MacDiarmid that the polymer would undergo an increase in conductivity of 12 orders of magnitude by oxidative doping raised the science community's curiosity and research about other conducting polymers soon followed.[57-63] The target was (and continues to be) a material which could combine the processibility, environmental stability, and weight advantages of a fully organic polymer with the useful electrical properties of a metal.

In this chapter, we will see how we can take advantage of different known techniques to obtain polymer thin films or nanofibers and use them to contact, organise or structure dye loaded zeolite L crystals in the polymer. The results of this study will provide optimal structures for the incorporation of zeolite crystals into OLED or into nanofibers which could be the first step towards the fabrication of zeolite based flexible nanodevices.

A. Zeolite L crystals embedded in electroluminescent electrospun nanofibers

Fibers with a diameter of between 100 nm-500 nm are generally classified as nanofibers. These fibers can be made from a wide variety of materials ranging from metals,[64] ceramics[65] to polymers. What makes nanofibers of great interest is their extremely small size and high aspect ratio. With higher surface area to volume ratios and smaller spaces between individual fibers than larger fibers, nanofibers offer an opportunity for use in a wide variety of applications. Increased awareness of the current and the potential applications of nanofibers have in recent years accelerated the research and development of these structures. Some important applications for these nanofibers include, but are not limited to, catalytic substrates, photonics, filtration, protective clothing, cell scaffolding, drug delivery and wound healing. To date, the most successful method of producing nanofibers is through the process of electrospinning.[66-77]

1. Electrospinning electroluminescent polymer blends

(1) The electrospinning process

Electrospinning traces its roots back to electrostatic spray painting, which has been in operation for almost 100 years. In 1934, a process for the production of polymer filaments using electrostatic force was patented by Formhals.[78-80] Formhals encountered a number of problems early in his work, but by 1940 not only had he overcome those initial problems, but he had developed methods of producing composite fibers using multiple polymers and fibers that were aligned parallel to one another. Although the fibers produced by Formhals were much larger than the nanofibers which can be obtained nowadays, his work set the stage for the production of these structures. The electrospinning process uses high voltage to create an electric field between a droplet of polymer solution at the tip of a needle or a capillary and a collector plate. One electrode of the voltage source is placed into the solution and the other is

connected to the collector. This creates an electrostatic force. As the voltage is increased, the electric field intensifies causing a force to build up on the pendant drop of polymer solution at the tip of the needle. This force acts in a direction opposing the surface tension of the drop. The increasing electrostatic force causes the drop to elongate forming a conical shape known as a Taylor cone. When the electrostatic force overcomes the surface tension of the drop, a charged, continuous jet of solution is ejected from the cone. The jet of solution accelerates towards the collector, whipping and bending wildly. As the solution moves away from the needle and toward the collector, the jet rapidly thins and dries as the solvent evaporates. On the surface of the grounded collector, a nonwoven mat of randomly oriented solid nanofibers is deposited.

Taylor did a study of the polymer droplet at the end of the capillary in an electrospinning setup in 1969. This study led to a better understanding of the process by which the polymer solution streams from the capillary. In 1987, the experimental conditions and factors that cause highly conductive fluids exposed to increasing voltages to produce unstable streams was studied by Hayati et al. These conditions cause the fluid stream to whip around in different directions as it leaves the needle. The work of Doshi and Reneker explored how changing the concentration of the polymer solution and the voltage applied to the solution affected the formation of nanofibers.

Numerous other studies have been done to examine the effect of changing both the polymer solution and the experimental setup. Based on these studies it is clear that characteristics such as fiber diameter and morphology depend on a large number of both experimental variables and material properties which include solution concentration, viscosity, surface tension, voltage, capillary diameter, flow rate and capillary-to-collector working distance.

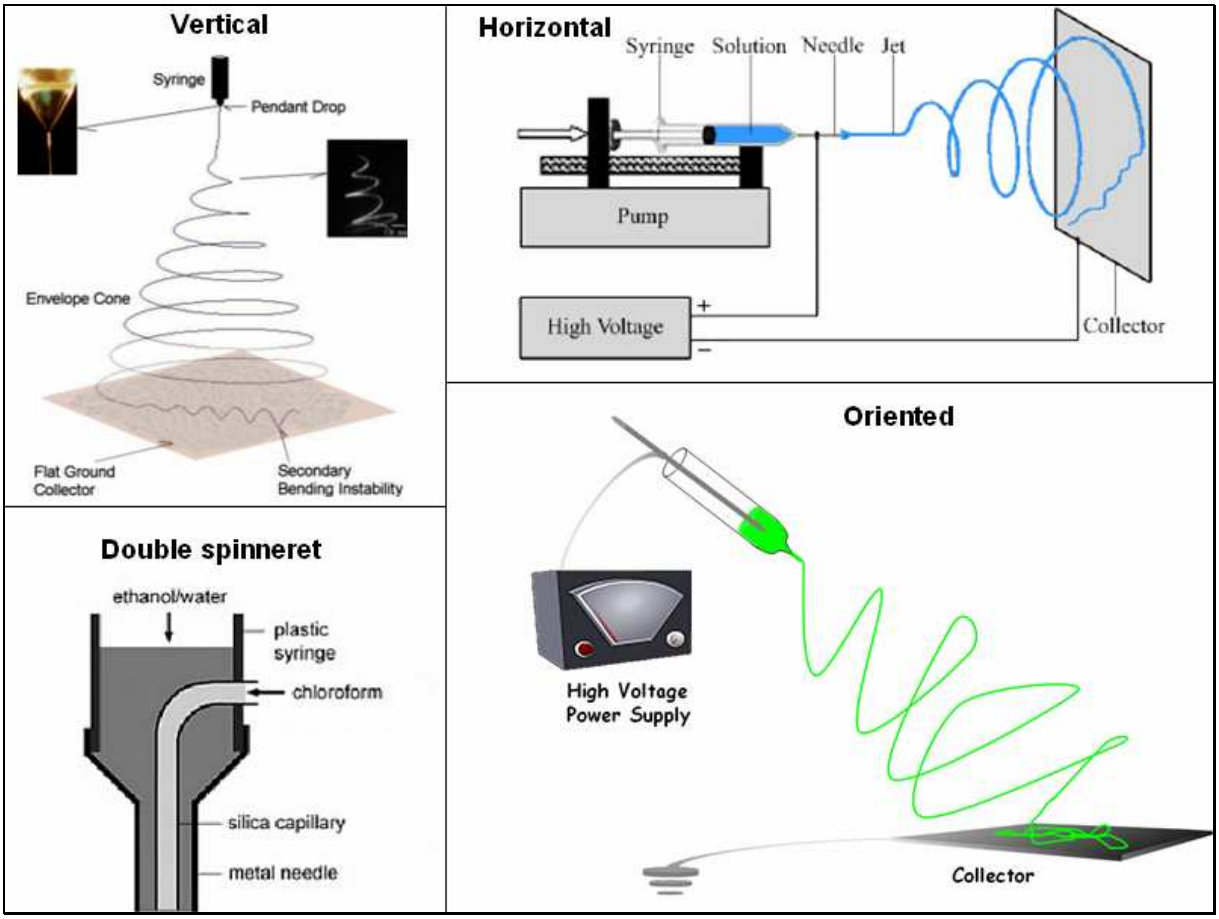

Figure III-1: different set ups for electrospinning going from the classic vertical set up (top left) to the horizontal (top right) through the oriented one (bottom right) and schematic representation of the double spinneret (bottom left)

Different set ups have also been introduced going from a simple vertical one involving gravitational forces to much more elaborated horizontal ones using an external pressure system to create the droplet at the tip of the capillary.[81] The vertical set up has one major drawback: during the initial part of the process, before stabilization, some drops of the polymer solution fall on the collector screen. The substrates covered with the polymer nanofibers are therefore also covered with some polymer drops. In the horizontal set up, the collector screen is not placed under the capillary and therefore the problem of the drops falling on it is avoided. Although, obtaining a much more controlled horizontal set up involves a lot of engineering and automatisation as a constant pressure should be applied to the polymer solution. By coming to a compromise between the simple horizontal set up and

the much more controlled but complicated horizontal set up, it is possible to have the advantages of both "extreme" set ups: if the set up is oriented with a consequent angle (in our case, 60° with respect to the vertical plane), drops will not fall on the substrates and gravitational forces can still be used to control the formation of the droplet at the tip of the capillary.

(2) Are conjugated polymers electrospinnable?

Electrospinning a conjugated polymer on its own is not an easy task. As we previously saw, the electospinning technique is based on a stretching of the polymer solution droplet created at the tip of the capillary. This stretching of the droplet closely depends on the polymer's intrinsic visco elastic properties. Conjugated polymers are known to have a rigid backbone which allows charge transport. Unlike the common polymers used for electrospinning, the rigid conjugated backbone prevents the stretching of the polymer. This lack of good visco elastic response towards stretching of the polymer chain has to be overcome in some other way. Different concepts were studied to help the process. Most of these techniques use complicated systems such as the double spinneret to obtain core shell co-electrospun structures.[82-85] In this approach, two immiscible polymer solutions are used. The double spinneret consists of two capillaries or metallic needles with different diameters placed one into the other. Each of them contains a polymer solution and typically for the co-electrospinning of conjugated polymers, the external capillary contains a polymer with good visco elastic properties in a polar solvent whereas the inner capillary contains the conjugated polymer in an organic solvent. It is very important that the two solvent are immiscible. Having such a system, once the electrospinning process starts, the polymer contained in the outer capillary will form a micro or nanotube through which the inner polymer solution will flow. The inner polymer solution will therefore fill the stretched polymer nanotube and form a nanofiber after solvent evaporation. The result of such co-electrospinning using double

spinneret is interesting as one directly obtains a threaded flexible nanowire but the technique has a major drawback: the morphology of the inner part of the nanowire cannot be controlled. The main advantage of this technique consists in the fact that one can obtain a nanofiber of pure conjugated polymer by selectively dissolving the polymer present in the external part of the core-shell nanotube.

The double spinneret technique is not the only way of obtaining pure conjugated polymer nanofibers. Blending the conjugated polymer with a polymer with good visco elastic properties such as Polyethyleneoxide (PEO) or Polystyrene (PS), obtaining the same results is possible but very selective towards the used materials. These blended electrospun fibers sometimes exhibit a phase segregation of the two polymers which induces a tubular structure (core made of the conjugated polymer and shell made of other polymer or vice versa) of the fiber. After the selective dissolution of the non conjugated polymer, one can obtain fibers or nanotubes of pure conjugated polymers. Another approach would be to use precursors of conjugated polymers for the electrospinning process which are consequently converted into conjugated polymers. With this last approach, the polymer still has good visco elastic properties during the electrospinning process and becomes rigid only after the thermal conversion. This last method is an easy way of obtaining very well defined pure conjugated polymer nanofibers with a diameter which can be lower than 100 nm but the choice of the polymer is very restricted. With respect to the double spinneret set up, the blend and the polymer precursor methods use much simpler set ups but they are also much more selective towards the conjugated polymer which is electrospun.

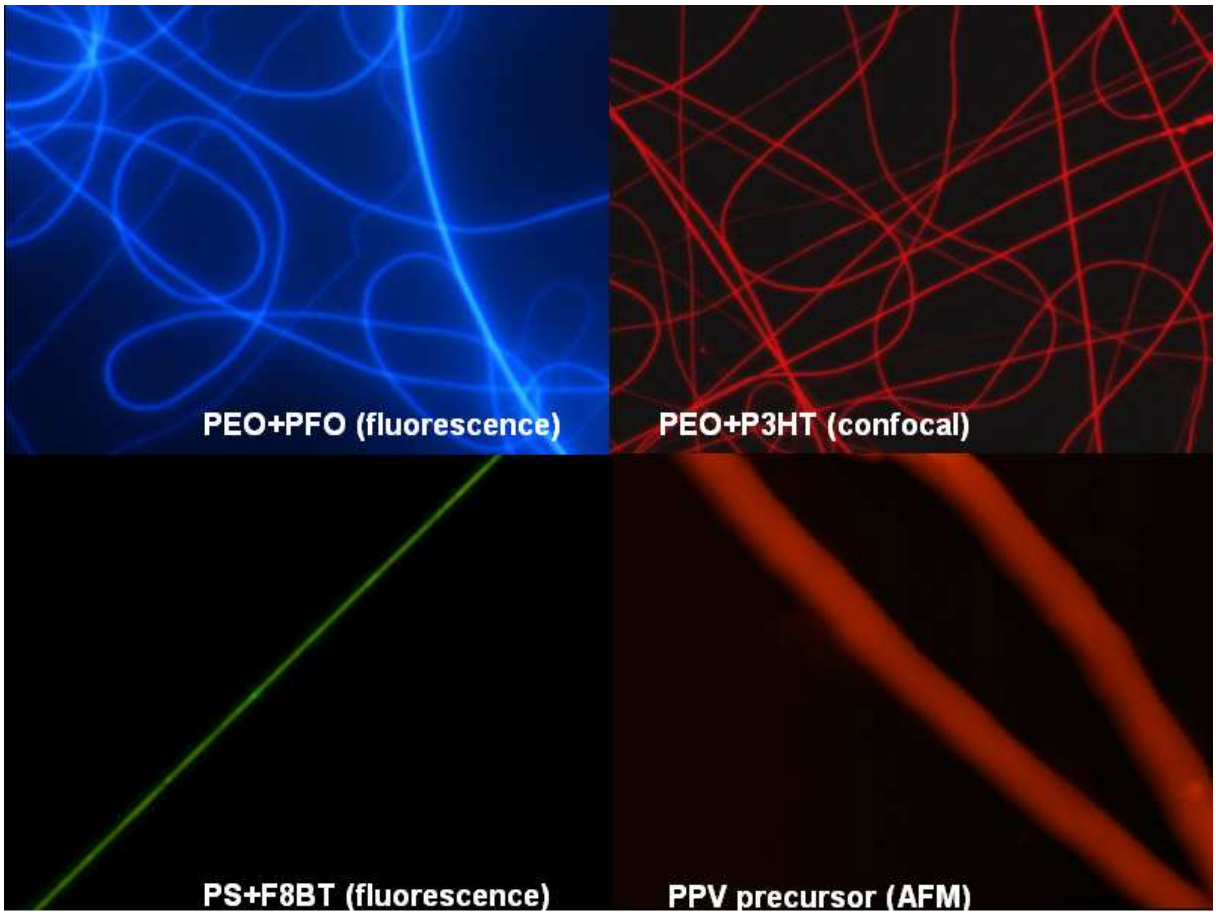

Figure III-2: examples of nanofibers obtained from blends based on polyfluorene (top left), P3HT (top right), F8BT (bottom left) and AFM image of the 100 nm fibers obtained from PPV precursors (bottom right)

In the following paragraph, we will see a number of examples of what can be achieved without the use of the double spinneret set up.

(3) Morphological study of the electroluminescent nanofibers resulting from electrospinning a blend of polymers

The use of blends for the electrospinning process can lead to different morphologies. When it comes to blending two polymers together, many parameters have to be taken into account to obtain the desired morphology. Those parameters include the ratio between both polymer quantities, the miscibility of the two polymers and all the experimental parameters which were previously introduced concerning the electrospinning process. We will focus our study on the following green emitting alternative copolymer: Poly[(9,9-dioctylfluorenyl-2,7-

diyl)-alt-co-(1,4-benzo-{2,1',3}-thiadiazole)] (**F8BT**). The function of the second polymer which will be added to the blend will be to help the F8BT to be electrospun, therefore, to undergo the study of the morphology of the fibers, two polymers known to be easy to electrospin and to be miscible with F8BT were selected: Polystyrene (PS) and Polyethylene oxide (PEO). As the miscibility of the two blended polymers is one of the major parameters to influence the morphology, it is necessary to understand that, due to the hydrophilic groups present along the PEO chains, PS will have a higher compatibility with F8BT than PEO.

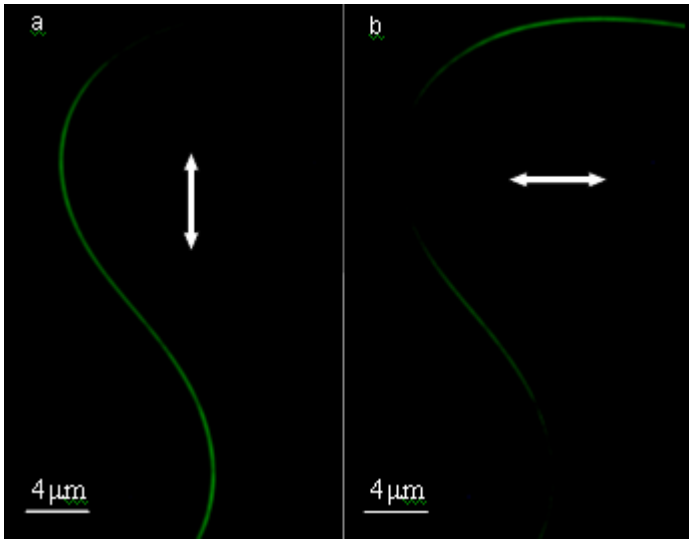

Figure III-3: Fluorescence microscope images with selectively (a) vertically and (b) horizontally polarized emissions of an electrospun fiber (blend of F8BT and PS)

Fibers obtained with a blend of F8BT and PS are obtained with a broad range of relative concentrations. The higher the quantity of F8BT becomes, the harder it is to obtain decent fibers. The fibers obtained with more than 60 w% of F8BT are not smooth fibers and they display many beads due to the high viscosity of the polymer solution. When the w% of F8BT is kept under 60%, nice and smooth nanofibers are obtained, the diameter of which can be tuned by playing on the relative concentrations of both polymers and the electrospinning parameters. Those nanofibers also exhibit an interesting property: polarized emission along the axis of the nanofiber. This can be easily explained. During the electrospinning process, the chains of PS are stretched and therefore align along the nanofiber axis. As there is no

demixing between the two polymers, the PS chains drag the F8BT ones which also align along the axis of the nanofiber leading to a polarized emission from the blended polymer nanofiber (**Figure III-3**).

The case of the PEO-F8BT blends is slightly different. Smooth fibers can be obtained with a w% of F8BT upto 85% without any problems. The polarized emission from the PS-F8BT blend is not seen on any of the fibers obtained with the PEO-F8BT blends. This already gives us the hint that the miscibility of both polymers plays an important role in the morphology of the obtained fiber. By electrospinning a range of different relative concentration, phase segregation of the two polymers can be studied. As long as the w% of F8BT is kept under 65%, no phase segregation is seen and fibers of a mean diameter on the nanometric scale are obtained. By further increasing the w% of F8BT, a demixing of the polymers can be observed which leads to the formation of a core-shell fiber. The diameter of the fibers obtained with such blends increases to a few microns and clearly displays emission mainly from the external part. PEO is soluble in water whereas F8BT is insoluble. This core shell structure can therefore lead to the formation of hollow F8BT microtubes by selectively dissolving the core in water. The dissolution of PEO can be observed directly thanks to its tension active properties. After the elctrospinning process is over, the collected fibers are immersed into water for 3 hours to allow complete dissolution of the PEO and we can observe bubble formation. Before and after the immersion, the tubular morphology of the fiber is maintained in the case of F8BT/PEO core shell fibers. To obtain fibers of pure F8BT, they can be further annealed over 150°C which allows chain mobility and induces the formation of fibers.

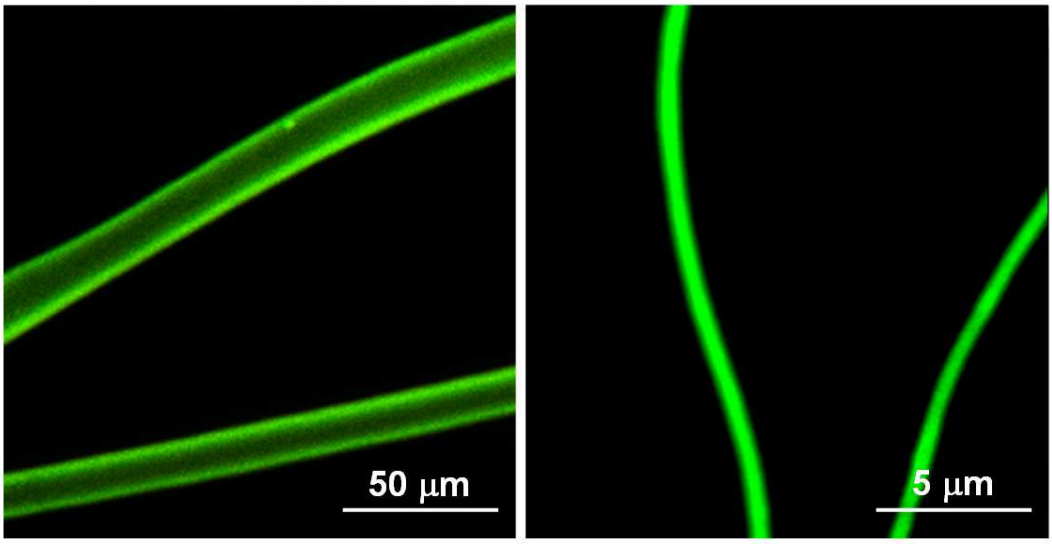

Figure III-4: confocal microscope images of (left) fibers obtained with 85 w% of F8BT after PEO dissolution in water and (right) fibers obtained with 60 W% of F8BT blended with PEO

Different morphologies and properties of electrospun fibers of electroluminescent polymer blends can therefore be obtained. In the following parts of this work, only nanofibers displaying no phase segregation will be used.

2. Inclusion of zeolite L crystals in polymeric nanofibers: Two step energy transfer from the polymer nanofiber to the guest dye molecules

As we saw in **Chapter II**, the host-guest organic/inorganic hybrid systems display enhanced fluorescent properties from the included dye, but, the major challenge consists in being able to address the fluorescent dye included in the nanocrystals optically or electronically to obtain interesting functional materials. Blending the crystals in a conjugated polymer can be an option to do so. As the zeolite L crystals cannot be diluted and destroyed in common organic solvents, the inclusion compounds can be dispersed in polymer solutions without loosing the crystal structure and therefore keeping their peculiar optical properties. Dye loaded zeolites can be embedded in electrospun nanofibers by simply suspending the crystals in the polymer solution used for electrospinning.[86] A second level of organization can be observed in zeolite L crystals embedded in nanofibers: crystals with a high aspect ratio

align along the nanofiber axis during the electorpinning process. If the dye loaded crystals can be linked to the external environment, a two step energy transfer from the electroluminescent polymer nanofiber to the dye inside the zeolite channels can be obtained.[87-88]

(1) Stopcock molecules: a link between the electroluminescent nanofiber and the organic dye included in the zeolite L channels

To obtain materials for innovative devices it is necessary to have an energy transfer from the electroluminescent polymer in the fiber to the dyes inside the zeolites. The stopcock molecule is composed of two parts: a head that cannot enter the zeolite channels due to size issues; and a tail which fits in those channels. Having such a structure, the molecule will stay at the channel entrances thus creating a "link" between the surrounding environment (the polymer in the case of fibers) and the dye inside the crystals. In this part, we will focus on the study of the previously introduced Cy02702 stopcock molecule.

The use of the stopcock molecule Cy02702 is not only to be an acceptor for energy transfer from the polymer fiber but also a donor for the dye molecules inside the zeolites channels. The oxonine and oxazine 1 are two potential acceptors for this second energy transfer. The overlap between Cy02702 stopcock molecule as donor and those two organic molecules is almost equivalent in both cases. The difference between the two systems comes from the specific orientation of the molecules inside the zeolite L channels. Oxazine 1's dipole moment is oriented along the channel axis whether oxonine's makes an angle of 72° with the channel axis. Taking into account these relative orientations of the dipole moments, the Förster's radius for the energy transfer between Cy02702 and oxonine and oxazine 1 become respectively 25 Å and 45 Å. Zeolites loaded with oxonine are refered to as ZLOx. Zeolites loaded with the stopcock molecule and oxonine and oxazine1 are respectively called CyZLOx and CyZLOx1.

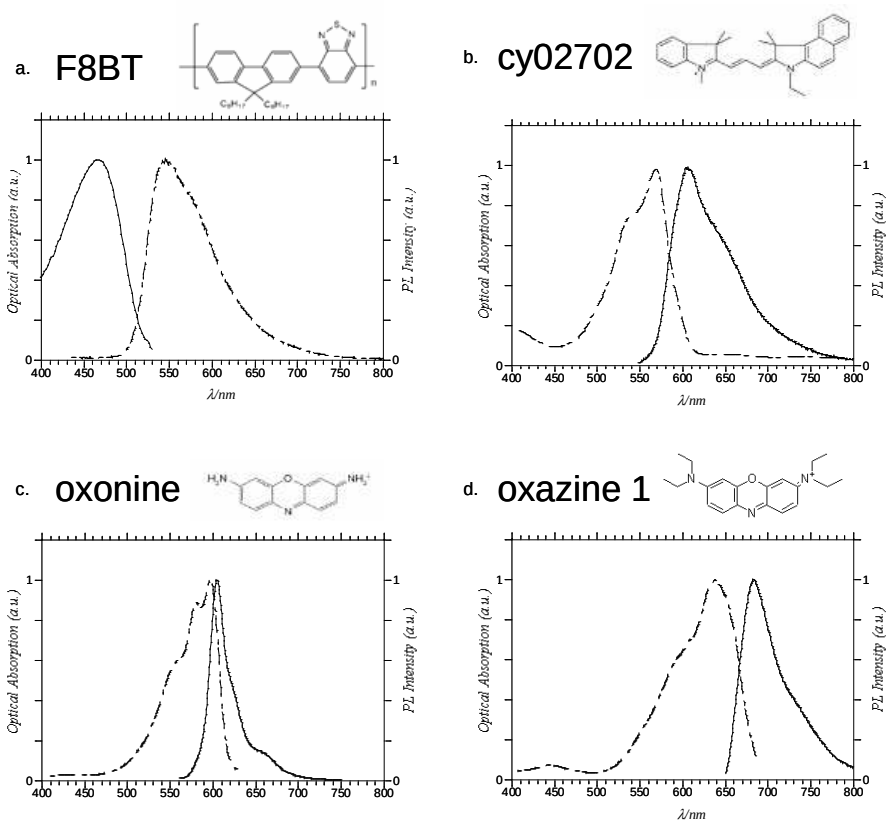

Figure III-5: chemical formula, excitation profiles and solid state emission spectra of (a) F8BT, (b) Cy02702 stopcock molecule, (c) oxonine and (d) oxazine 1

The fact that the emission from the stopcock and oxonine molecules are in the same wavelength range makes it difficult to discern one from the other especially as, by exciting one directly, we also excite the other. Though, as we can see on **Figure III-6**, when the zeolites CyZLOx are excited at 480 nm, the response obtained is a sum of both signals from oxonine and the stopcock molecule. On the other hand, in the case of zeolites CyZLOx1, by exciting specifically the stopcock molecule (excitation at 500 nm), the recorded fluorescence spectra display an intense emission from the oxazine 1 while the signal from Cy02702 is strongly reduced due to nearly complete energy transfer to oxazine 1.

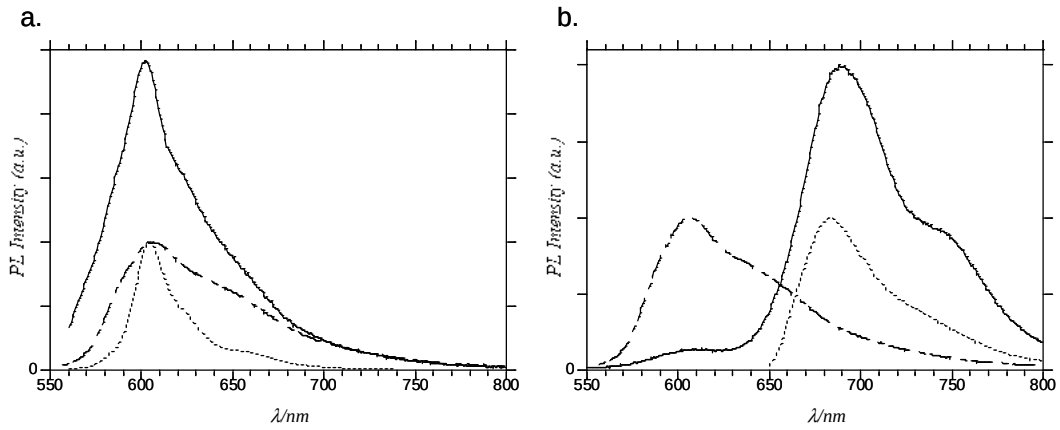

Figure III-6: (a) emission spectra of CyZLOx excited at 480 nm (solid) and zeolites loaded with Cy02702 (dashed) and oxonine (spotted) and (b) emission spectra of CyZLOx1 excited at 500 nm (solid) and zeolites loaded with Cy02702 (dashed) and oxazine 1 (spotted)

The conjugated polymer used in the fiber was Poly[(9,9-dioctylfluorenyl-2,7-diyl)-alt-co-(1,4-benzo-{2,1',3}-thiadiazole)] (F8BT, **Figure III-5**) blended with polystyrene (PS) which can easily be electrospun.[90] The blend of polymers consisted of 25% of F8BT and 75% of PS in wt.%. The diameters of the fibers obtained can be tuned from 300 nm to 2 microns by changing the diameter of the capillary and the polymer concentration in the solution used for electrospinning. The resulting fibers display a polarized emission along the fiber axis due to the stretching of the polymers during the electrospinning process and therefore an orientation of the polymer chains. To obtain zeolite embedded fibers, 2,5 % of the selected zeolites (in mass with respect to total polymer mass) was added to the electrospun solution. Fibers FB-ZLOx, FB-CyZLOx and FB-CyZLOx1 correspond respectively to fibers containing zeolites ZLOx, CyZLOx and CyZLOx1. The horizontally and vertically polarized emissions show us as well that, unlike the rest of the fiber, the polymer surrounding the zeolite is not oriented.

To study whether there is or not an energy transfer from the polymer to the dye loaded zeolites, one has to measure the emission spectra in two different points of the fiber, one only with the polymer and one with the polymer and zeolite L crystals (**Figure III-7**).

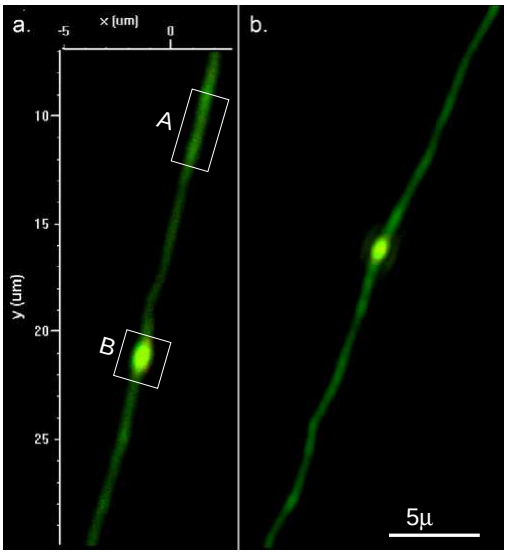

Figure III-7: Confocal (a) and fluorescence (b) microscope images of an electrospun fiber (F8BT/PS) FB-CyZLox1 excited at 488 nm. A and B are the regions of integration of the photoluminescence for the fiber and the embedded zeolite respectively (A: Fiber without zeolites; B: Fiber embedding the zeolites CyZLOx1)

In order to specifically excite part A or part B of a given fiber, the confocal microscope was used. By using such a system, we were able to compare the fluorescence from the dye loaded zeolites when they are inside the fibers (in contact with the electroluminescent polymer) and when they are on their own. To demonstrate whether there is or not an energy transfer, one has to introduce a few terms: $I_{wavelenght}$ corresponds to the integration of the signal from the dye loaded zeolites when excited at the given wavelength. I_{bl} is defined as I_{488nm} over I_{543nm} (the latter corresponding to a direct excitation of the dye loaded zeolites).

Table 1 displays the results obtained for the integrations of the different systems.

	I_{bl} ZLOx	I_{bl} CyZLOx	I_{bl} CyZLOx1
ZL	**0,05**	**0,14**	**0,17**
FB-ZL	**0,03**	**1,22**	**0,71**

Table 1: I_{bl} for ZLOx, CyZLOx, CyZLOx1, FB-ZLOx, FB-CyZLOx and FB-CyZLOx1.

If energy transfer from the conjugated polymer to the zeolite crystals occurs, the emission from the organic dyes should increase where the polymer is excited. Therefore, we expect to observe I_{bl} with higher values for the zeolites embedded in the fibers with respect to those of the zeolites alone. In the case of the fibers FB-ZLOx (zeolites without stopcock molecules), we do not observe an enhancement of the emission from the dye with direct excitation of the polymer. On the other hand, the fibers FB-CyZLOx and FB-CyZLOx1 display a remarkable increase of I_{bl} which means that in the case of these fibers we have an energy transfer from the polymer to the dye loaded zeolites. The Förster's radius for the energy transfer between F8BT and the organic dyes are 45 Å and 55,5 Å for oxonine and Cy02702 respectively considering an isotropic orientation of the polymeric chains surrounding the zeolites. Since both organic guests have similar absorption properties, the particular position of the Cy02702 molecules on the zeolite L crystals thus increases the amount of energy transferred. By adding the stopcock molecules to the zeolites, we have provided a link between the electroluminescent fiber and the inclusion complex, a link that could also be used as a donor in order to transfer energy to the dye included inside the channels. In the case of FB-CyZLOx, the energy is transferred only to the stopcock molecule. On the other hand, in the case of fibers FB-CyZLOx1, the energy is transferred to the oxazine 1 molecules inside the zeolite channels through the stopcock molecule.

The energy transfer obtained using such a method, although not very efficient, is a proof of principle that three simultaneous emissions can be obtained from an electrospun nanofiber. By adding the stopcock molecules to the zeolites and loading them with the dyes having the right properties (optical and geometrical), we have provided a link between the electroluminescent fiber and the inclusion complex which opens new perspectives to the development of nano devices based on hybrid host/guest systems.

(2) Functionalized zeolite L crystals for efficient two step energy transfer

An alternative way of addressing the dye inside the zeolite L crystals is through energy transfer from an organic dye grafted on the external surface of the crystal. Those crystals are then again embedded in an organic light emitting nanofiber being used as acceptors for FRET. The fibers obtained from the electrospinning process were prepared from a blend of a fluorene-based copolymer containing triphenylamine groups (PFTPA) and Polyethylene oxide (PEO). PFTPA was shown to avoid formation of fluorenone which quenches the emission from the fluorene inducing a green shift of the emission of the polyfluorene (as can be seen with commercial polyfluorenes).[91,92] Oxonine (Ox+) loaded zeolites with the derivative of a dialdehyde substituted tetra-hexylsexithiophene[93,94] (T6) grafted on the outer surface were added to the electrospun solution in order to obtain zeolite crystals dispersed in the polymeric nanofiber. **Figure III-8** presents the structures of the different molecules that were used along with their optical characterisation.

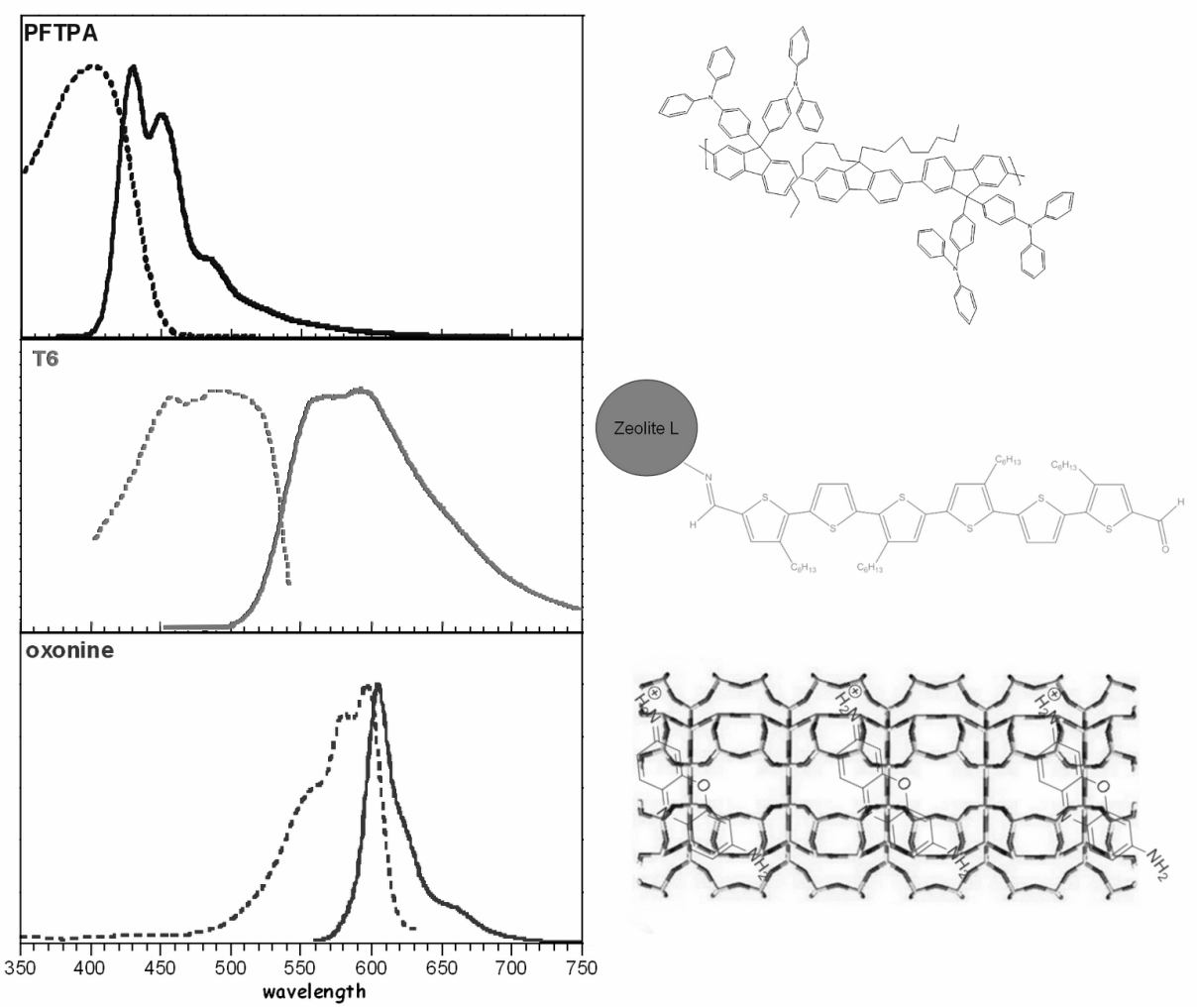

Figure III-8: (dotted) excitation profiles, (solid) fluorescence spectra (left) and formula (right) of the different molecules composing the system. Top: PFTPA (film). Middle: T6 on zeolites (powder). Bottom: oxonine in zeolites (powder)

The loading of the zeolite L crystals with organic dye molecules is done as described previously. The zeolite crystals used were nanozeolites of a mean diameter of 25 nm and a mean height of 25 nm which tend to form nanoaggregates of around 100nm x 100nm. The procedure for grafting the T6 molecule on the zeolite external surface is the one described in **Chapter II.**

To obtain a material which simultaneously emits in three different ranges of wavelengths, it is necessary to have a controlled energy transfer from the electroluminescent polymer in the nanofiber to the dye grafted on the zeolite and consequently to the dye inside

the channels. The important parameters for a good resonant energy transfer are the spectral overlap between the donor's emission and the acceptor's absorption spectra, as well as the quantum yield of the donor molecule. These parameters allow us to calculate the Förster's radius (R_0) which corresponds to the distance at which the acceptor should be from the donor in order to have half of the energy transferred. The calculated values for R_0 for the systems PFTPA-T6 and T6-Ox+ are respectively 5,73 and 5,01 nm.

Figure III-9 displays the excitation profiles of ZLOx alone and T6ZLOx dispersed in a blend of PFTPA:PEO (65:35 in w%). The compatibility between the T6 present on the surface of the zeolite crystals with polymer materials induces a far better dispersion of the host-guest inclusion compound in the prepared solution and consequently in the polymer film obtained. The emissions from the samples were integrated between 680 and 700 nm where only the emission from Ox+ is present. This demonstrates that a two step energy transfer from the conjugated polymer to the dye inside the zeolite L crystal is achieved.

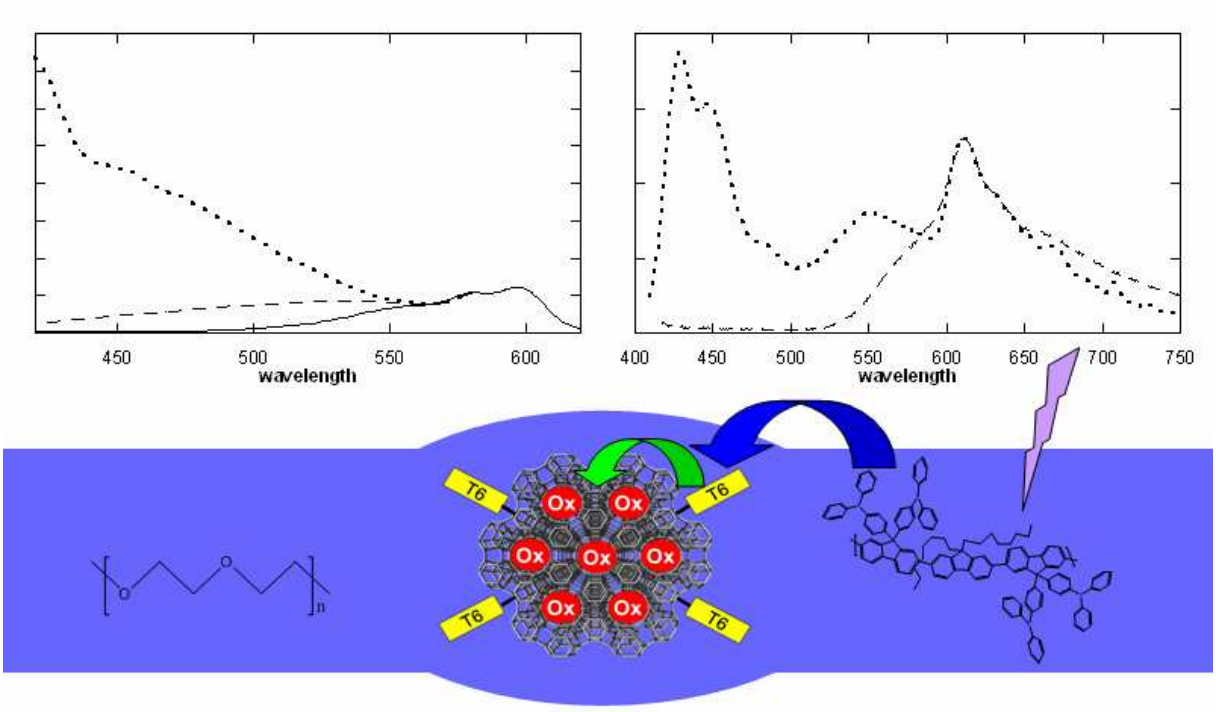

Figure III-9: top: excitation profiles (left) of ZLOx (solid) T6ZLOx (stripped) T6ZLOx dispersed in a PFTPA-PEO blend (dotted) integrated between 680 and 700 nm and emission (right) from T6ZLOx (stripped) and T6ZLOx dispersed in a PFTPA-PEO blend (dotted) excited at 350 nm; bottom: schematic representation of the two step energy transfer within the electroluminescent nanofiber

In **Figure III-9**, the photoluminescence of loaded zeolites in the PFTPA-PEO blend exhibits white light by combining the emission from PFTPA, T6 and Ox+. As shown in **Figure III-10,** the CIE (Comission Internationale de l'Eclairage) coordinates of the emission recorded with a single excitation at 350 nm are (0,33; 0,26).

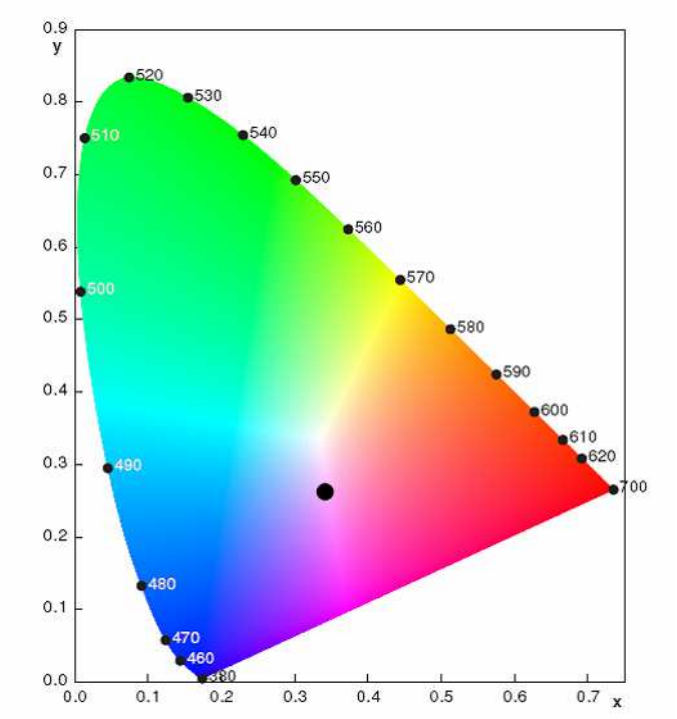

Figure III-10: CIE coordinates of the blend of electroluminescent polymer with dye loaded zeolites

The electrospinning step will now allow us to obtain nanofibers of an electroluminescent polymer blended with PEO (**Figure III-11**) embedding T6ZLOx crystals displaying the emissions from the three materials. The confocal images, obtained with a single excitation at 407 nm, exhibit emissions at the different wavelengths corresponding to the polymer, the grafted T6 and the Ox+ molecules. The nanofibers embedding zeolites display mainly blue emission from the polymer but locally exhibit white emission in the parts of the fiber containing zeolites.

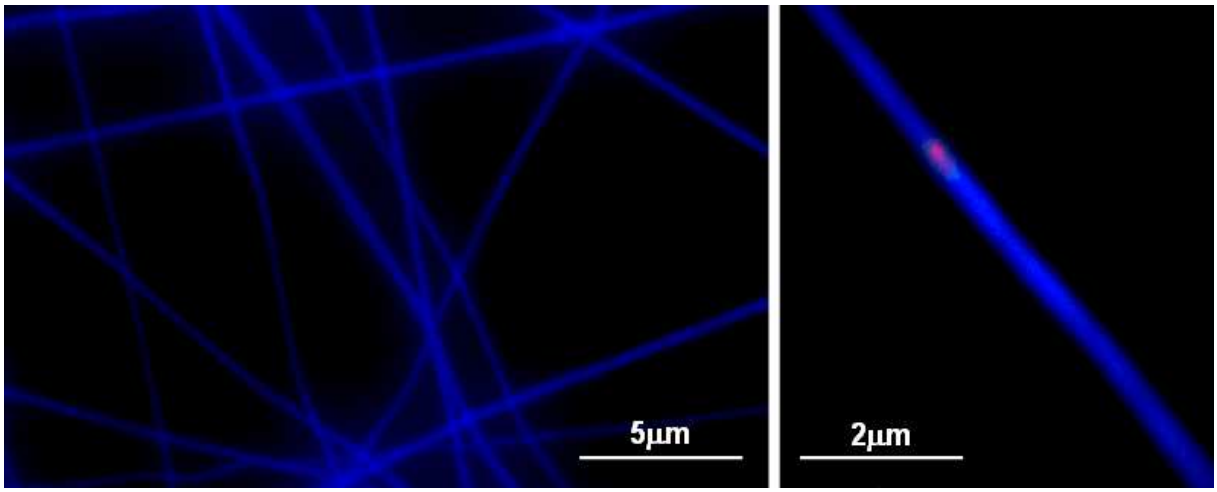

Figure III-11: fluorescence microscope image of fibers of PFTPA-PEO (left) and confocal microscope image of T6ZLOX in PFTPA-PEO nanofiber (right)

In **Chapter II** we have demonstrated that energy transfer from the molecules grafted on the external surface is much more efficient than using a stopcock molecule. The functionalisation also presents other advantages. The grafted molecules and the conjugated polymer are in direct contact which makes the first energy transfer very efficient. The compatibility of the conjugated polymer with the grafted conjugated oligomer leads to a better dispersion of the zeolite crystals in polymers allowing us to increase the zeolite concentration in the polymer. Adding the zeolites to the electroluminescent blend used for electrospinning led to the creation of nanofibers which exhibit a highly efficient two step energy transfer to the dye included in the zeolite channels. The conjugated polymer partly transfers its energy to the organic molecule on the surface of the crystals which consequently injects the energy to the final acceptor molecule inside the zeolite channels. Such fibers display emissions of the three fundamental colours: blue, green and red. Playing on the concentrations of the different molecules, one could realize electroluminescent white light emitting nanofibers which could be used to create a hybrid organic/inorganic nanofiber based light emitting device.

B. Zeolite L crystals in hexagonally arranged in conjugated polymer thin films

Studies of the very well arranged light harvesting systems in plants revealed that the concept of enhancement through hybrid organization can also be applied to opto electronics.[95] Many examples in literature are related to hybrid solar cells with increased efficiencies[96] or hybrid light emitting devices based on an organic matrix embedding inorganic nanoparticles for colour tunning.[97] By including cationic dyes through ion exchange in the zeolite L framework, the aggregation of the dye molecules is avoided which further leads to an increase of the emission quantum yield. As nature teaches us, a well organized system is what is needed to obtain good opto electronic devices (like the solar energy conversion during photosynthesis), therefore, in this chapter, the methods to obtain highly organised zeolite L crystals in polymeric materials will be discussed.[98,99] This is one of the key factors to obtain highly efficient hybrid functional thin films.

1. Breath figure formation combined with soft lithography: a cheap and easy way to obtain micro/nanopatterned polymeric thin films

In the past years, obtaining micro- or nano patterns with easy to use and cheap techniques has been the centre of interest in a broad range of fields going from biotechnological applications to microelectronics.[100-102] The well known techniques using photolithography work perfectly but the cost of it raises the whole process price. Consequently, a greater importance has been given to phenomena such as self-assembly and other self-organization processes.[103,104] The formation of breath figure arrays[105-107] on a polymeric thin film is one of those investigated techniques which can, once combined with soft lithography,[108] lead to a cheap and easy way to obtain micro patterns on different materials.

(1) Breath figure formation process

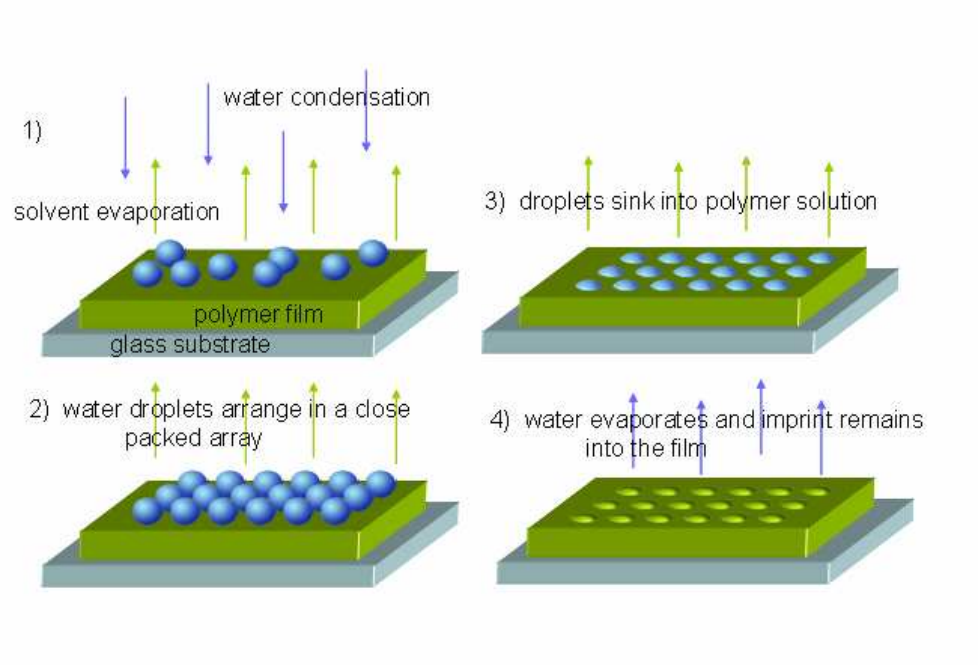

Figure III-12: schematic representation of the breath figure formation mechanism leading to the formation of honeycomb structures on thin polymer films

The term breath figure refers to the arrangement of water droplets formed by the condensation of water vapour on either a cold solid or liquid surface. Using the right polymer material and solvent, during solvent evaporation from solution, water vapour present in the atmosphere will condense and self-organize into a hexagonal arrangement of water droplets on the evaporating solution. Once both the solvent and the water droplets are evaporated, the latter leave the imprint of their honeycomb-like structure in the polymer film.

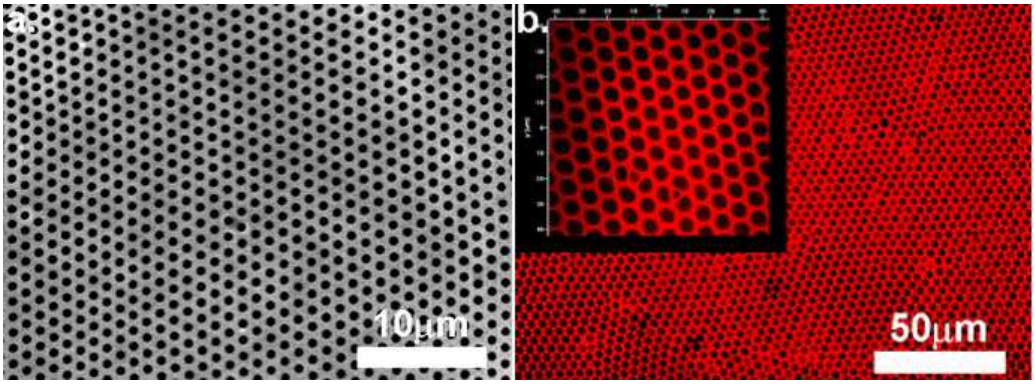

Figure III-13: a) Scanning Electron Microscopy (SEM) picture of a holey PS film and b) confocal and fluorescence microscopy images of a holey P3HT film

Such a technique allows us to easily obtain a hexagonal arrangement on some polymer films. Unfortunately, the formation of breath figures cannot be obtained with any polymer. The choice of the polymer is one of the key factors for the breath figure formation. In order to select the polymer which can be used, one has to keep in mind that the process involves condensation of water droplets on a polymeric film. Therefore, if the polymer is completely hydrophobic, the water droplets will tend to coalesce which will lead to a loss of the regular hexagonal structure. Polymers which are commonly used can be listed into two categories: amphiphilic polymers (e.g. polystyrene terminated with a hydrophilic head)[109] and substituted conjugated polymers (e.g. poly-3-hexylthiophene).

The choice of the polymer is not the only important parameter to obtain a regular hexagonal array. The moist air flow, the polymer concentration, the temperature and the solvent are among other parameters which influence the quality of the formed pattern. Playing on these parameters, one can tune the diameter of the cavities obtained on the polymeric thin film from 400 nm to a few microns. **Figure III-13** displays arrays obtained with different polymers inducing different sizes of the hexagonally arranged cavities.

(2) Soft lithography for more versatility

The breath figure technique can be useful for many applications but it still presents a few drawbacks when it comes to creating nanostructures for organic light emitting devices type structures. The BF formation is based on a casting technique which leads to thicknesses of more than an order of magnitude larger than what is used for the active layers of OLED. Other than that, regular structures can only be obtained with some particular polymers and therefore, there isn't much versatility towards the choice of the electroluminescent polymer one would use in an OLED. Using a simple technique such as soft lithography or more specifically in this case nanoimprinting, replicas of the hexagonal array formed by the BF

technique can be obtained on most of the polymeric materials. The combination of breath figure formation and soft lithography allows us to overcome the material selectivity.

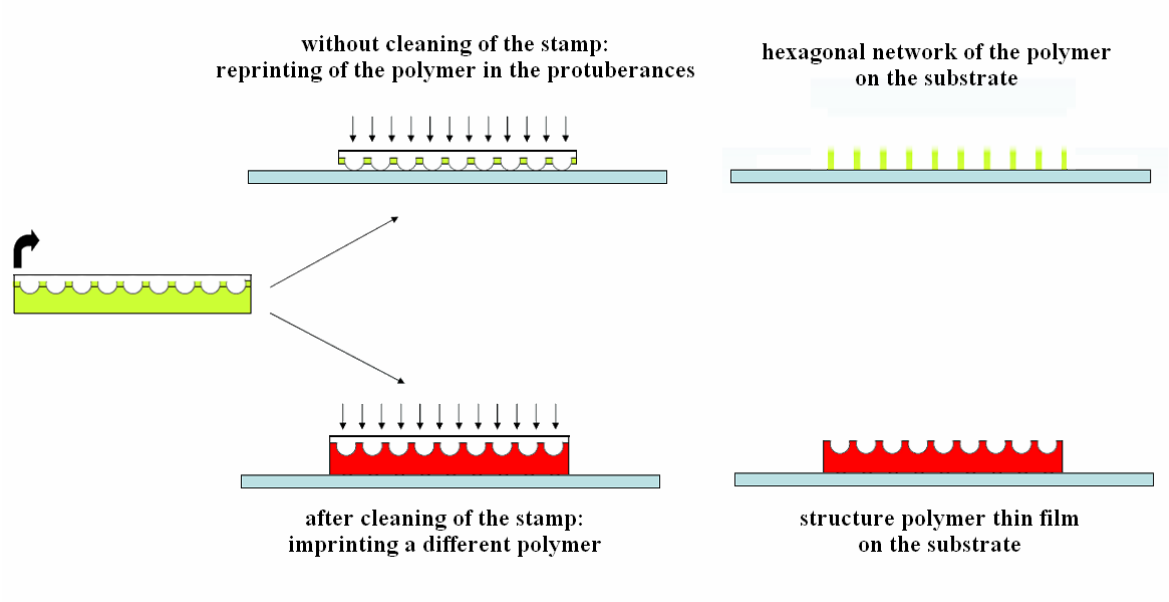

Figure III-14: combining breath figure formation and soft lithography

In order to do that, a PDMS mold or negative is made (using the breath figured thin film), which will then be used to imprint the desired polymeric materials. The problem of the thickness of the film can be overcome as the replica can be printed on a spin coated film (thickness of a few hundreds of nm). The choice of the material, which is one of the key factors to obtain breath figured films, becomes less important thanks to the soft lithography. Once the stamp is obtained, almost any polymer material can be nanopatterned by simply adjusting the experimental parameters (pressure on the BF replica, temperature and time of the process).

An alternative to nanoimprinting was also developed to obtain hexagonal networks of polymer on a substrate (**Figure III-14, III-15**). This second method consists in putting the desired polymer inside the free space between the protuberances of the PDMS negative which is consequently repressed against a substrate at a high enough temperature to melt the polymer. With this method, we are able to obtain an hexagonal network of polymer on a

substrate with a thickness going from 1 µm down to 100 nm. The thickness of that polymer network depends on the quantity of polymer added on the PDMS negative. The substrate can be of any nature as long as it resists to temperatures higher than the melting temperature of the polymer. This method opens new perspectives of novel architectures for OLED which we will see in **Chapter IV**.

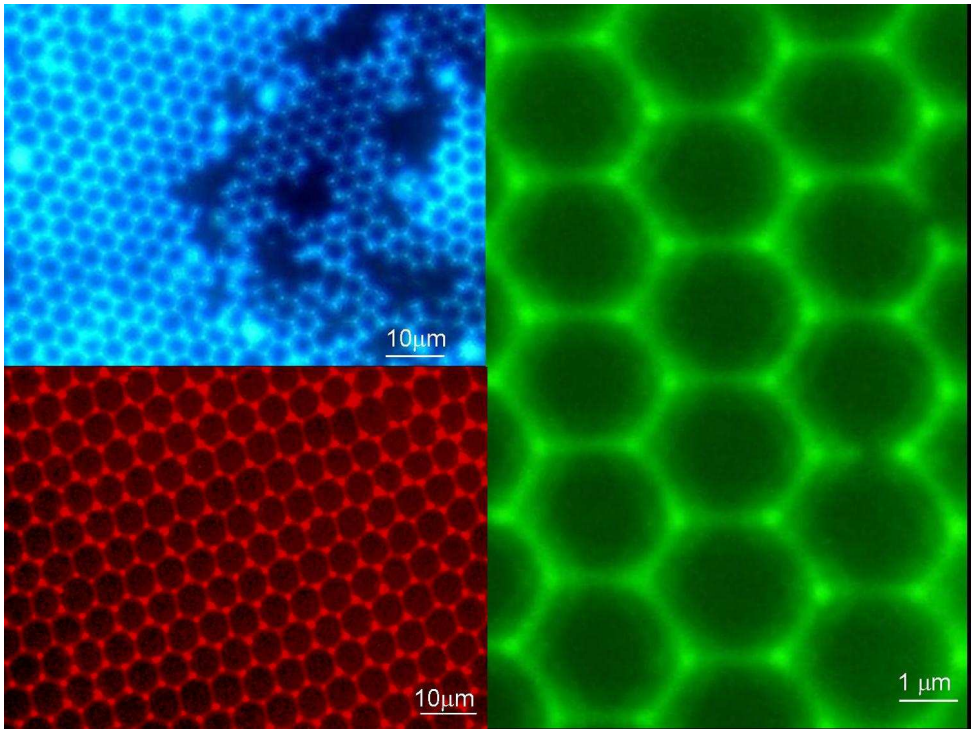

Figure III-15: PFO (top-left), P3HT (bottom-left) and F8BT (right) hexagonal networks printed on glass substrates

2. Hegaxonal arrangement of zeolite L crystals in conjugated polymer thin films

(1) Amphiphilic zeolite crystals for direct organization during the breath figure formation

Ox loaded zeolite L nanocrystals' external surface was chemically modified, as shown in **Figure III-16**, in order to give hydrophilic properties to the inclusion complex. The silanol groups on the external surface easily react with APTES to give rise to surface amine functionalized zeolite crystals (ZLOxNH2). The resulting amine groups present on the external surface of the inorganic host are hydrophilic. ZLOxNH2 can be further

modified using a fumaric acid. One of the acidic functions reacts with the amino groups of ZLOxNH2 to form an amide while the second gives rise to carboxylic acid groups present on the outer surface of the zeolites connected to the crystals through a bridge containing a C=C double bond. This second type of modified crystals are designated as ZLOxCOOH and present hydrophilic properties as well as hydrophobic ones.

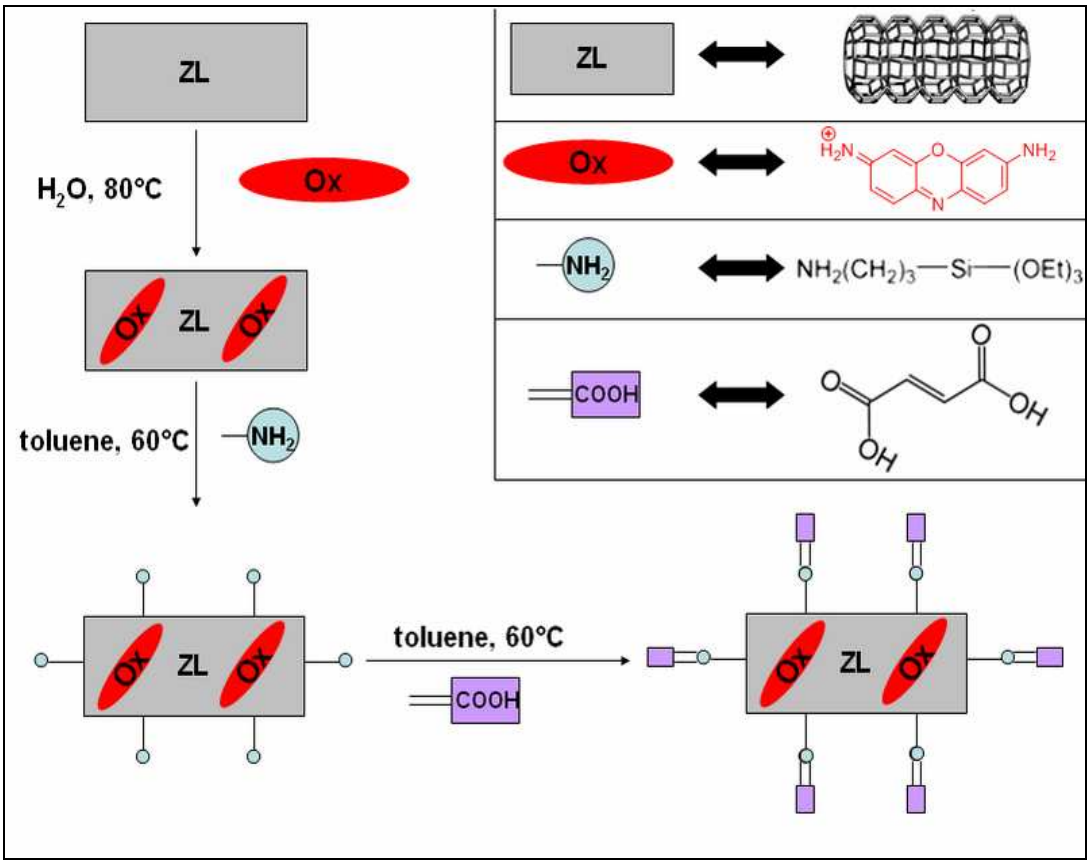

Figure III-16: schematic representation of the different functionalized zeolite L crystals and molecules

The formation of BF arrays on a polymeric thin film depends on many parameters. One of the major parameters is the nature of the molecules present in the cast solution. Ambipolar polymers are the best candidates for the process as they easily form films and stabilize the amphiphilic interface between the hydrophobic film and the water droplets. Some conjugated polymers, such as PF8BT, when dropcast from a low concentration solution in CS_2 under moist airflow induce formation of BF. Such films can also be obtained using an amphiphilic polystyrene (aPS). The dimensions of the pores resulting

from the presence of the water droplets vary between 400 nm and 5 microns depending on the nature of the polymer used: the better the polymer can stabilize the water droplets, the smaller the pore diameter. Other parameters such as the moist air flow and the concentration of the solution have also to be taken in account to be able to obtain nice and regular arrays.

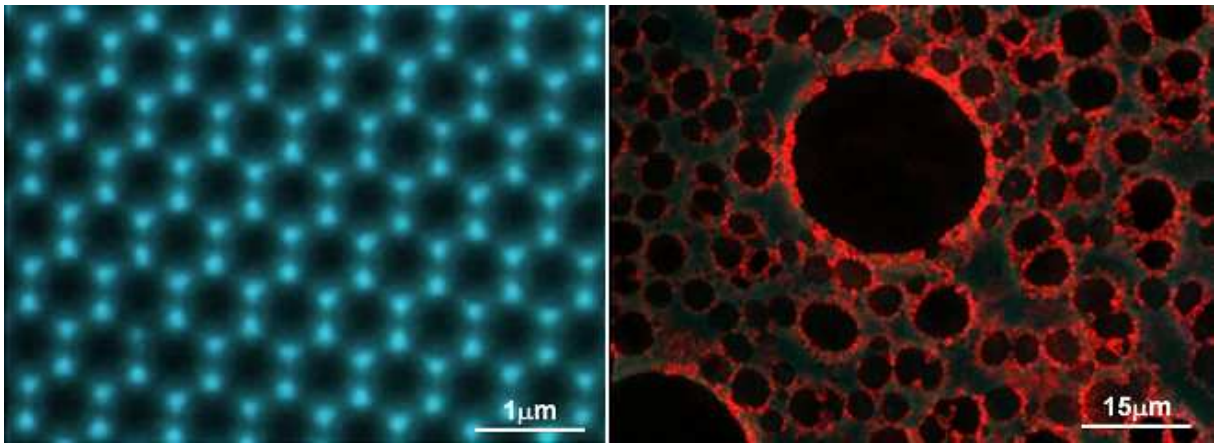

Figure III-17: confocal images of aPS (left) and ZLOxNH2 in aPS (right) films formed under moist air flow

Amino functionalized zeolites are added to the polymer solutions. The hydrophilic zeolites are expected to diffuse close to the water droplets during the film formation and stay at the polymer air interface in the cavities as the water droplet evaporates. **Figure III-17** presents the thin film obtained from ZLOxNH2 dispersed in an aPS solution to which a blue pigment (fluorescamine) was added (2 w% with respect to the weight of the polymer) to give a blue-green emission from the polymeric film. The confocal image clearly shows that the ZLOxNH2 crystals are present only where the water droplet was before its complete evaporation. The other information we get from these images is that the presence of ZLOxNH2 actually disturbs the formation of BF. aPS forms regular pores of a mean diameter of 600 nm when used without those zeolites. As the modified zeolite crystals recover completely the polymer-water interface during the BF formation, it becomes harder for the polymer to stabilize the water droplet. Therefore, irregular arrays

are obtained which display larger pore diameters. ZLOxNH2 is not amphiphilic, therefore, it is not able to stabilize the water droplet. In order to overcome this issue, a new system was introduced.

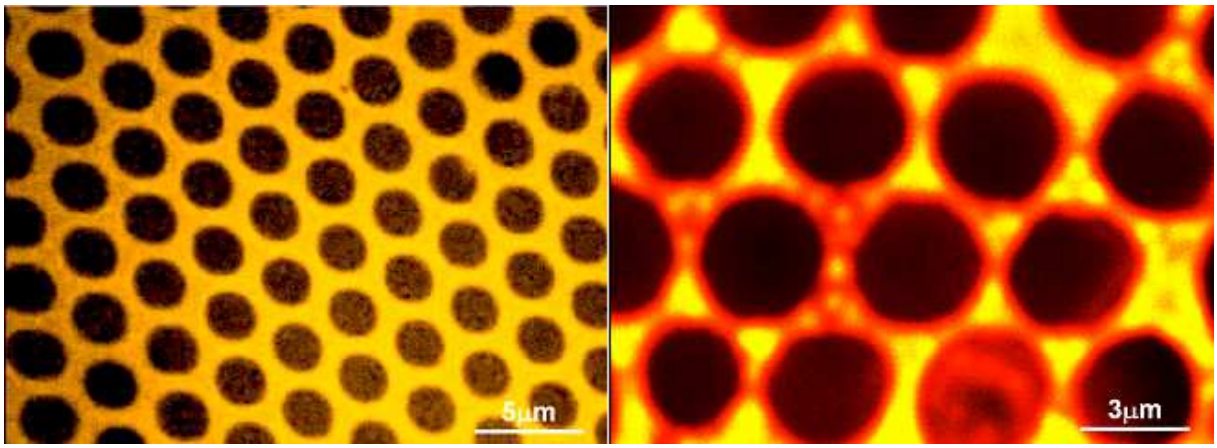

Figure III-18: : confocal images of BF formation on PF8BT (left) and self assembled ZLOxCOOH at the polymer-air interface in the cavities of a BF PF8BT (right)

ZLOxCOOH, unlike ZLOxNH2, has amphiphilic properties. The presence of the C=C double bond and the functional groups in the diacid molecule grafted on the crystals induce compatibility of ZLOxCOOH with both conjugated polymers and water. The modified zeolite crystals therefore tend to further stabilize the polymer-water interface as they can stabilize the water droplets directly. **Figure III-18** shows a confocal image of BF arrays obtained from a solution of PF8BT containing ZLOxCOOH. The image clearly shows two different emissions from the borders of the cavities and from the rest of the film. The array obtained in this case is regular with dimensions of the cavities in the same range as the ones formed with conjugated polymers when no zeolites are present. The amphiphilic loaded crystals move towards the water droplet to stabilize it but can be mixed with the polymer which also stabilizes the droplet. Unlike the previous case, here the zeolites and the polymer are not incompatible and therefore, during the film formation, the zeolites are entrapped in the polymer close to the water-polymer interface. Using such a system, three levels of organisation are obtained: a regular hexagonal array of

microcavities in a polymeric film; a selective positioning of the inclusion compounds in the polymeric micropatterned film; and a molecular arrangement of the dye molecules within the hexagonal channels provided by the inorganic host.

(2) Breath figured polymeric thin films as a template for zeolite L organization

A similar arrangement can be obtained through a different approach. This second method also aims to suppress the chemical reaction steps and to give more versatility towards the polymeric materials which can be used. The idea of using soft lithography to reproduce the BF array on polymers which do not form BF arrays with the conventional process was introduced in previously. This method consists in creating a negative PDMS film of the BF array. The PDMS film is consequently used as a stamp for creating replica BF on a different polymer thin layer. The cavities present in such polymeric films or films obtained by direct BF formation are consequently filled with ZLOx by simply casting a dispersion of crystals in water on top of the film. After water evaporation, the zeolites cover the whole polymeric surface and fill the cavities. In order to obtain zeolite crystals organized in a honeycomb arrangement, the excess of ZLOx present on the surface is removed by pressing a flat PDMS block on top of the hybrid film. The zeolite crystals which are not in the cavities are therefore transferred on the inorganic elastomere. The only zeolites which remain in the film are the ones in the hexagonally arranged cavities. Depending on the size of the zeolites used, the cavities will contain one or more zeolite crystals. This second method therefore gives more versatility towards the polymer material used as well as the quantity of zeolite crystals present in one cavity. Although dye loaded zeolites' optical properties are not affected by the aggregation in solid state, the good dispersion of the crystals is one of the major issues to obtain good functional thin

films which could be used for applications such as zeolite based organic light emitting devices.

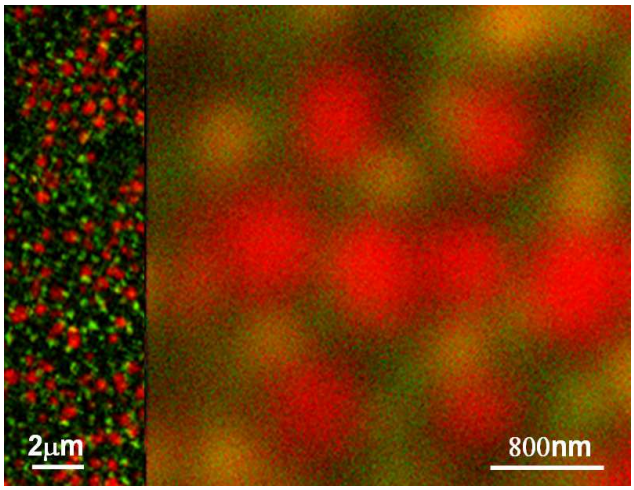

Figure III-19: confocal images of ZLOx in F8BT embossed using PDMS replicas of BF on aPS

.

Figure III-19 displays a confocal image of a thin film of F8BT loaded with ZLOx of a mean diameter of 600 nm and a mean length of 800 nm. Unlike the nanocrystals (25nm x 25nm) used for the method based on hydrophilic interactions, only one crystal will be present in the cavities due to spatial and geometrical restrictions. The confocal images show a bicolour fluorescent film. The green emission corresponds to the photoluminescence of F8BT, whereas the red emission comes from the Ox molecules present in the zeolite crystals. The crystals are trapped in the cavities within the film which leads to this bicolour microstructured emission.

C. Self assembly of zeolite L crystals and conjugated polymer

1. Polyphenylene vinylene precursors: a polycationic precursor presenting many advantages

One of the major issues when it comes to electroluminescent polymers is their poor solubility in organic solvents. Different approaches have been studied in order to overcome that problem leading to easy to process materials. The most common way to make the conjugated polymers more soluble is to use long alkyl chains or polar groups as substituents or building block of the unsoluble rigid backbone.[110-112] Here, we will discuss an alternative approach to obtain conjugated polymer films or structures from very easy to process materials. This approach consists in processing some non conjugated polymers which can then be converted into conjugated ones. This family of polymers is called conjugated polymer precursors.

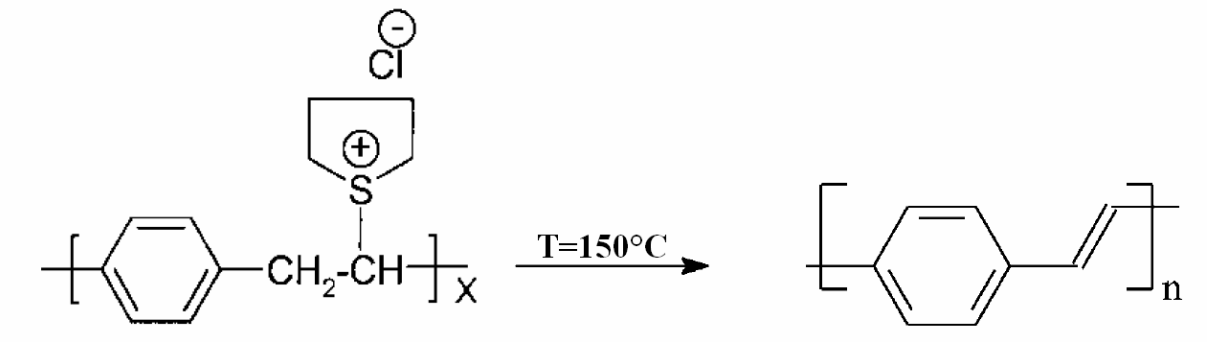

Figure III-20: thermal conversion of the PPV precursor into unsubstituted unsoluble PPV

The precursor we will mainly be discussing about is a cationic polymer (as shown in **Figure III-20**) which is converted into unsubstituted PPV after a thermal annealing at 150°C in an inert atmosphere. The unsubstituted polymer then becomes insoluble which opens the way to the preparation of some original architectures of polymer and composite thin films. Another advantage of this precursor is that it presents polycationic properties before it is converted and therefore also has a great potential to create original self assembled structures. We saw at the beginning of **Chapter III** that such precursors also have quite good visco

elastic properties and therefore are not only soluble in solvent such as water or methanol but can also easily be electrospun. In the following parts, we will see that not only are they a good candidate for electrospinning, but they can also be very interesting to obtain hybrid self assembled structures or innovative bilayers of conjugated polymers.[113]

2. Polyelectrolytic assembly of functionalized zeolite L crystals and polyphenylene vinylene precursors

(1) Principle of polyelectrolyte assemblies

Polyelectrolytes are polymers whose repeating units bear an electrolyte group.[114-118] As they are polymers, their viscoelastic properties are good and when in solution, they usually display a high viscosity which is one of the keys to making nice multilayer films in an efficient and low cost way. Many biological molecules such as polypeptides and DNA are polyelectrolytes.

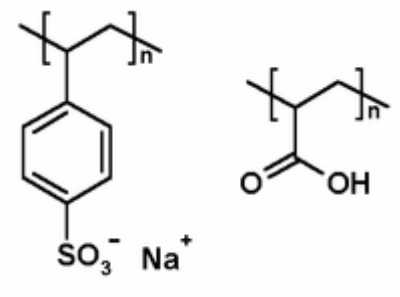

Figure III-21: chemical formula of two polyanions: (left) poly(sodium styrene sulfonate) (PSS) and (right) polyacrylic acid (PAA)

Figure III-21 displays two molecules which are considered as polyanions: poly(sodium styrene sulfonate) (PSS) and polyacrylic acid (PAA). Although both of these molecules are polyanions, PSS is considered a “strong” polyelectrolyte as it is fully charged in solution whereas PAA is said to be a “weak” polyelectrolyte (partially charged). When solutions of oppositely charged polyelectrolytes are mixed together, it usually leads to the formation of bulk complex as the opposite charges attract each others and therefore irreversibely bind the two polymers together. Therefore, polyelectrolytes can assemble in many different ways

using these peculiar properties. Among the different assemblies of polyelectrolytes which can be obtained, two have drawn a particular interest in the past decade: the layer by layer assembly (LbL) and the nanoparticle coating. During LbL deposition, a suitable growth substrate (usually charged) is dipped back and forth between dilute baths of positively and negatively charged polyelectrolyte solutions. (**Figure III-22**)

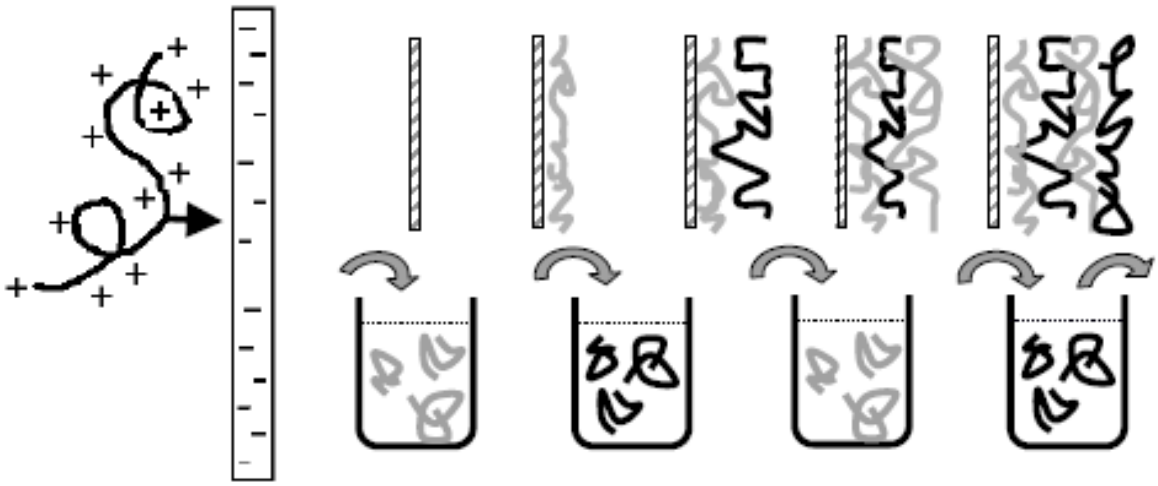

Figure III-22: schematic representation of the layer by layer polyelectrolyte assembly

During each dip a small amount of polyelectrolyte is adsorbed and the surface charge is reversed, allowing the gradual and controlled build-up of electrostatically cross-linked films of polycation-polyanion layers. When a substrate with a negative surface charge is immersed into a solution with positively charged polyelectrolyte chains, the electrostatic attraction leads to an irreversible binding of the chain to the surface, while the counterions remain in the electric double layer. Thus, a monomolecular layer with a thickness on the order of one nanometer is formed.[119] Under suitable conditions, the net surface charge is positive, such that as a next step, a negatively charged polyion can be adsorbed by immersion into a solution of polyanions. This technique is an alternative to Langmuir-Blodgett deposition. These two techniques are in a certain way complimentary as they are both restrictive on the nature of the material which can be deposited. The polyelectrolyte LbL deposition allows to prepare really

thin films (on the nanometric scale if only one layer is deposited) or can lead to sandwich structures of alternative polyelectrolyte or hybrid layers with novel and interesting properties in many different fields. The process can go on forever, therefore, the film thickness can be controlled by the number of alternative layers which are deposited.

The principle of LbL deposition of polyelectrolytes can also be applied to nanoparticle coating. If a nanoparticle displays a charged external surface, when mixed with an opposite charge polyelectrolyte, the two species will assemble. After recovering the covered nanoparticles, one or more additional layers of alternated polyelectrolytes can be added (**Figure III-23**).

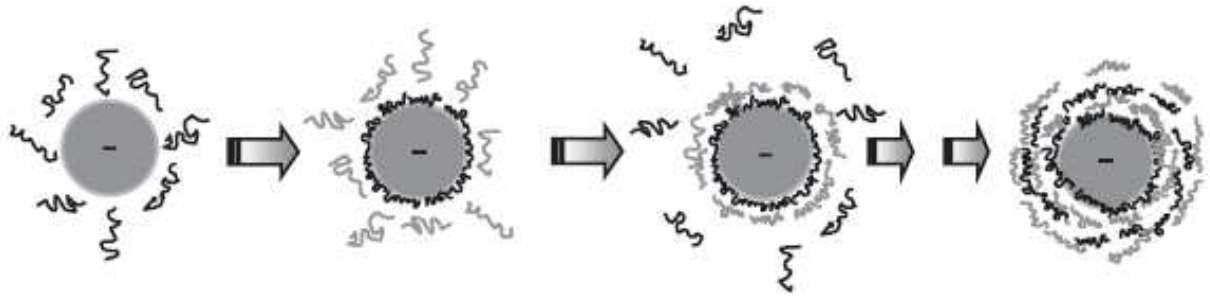

Figure III-23: schematic representation of polyelectrolyte layer by layer assembly on nanoparticles

Thin films and nanoparticles prepared using the polyelectrolytic approach can lead to very interesting materials in different fields ranging from biomedical applications to water treatment, sensor materials and functional coatings. In the following part, we will see how polyelectrolytes can lead to novel self assembled structures involving dye loaded zeolite L crystals.

(2) Surface modified polyanionic zeolite L crystals

In order to be able to use the polyelectrolytic approach to assemble zeolite L crystals with a polymer, it is first necessary to modify the external surface of the inorganic crystals. As polyelectrolyte assembly is based on charge compensation, the functionalisation of the surface should lead to a polyanionic zeolite L as in our case, the polyelectolyte is a cationic precursor of PPV. The zeolite L crystals are first loaded with a cationic dye (oxonine) to easily probe the position of the crystals. Once the oxonine loading procedure is done and crystals are recovered, external surface modification of the zeolite L can take place. The silanol groups present on the external surface of the crystals react with the Aminopropyltryethoxy Silane (APTES) through formation of Si-O-Si bridges. The resulting zeolite L crystals have amine groups on their external surface. These amine groups are then further modified with fumaric acid to present carboxylic acid groups on the zeolite surface following the reaction pathway presented in a previous section **(Figure III-16)**.

The carboxylic acid groups are then put in presence of NaOH and transformed into anions. After all these modifications, the dye loaded zeolite L crystals present the same assembly properties as a “strong” polyanion which can be easily coupled with the PPV precursors.

(3) Morphological and spectroscopical study of the assembly of modified zeolite L crystals and polyphenylene vinylene

Two different types of zeolites are used for the formation of such assemblies: the first set (ZL1) corresponds to crystals of a mean diameter and a mean length of both 40 nm whereas the second set (ZL2) has a mean diameter of 600 nm and a mean length of 5 microns. The zeolites were first loaded with an organic molecule: the oxonine. The first step to obtain

zeolites encapsuled in PPV is to modify the zeolite surface as described in the previous section to obtain polyanionic zeolites.

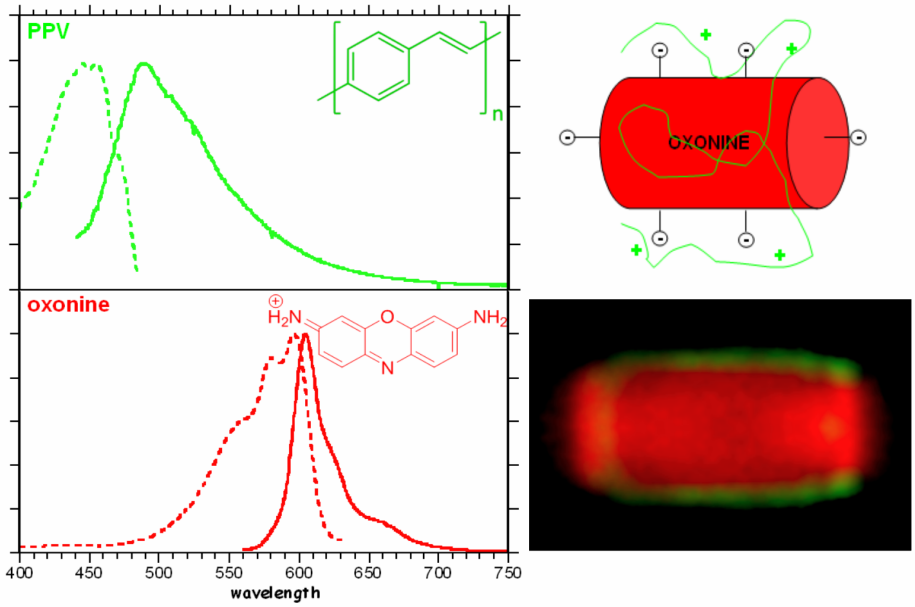

Figure III-24: excitation profiles (dotted), photoluminescence spectra (solid) of PPV and oxonine (left), confocal image of a oxonine loaded ZL2 crystal having PPV adsorbed on its coat after thermal treatment at 150°C and schematic representation of the covered zeolite (right)

PPV precursors are polycations that can be converted into PPV through a thermal conversion in an inert atmosphere. The precursors can be used for electrolytic self assembly with the zeolite L crystals. To visualize the morphologies obtained, a careful confocal microscopy study was conducted on modified oxonine loaded zeolite crystals which have a mean diameter of 600 nm and a mean length of 5 microns. The base and the coat of the zeolite crystals have different reactivities due to the presence of the channel entrances. Although the functionalization of the zeolite also occurs on the bases of the crystal, at the channel entrances, the presence of cationic species (counter ions or exchanged oxonine molecules) screen the anionic properties of the carboxylate groups leading to a preferential adsorption of the PPV precursors on the coat of the zeolite (**Figure III-24**). Adding PPV precursors to the zeolite suspension leads to the formation of cylindrical core shell structures which are

consequently thermally annealed leading to the conversion of the PPV which becomes insoluble and rigid.

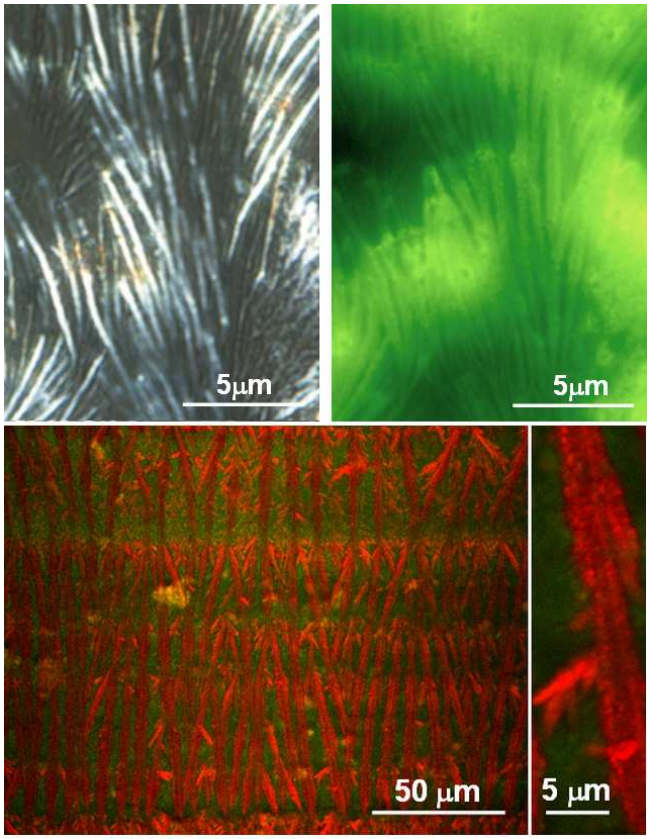

Figure III-25 : (top) Optical (left) and fluorescence (right, excitation wavelength: 488 nm) microscope images of PPV-oxonine loaded nanozeolite 200 nm large nanofibers obtained by adding 300 μL of PPV precursor solution to 25 mg of zeolites suspended in water; (bottom) confocal microscope images of PPV-oxonine loaded nanocrystals assemblies obtained by adding 900 μL of PPV solution to a suspension of 25mg of zeolites in water (simultaneous excitation wavelengths: 405, 488 and 543 nm).

Adding PPV precursors to a suspension of zeolite L nanocrystals (40 nm x 40 nm) in water and casting the solution on a glass substrate can lead to different morphologies. The PPV precursors can be consequently thermally converted into PPV to make those structures unsoluble in most solvents (polar and organic). As we previously saw in **Figure III-24**, adding a small amout of PPV precursors allows us to fabricate core shell polymer zeolite structures where the polymer envelops a single zeolite crystal. A higher PPV precursor concentration can give rise to the formation of self assembled nanofibers by simply dropcasting the polymer-zeolite solution on a clean glass substrate. Playing on the relative

concentrations of PPV and zeolites, we can obtain nanofibers of less than 200 nm of diameter and which grow up to lengths of more than 20μm (**Figure III-25**).

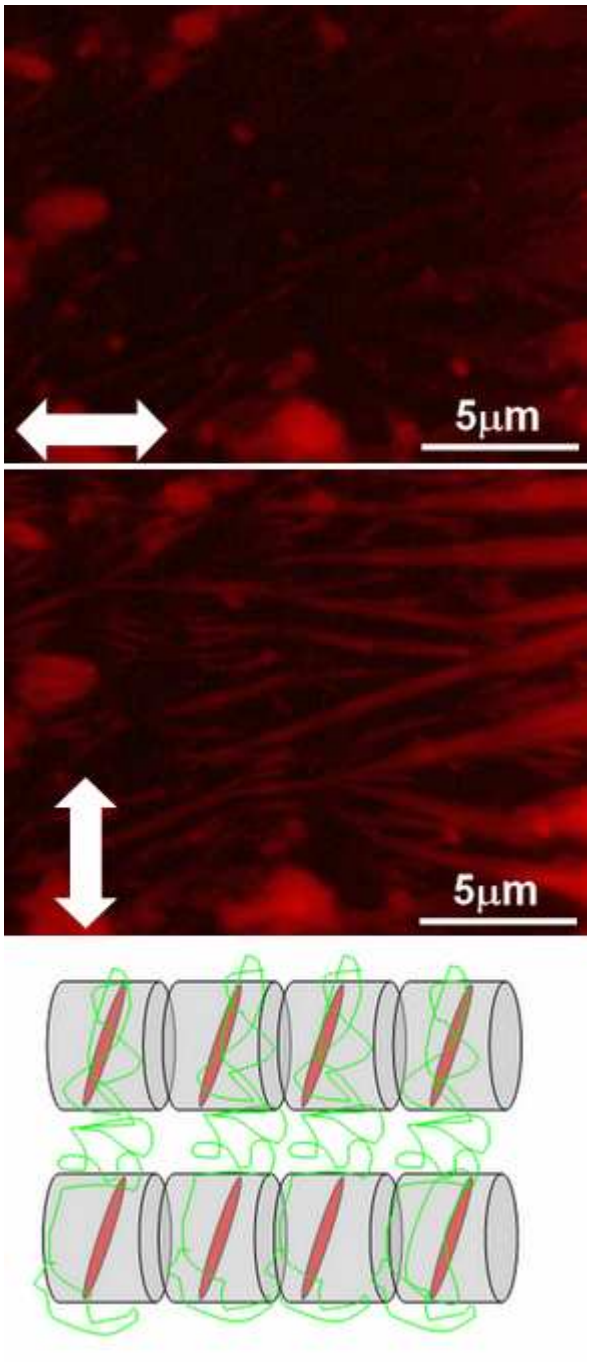

Figure III-26 : Fluorescence microscopy images of horizontally (top) and vertically (middle) polarized emission of almost horizontal hybrid fibers and (bottom) schematic representation of the self assembled structure.

In **Figure II-26**, the polarized fluorescence images obtained from larger fibers allow us to understand better the arrangement of the zeolites inside the fibers. The zeolite nanocrystals

are loaded with a dye molecule which stays almost perpendicular (72°) to the zeolite channel axis and through this fluorescent microscopy study, it can be concluded that the emission from the dye is also polarized at an angle of around 72° with respect to the fiber axis. The zeolites are therefore oriented along the fiber as schematized on **Figure II-26**.

The nanofibers displayed in **Figure II-25 and 26** result from the combination of different phenomena. In previous works, it has been demonstrated that drop casting a colloidal solution of carbon nanotubes from a non volatile non solvent leads to such an arrangement with high aspect ratio nanotubes. The mechanism of such carbon nanotubes nanofiber formation is linked to the microfluidic forces created during solvent evaporation. Several groups have studied and modelled the drying of drops of colloidal dispersions. Although it has been shown that such phenomena can occur with spherical silicalite-1, we could not obtain such arrangement by simply drop casting zeolite L nanocrystals (with or without surface modification) on their own from water solution. We therefore believe that the mechanism leading to the nanofiber formation is related to the rod-coil nature of the PPV precursors dressed zeolite crystals. In literature, many examples of rod-coil block polymers which self assemble can be found. The polymer–zeolite core shell structure can be considered as a similar case in which the central inorganic crystal acts as the rod and the unconverted polymer surrounding the crystal would be the coil. Increasing the amount of PPV precursors, fibers become larger but also more ordered (**Figure II-26**). Self assembly phenomena involving rod-coil block copolymers depend on the relative lengths of the different blocks. The case of our core shell structures is somehow similar: a larger amount of PPV precursors induces a higher quantity of adsorbed polymer on the zeolite surface which will consequently increase the self assembly properties of the core shell structure. Once the structure is obtained, thermal annealing of the conjugated polymer precursors into unsubstituted PPV will lead to unsoluble nanofibers encapsulating highly ordered dye loaded zeolite crystals.

Functionalization of the loaded zeolite crystals with an anion was obtained. The resulting zeolites are used as polyanions to self assemble with PPV precursors having cations along the polymer chain. Playing on the relative concentration of PPV precursors and zeolites, different self assembly morphologies are obtained. A higher precursor concentration allows us to obtain self assembled core shell nanofibers formed by stacked zeolite L nanocrystals surrounded by the polymer. The highly ordered zeolite L crystals display polarized emission almost perpendicular to the fiber axis. The zeolites' axis is therefore parallel to the axis of the fiber. After thermal threatment, the polymeric shell of the fiber is converted into an unsoluble conjugated polymer. Since the dye inside the zeolite crystals can be addressed through energy transfer from the electroluminescent polymer, such hybrid self assembled nanofibers open new perspectives in the fabrication of nano devices.

IV. Third level of organization: innovative Organic Light Emitting Device

A. Organic Light Emitting Device (OLED)

1. What is an OLED?

If you ever thought about having a display built up in your clothes, a newspaper where images are dynamic, a TV that you could fold and put in your pocket or a high definition screen which would be thinner than your finger, it's not science fiction anymore. The OLED technology is advancing everyday and we should soon be able to build such devices thanks to it. But what is an OLED? OLEDs are solid-state devices composed of thin films of organic molecules that create light with the application of electricity.[120-128] They can be used in many different fields going from energy saving lighting to high definition displays.[129,130] OLEDs can have either two layers or three layers of organic material; the third layer helps transport electrons from the cathode to the emissive layer. The OLEDs built during our studies were two organic layer OLEDs as the one described in **Figure IV-1.**

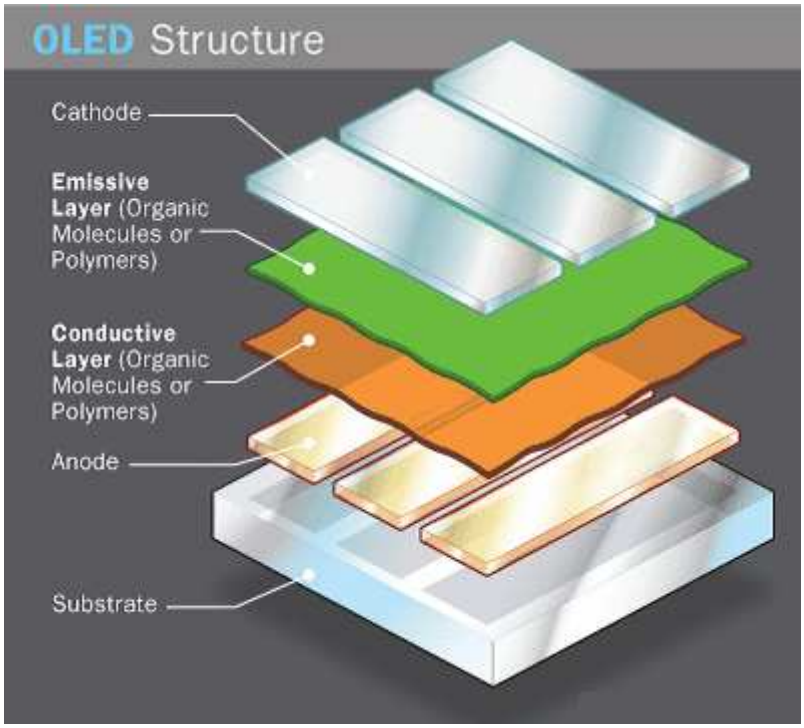

Figure IV-1: schematic representation of a single emissive layer OLED

The OLED structure schematically represented corresponds to a stack of the following layers: First comes the substrate which supports the OLED. Depending on the application, it can be a transparent polymer foil or like in our case, glass. The substrate is covered with the anode. The anode has to be transparent (so that light emitted by the device can go through it and through the substrate) and its function is to remove electrons (also called add holes) when a current flows through the device. The first organic layer is called the hole transporting layer. It is usually made of hole transporting (electon blocking) layers of polymers such as PEDOT:PSS or polyaniline. On top of this hole injecting layer, the active layer is deposited. This second organic layer can be deposited in different ways depending on the material and the applications: these include (but are not limited to) spin coating from a solution, vacuum thermal evaporation, organic vapour phase deposition and inkjet printing. This last method have drawn a particular attention as it could be the key step to the fabrication of very efficient flexible OLED or displays.[131-133] This is the layer which we will focus on in the coming chapter: this layer is based on conjugated polymer and is the layer where holes and electrons will recombine in order to create light. Finally, the top electrode (the cathode) is not necessarily transparent and is used to inject electrons when a current flows through the device.

2. How does the OLED work?

Figure IV-2 displays the mechanism to obtain light through electroluminescence of the active layer in an OLED. A voltage is applied across the OLED which leads to a current from the cathode to the anode through the organic layer. The cathode injects electrons to the active layer (emissive layer) of the device while the anode injects holes into the conductive layer (PEDOT:PSS). When an electron finds a hole in the active layer, the electron fills the hole which means that it falls into an energy level of the atom that's missing an electron.

When this happens, the electron gives up energy in the form of a photon of light and the OLED emits light.

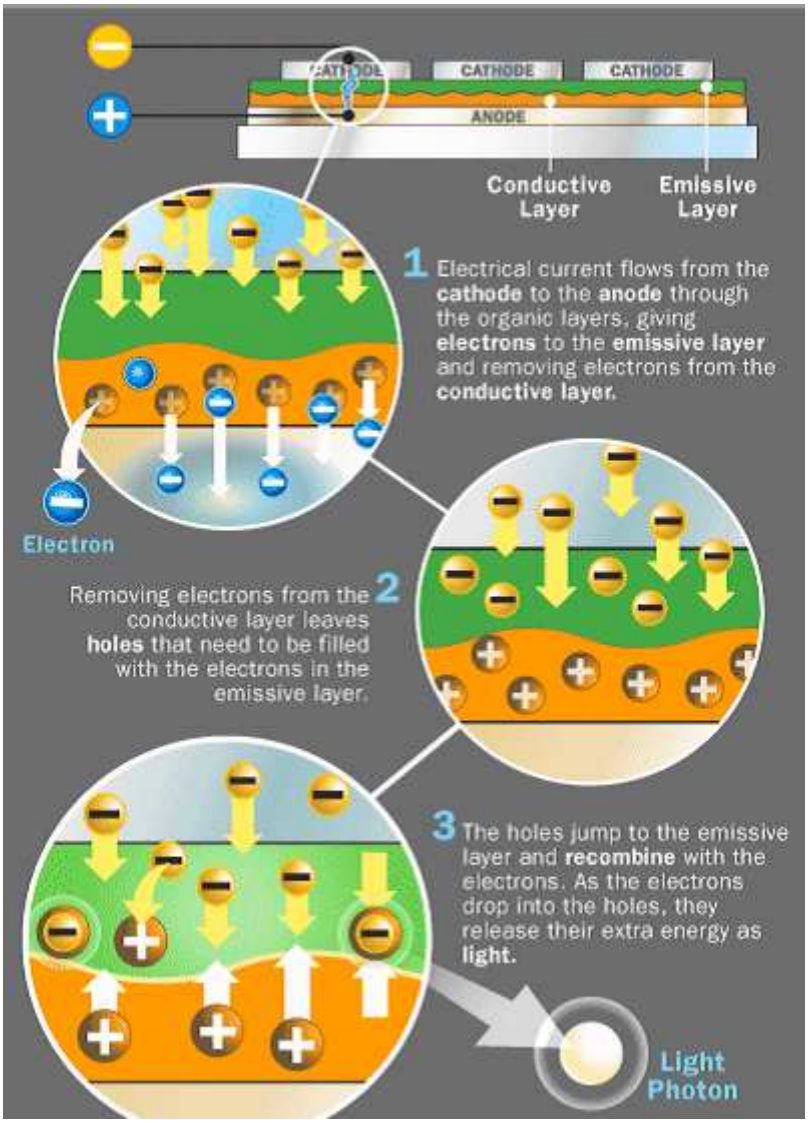

Figure IV-2: working principle of an OLED

In literature, we can find many works concerning the optimisation of the materials used for the electrodes[134] and the architectures of the OLED[135] in order to obtain high efficiencies which will not be the focus of our work.

3. Preparation and characterization of the devices

In the previous section, we had an overview of what the OLED architecture should be. The OLED which will be described in the following sections were prepared as follows:

To obtain a functional OLED, one has to keep in mind that the design should provide a way to contact both the anode and the cathode separately without having any short circuits.

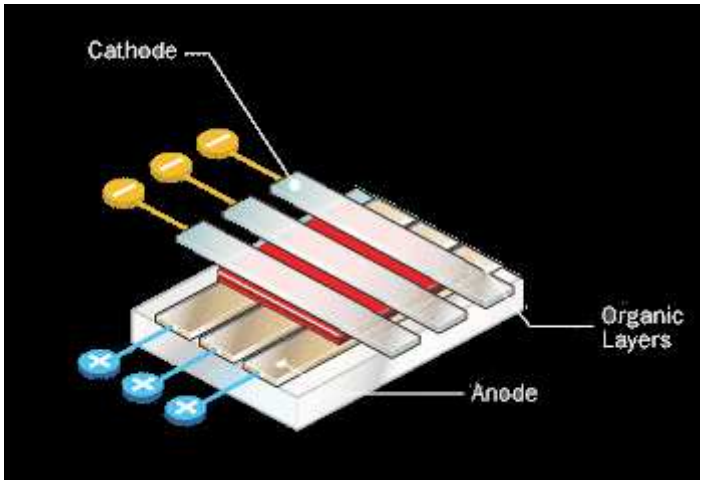

Figure IV-3: typical architecture of the studied OLED

The preparation of the device therefore starts with the preparation of the substrate. The substrate has to be partly covered with ITO. In order to do that, the first step is to obtain ITO covered glass substrates which will then be selectively etched in aqua regia (a volumetric ratio of 1:3 mixture of nitric and concentrated hydrochloric acid). Once the etching is over, and after a careful cleaning of the surface in different solvents, the sample will be placed for UV-ozone surface treatment to create an oxidized layer. This step will increase the properties of the interface between ITO and PEDOT:PSS which is spin coated on top of it. The PEDOT:PSS is deposited from a water solution and then annealed at 100°C for ten minutes to eliminate the dishomogeneities of the film. Active layers were prepared by spin-coating blend toluene solutions with a concentration of approximately 15mg/ml. The total concentration of

the solutions and deposition parameters are unchanged to give comparable thickness films. Calcium/Aluminium (Ca/Al) cathodes were then selectively growth using protective masks on the active layer (perpendicular to the ITO electrodes as shown on **Figure IV-3**) in 10^{-6}mbar vacuum. The dimensions of the deposited metal layers were also kept unchanged in order to have reproductible results and were respectively of 30 and 70 nm for calcium and aluminium. The perpendicular bottom and top electrodes allow one to easily contact both electrodes with reduced chances to have short circuits.

There are two different ways of characterising the devices: one consists in measuring its electroluminescent spectra to obtain information about the active layers' colours and the second one corresponds to the calculus of the efficiency of the device. This second characterization is done through current-photocurrent-voltage (I-PhI-V) measurements. In order to calculate the external quantum efficiency of the device it is necessary to have the photocurrent (intensity of light emitted by the device) as well as the current flow through the device for an applied voltage.[136]

As OLED external emission profile is supposed to be Lambertian ($I(\vartheta) = I_0 \cos\vartheta$), the radiant flux Φ_{EXT} leaving the device can be calculated using the following procedure:

$$\Phi_{EXT} = \int_0^{\pi/2} 2\pi L_0 \cos\vartheta \sin\vartheta d\vartheta = \pi I_0$$

where I_0 is the radiant intensity of light leaving the device in the forward direction. The solid angle from detector to light source is:

$$\Omega = A_{DET} / r^2$$

where A_{DET} is the area of the detector and r is the distance between the OLED and the detector.

$I_0 = P_{DET}/\Omega$ and therefore, the number of photons N_p collected by the detector can be calculated as:

$$N_p = \frac{\pi r^2 P_{DET} \lambda}{A_{DET} hc}$$

where e is the charge of an electron, P_{DET} is the power that the detector measures, λ is the emission wavelength, h is Planck's constant, c is the speed of light in vacuum.

The number of electrons N_e can be calculated from the input current I:

$$N_e = I_{OLED}/e$$

and external quantum efficiency forward direction η_{ext} is the ratio N_p/N_e:

$$\eta_{EXT} = \frac{\pi r^2 e P_{DET} \lambda}{A_{DET} hc I_{OLED}}$$

Even though the external quantum efficiency is very important as it allows us to compare the quantity and the intensity of light emitted by the devices, we will focus more on the other type of characterisation which corresponds to the electroluminescent spectra of the device. In the coming parts, we will try to detect different elements included in the active layers of the OLED and this can be easily done by simply looking at the emission spectra. The electroluminescent spectra are obtained using the same detector as the photoluminescent spectra.

4. Original active layers for the OLED

As was discussed previously, our concern is to create new architectures and designs of the active layers in order to obtain original functional devices. In the previous section (presentation of OLEDs), the description of the active layer always consisted of a simple monolayer of an electroluminescent polymer. With this first approach, very efficient and

bright monochromic OLEDs can be obtained. Thanks to organic chemistry, it has been demonstrated that with a copolymer containing donor and acceptor moieties bound together, one can also obtain dichromic OLEDs or even white emitting OLED (WOLED) based on just one electroluminescent polymer.[137] Although these results are very interesting, it takes a very big amount of time and chemistry to synthesize such polymers. An alternative approach is to use more than one material for the active layer and combine those different materials using energy transfer processes.[138,139] In the previous chapters, we discussed about the energy transfer process which occurs when two fluorescent molecules are close enough to have their dipole moments resonating (FRET). In the case of OLEDs, the situation is slightly different. Here, the excitation of the donor is not optical but electrical, therefore, charges are accumulated in the material and move within the layer until they meet the opposite charge and recombine. In the presence of a second material, if the energy levels of this second material fit to the situation, charges (electrons or holes or both) will be trapped on the second material. **Figure IV-4** displays the different traps which can be obtained.

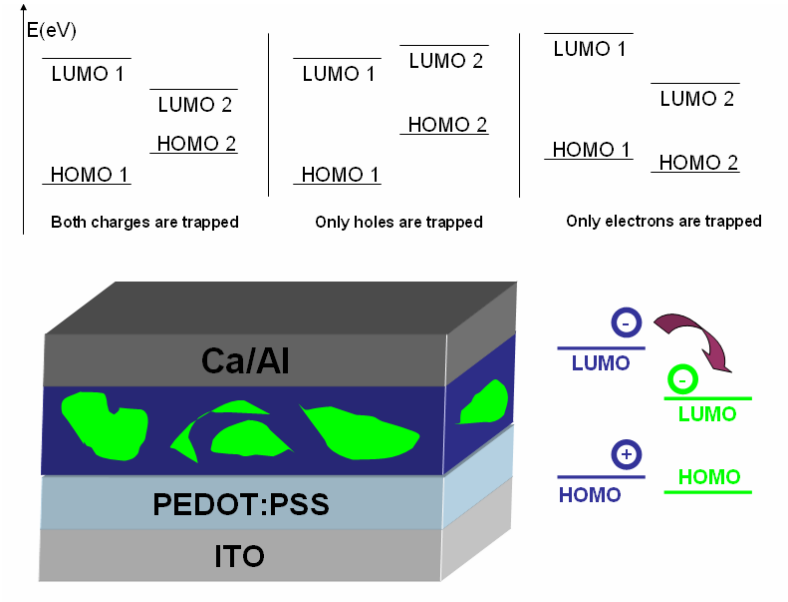

Figure IV-4: (top) different charge trapping situation; (bottom) example of a blend of polymers where the lower bandgap material is a trap for electrons

If one charge is trapped on a lower band gap material, it is likely that charges will recombine on this molecule or at the interface between the two materials (higher and lower band gap materials). For a better understanding, let us take the example of an active layer made of a blend of two conjugated polymers as shown in **Figure IV-4.** The HOMO and LUMO levels of both conjugated polymers tell us that one part of the electrons will be trapped on the green polymer while all the holes will move within the blue polymer. Therefore, when a hole will come close to the interface, it will recombine with the electron trapped to emit a photon. With such a system, we can obtain bicolour OLEDs. Using the same approach and tuning the quantities of the different materials, one can even obtain white light. Charge trapping and FRET are complementary in such systems, but it is predominantly the charge trapping which will give the stronger emission from the lower energy material. The easiest way to detect whether the emission from the lower band gap material is due to resonant energy transfer or charge trapping on a relatively well dispersed blend is done through electroluminescent spectroscopy. By increasing the voltage applied to the OLED, in the case of FRET, the relative intensities of the donor and the acceptor emission in the electroluminescent spectra stay the same. On the other hand, when it comes to charge trapping, increasing the voltage leads to an increased amount of charges trapped and therefore the emission from the lower band gap material becomes more intense with respect to the one from the higher energy material. The same observation can be made by simply comparing the electroluminescence and the photoluminescence of the active layer.

B. Dichromic microstructured electroluminescent polymer thin films: potential active layers for OLED

Original structures obtained with conjugated polymers can be really interesting in the fields of organic solar cells[140] and organic light emitting devices. One of the challenges of this area is the preparation of a double layer system, where the layers are formed by two different polymeric materials. The chance to get at least one of the two polymer layers in an ordered way opens new possibilities for advanced application in the field of microstructured material science. PDMS stamps can be used to emboss a polymer film (spin coated on a substrate) by heating the polymer over its glass transition temperature (Tg) keeping it lower than its Tf in order to avoid melting of the polymer (loss of the film thickness regularity). Here we describe two innovative approaches to print a semiconducting polymer onto another one without the use of wet techniques thus avoiding a mixing between the two materials.

In the first one, a thin film of substituted polyphenylenevinylene (red emitting soluble polymer, red PPV) was prepared by spin coating on a glass substrate. By pressing on the top of this PPV film a PDMS stamp obtained from a PFO prepared by means of the BF technique, PFO is released by PDMS (**Figure IV-5**) forming a net of photoluminescent material on PPV.

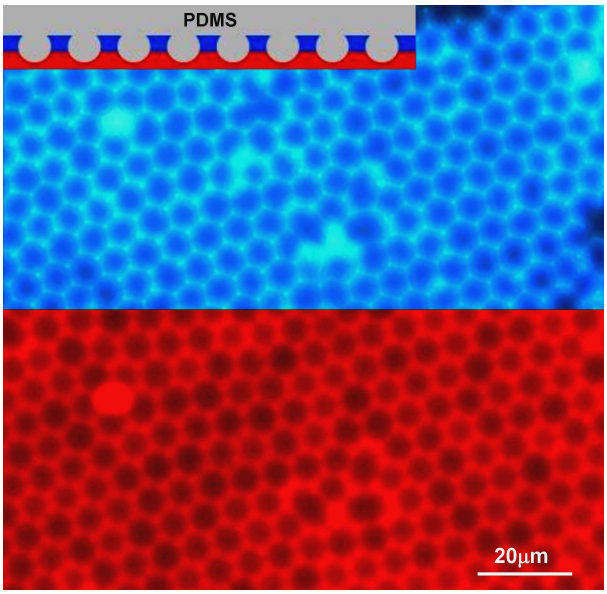

Figure IV-5: spin coated red PPV with printed PFO pattern (top: direct excitation of red PPV at 543 nm; bottom: direct excitation of the PFO at 405 nm)

During the PFO print process, the temperature is increased over the Tg of the red PPV. Therefore, in the mean time the red PPV is embossed. We therefore obtain a film that is composed of two structured conjugated polymers on top of each others.

In the second approach a thin film of soluble PPV precursor was obtained by spin coating and transformed by a thermal treatment into the conjugated unsoluble green emitting PPV. On top of this film a second emitting polymer (red PPV) was printed by using a PDMS stamp containing the red PPV. The result is shown in **Figure IV-6** where an image collected with the fluorescence microscope clearly shows the green emitting PPV as a background which is covered in an ordered fashion by the red PPV which was released during printing from PDMS.

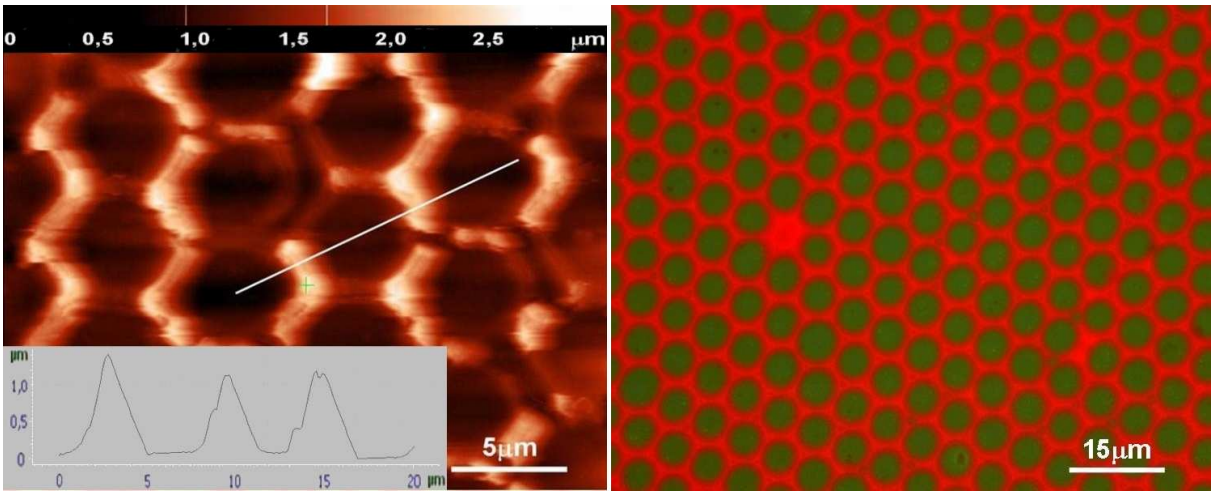

Figure IV-6: a) Atomic Force and b) Confocal Microscopy Images of red PPV pattern on green PPV

Unlike the first method, in this case the bottom layer is not structured, since the thermally polymerized PPV can not be moulded (due to the cross linking). With this second structure we can see cotemporally the emissions from the two polymers by exciting at two different wavelengths which is an alternative to the first structure obtained where both layers of the film where structured exactly the same way. The potential of these structured films for OLED applications is enormous. Such thin films could lead to a novel and innovative way of

creating a network of pixels with dimensions which can be tuned down to a few hundreds of nanometers using a low cost technique.

C. Zeolite L based hybrid Light Emitting Device

As we saw in **Chapter II**, host/guest systems based on zeolite L crystals can be addressed through photo excitation of a conjugated polymer nanofiber and energy transfer to the dye included in the channels. The question which now arises is to know whether they can also be contacted electrically through the conjugated polymer.

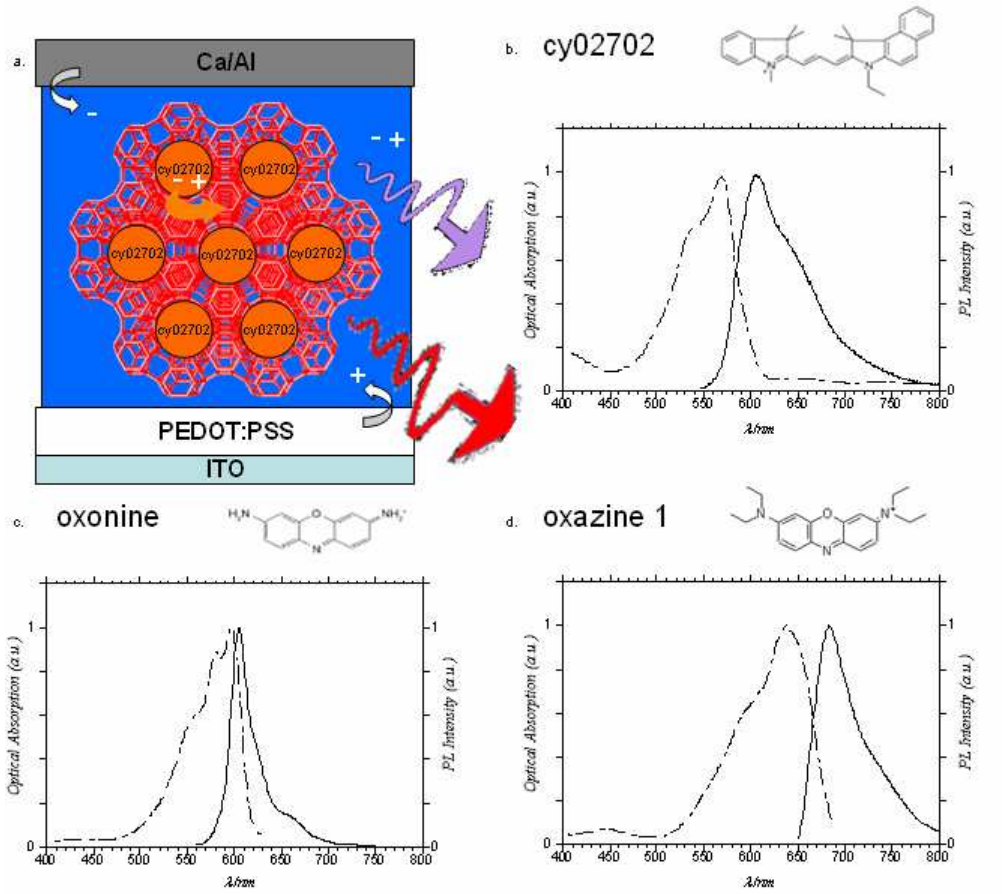

Figure IV-7: (a) schematic representation of the zeolite based device and Chemical structures, absorption (solid lines) and photoluminescence (dotted lines) of (b) Cy02702 stopcock molecules, (c) oxonine and (d) oxazine 1 in zeolite L crystals

The active layers that we prepared are based on two electroluminescent polymers: Polyvinyl Carbazole (PVK) and Poly[(9,9-dioctylfluorenyl-2,7-diyl)-alt-co-(1,4-benzo-

{2,1',3}-thiadiazole)] (F8BT). Inclusion compounds based on zeolite L crystals were also prepared: zeolites loaded with oxazine1 (ox1) and Cy02702 stopcock molecule (CyZLOx1).

Förster Resonant Energy Transfer (FRET) processes from F8BT to the stopcock molecule Cy02702 and from the latter to the oxazine1 molecules inside the zeolite channels, although not very efficient, have been demonstrated previously. On the other hand, the overlap integral between the emission spectra of PVK and the absorption spectra of Cy02702 being low, no energy transfer from PVK to the stopcock occurs. Therefore, by building devices that both contain zeolites CyZLOx1 with either F8BT (Device type 1; DT1) or PVK (DT2), we can compare two systems with and without energy transfer but also with different charge trapping properties. **Figure IV-8** displays the recorded electroluminescence for both DT1 and DT2. Although in the photoluminescence spectra the contributions from the zeolites are almost inexistent, in the electroluminescence, a strong emission from the zeolites is recorded in the case of DT2 but not in the case of DT1 (system where there is FRET from the polymer to the crystal). To understand why there is no emission from the zeolites in the system DT1, we have to take a closer look to the energetic levels of the different molecules. The energetic levels of the different polymers involved as well as the ones of Cy02702 stopcock molecule are to be taken in consideration. The HOMO and LUMO of Cy02702 are respectively at - 5,06 and - 3,04 eV. Therefore, in system DT2, the electrons as well as the holes will be trapped on the stopcock molecule as the HOMO of PVK is lower and its LUMO is higher than the ones of Cy02702. The process involved in this case is a two step process. In a first place, charges are transported within the polymer layer of the device and recombine in the polymer or are trapped on the stopcock molecules (lower band gap molecule). The energy will then be transferred to the dye inside the zeolite through FRET from Cy02702. The energetic levels of F8BT allow the holes to be trapped on the stopcock molecule but the

electrons remain in the polymer. Therefore, there is no recombination on the stopcock and no energy transfer to the dye inside the zeolite.

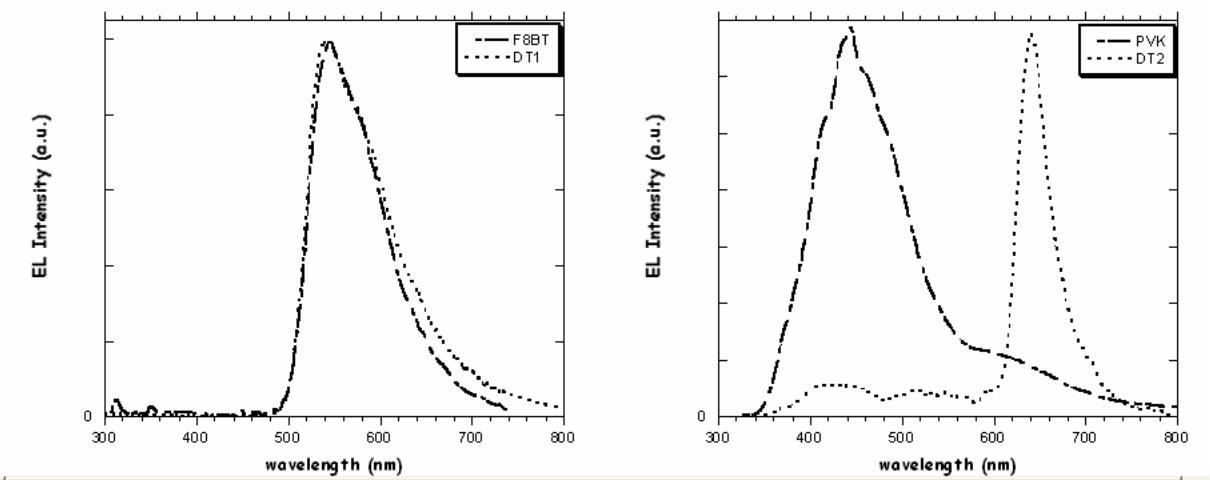

Figure IV-8: comparative electroluminescence of (left) F8BT and DT1 and (right) PVK and DT2

In order to verify that the stopcock molecule remains on the zeolite crystals and is not dispersed in the polymer film, confocal images of the film were taken photoexciting directly the different molecules. The confocal image displayed in **Figure IV-9** clearly shows a confined red emission from the zeolites (red spots) on a blue background emission that correspond to the photoluminescence of the PVK.

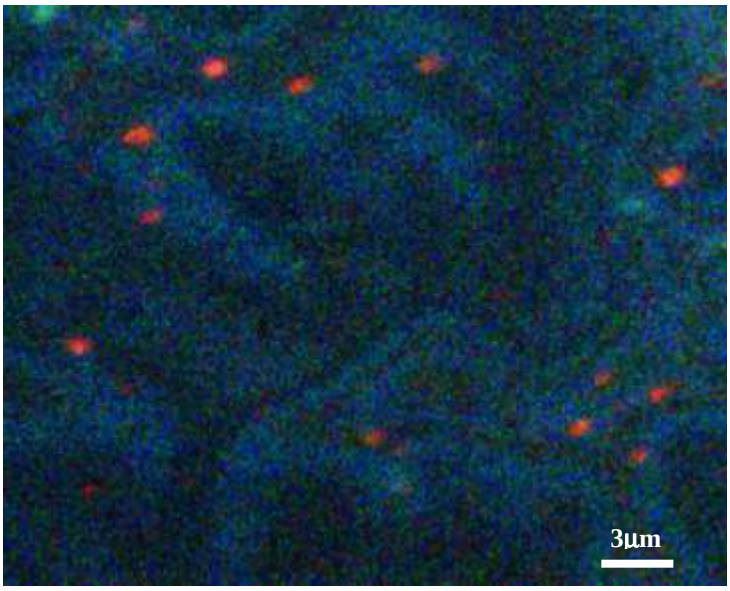

Figure IV-9: confocal image of DL2 (excitation wavelengths: 405nm and 543 nm)

If the stopcock molecule was dispersed in the polymer film, we would see a red emission from the whole film.

By increasing the voltage applied to the DT2 from 8 to 12 V, we see an increase of the emission from the zeolites with respect to the one from the polymer. This confirms the first step of the mechanism which was introduced before. The stopcock molecules are excited electronically through charge trapping and not through resonant energy transfer from the polymer. We can therefore tune the relative intensities of the different colours by adjusting the voltage applied to the devices.

This result provides an enormous breakthrough in the field of hybrid Light Emitting Devices but devices based on stopcock loaded zeolite crystals present some disadvantages: as no functionalisation of the zeolites is done, it becomes hard to disperse them into the polymer which leads to the formation of zeolite aggregates. The zeolite aggregates lead to major problems: the performances of the devices are not always reproducible as we cannot control the formation of such aggregates which could lead to big dishomogeneities of the active layer. The solutions provided in the previous chapter could be very efficient to have unaggregated zeolites in the active layers of the devices by including the zeolites in nanofibers or in a prepatterned polymer which should then be annealed in order to completely embed the zeolite. Concerning the nanofibers, a further study which will be presented in the next section needs to be done in order to be sure that they are not only optically active but also electrically.

D. Electroluminescent nanofibers in OLED

Electroluminescent nanofibers obtained by electrospinning a blend of a conjugated polymer with a polymer with good visco elastic properties present interesting properties both on the optical and the electronical point of view. We previously saw that some nanofibers

present peculiar optical properties which could lead to novel devices based on nanometer scale wires of electroluminescent polymers. The challenge now consists of seeing if those polymer nanofibers can be addressed electronically. A simple experiment to verify if those fibers are electroluminescent consists in embedding them in an active conjugated polymer film which is used as the active material of an OLED. In order to do that, one major problem has to be overcome: the polymer nanofiber should not be destroyed during the embedding step in the conjugated polymer film.

The nanofibers that were used in the devices are composed of 67 w% of F8BT and 33 % of PEO. Therefore they display no phase segregation and have a small diameter which is necessary for them to work in the devices. In order to see whether or not one can obtain electroluminescence from these nanofibers, one has to think of a way of contacting them or addressing them. In our work, the electrospun nanofibers were embedded in an active matrix of Polyvinylcarbazole (PVK). To do so, the electrospinning process was executed using glass patterned with Indium Tin Oxide (ITO) and consequently covered with Poly(3,4-ethylenedioxuthiophene) poly(styrenesulfonate) (PEDOT:PSS) as the substrate to collect the fibers.

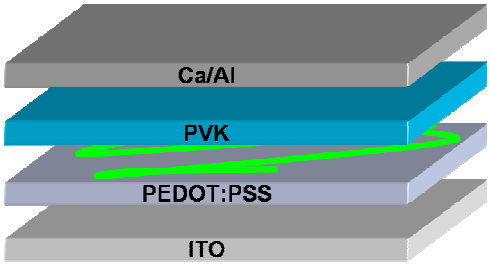

Figure IV-10: schematic representation of the nanofiber based OLED structure

The fibers, once electrospun on PEDOT:PSS, were separated into two groups: the first group was kept untouched after the electrospinning process while the second group was annealed at 150°C for 30 minutes. The annealing step induces the crystallisation of the F8BT

but the temperature has to be kept low enough to avoid coalescence of the fibers with each others. The next step consists in covering the electrospun nanofiber with a layer of PVK spin-coated from toluene to obtain the desired structure of the OLED as shown in **Figure IV-10**. As toluene is also a solvent for the fiber, the annealing step becomes even more essential: the crystallized fibers become less soluble in toluene. Through a careful study with the fluorescence and atomic force microscopes, we have seen that by annealing those nanofibers, the partial dissolution of the fibers (which leads to F8BT dispersed in the PVK layer) is completely avoided as shown on **Figure IV-11**. By giving energy to the fibers through the annealing step, chain mobility is induced which also leads to a flattening of the fibers which become ribbon like. Even though the diameter of the fibers is below 600 nm, in order to have a device that works, the thickness of the active layer should be kept as low as possible. The flattening of the nanofibers also induces less dishomogeneities of the active layer thickness. The cross sections on **Figure IV-11** show a surface roughness of around 30 nm for the devices containing annealed fibers whereas the ones containing unannealed ones display dishomogeneities of around 300 nm.

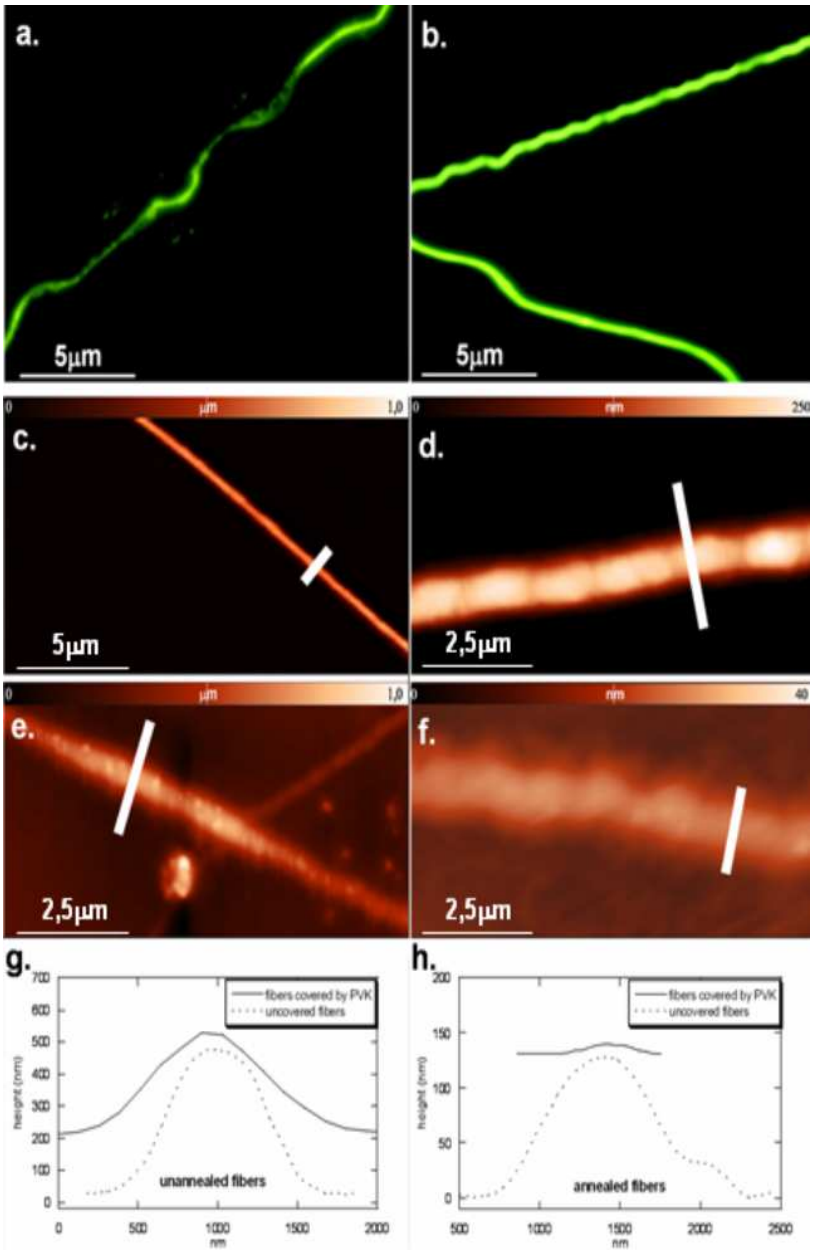

Figure IV-11: fluorescence images (a,b) of fibers of F8BT-PEO covered with spin coated PVK and AFM images of fibers on PEDOT:PSS (c,d) and covered with PVK (e,f) along with their cross sections (g,h); left: unannealed fibers; right: fibers annealed for 15 min at 150°C

The electroluminescence spectra presented in **Figure IV-12** confirm the necessity of the annealing step. The devices made without annealing of the fibers exhibit a low electroluminescence and display emission from the F8BT only at low voltage (4V), which then disappears when increasing the voltage. Taking in consideration the size of the fibers, the F8BT emission that can be seen is due to the F8BT dispersed in the PVK film next to the

fibers. Dishomogeneities are created in the device due to the thickness of the fibers. This leads to a higher emission from the parts of the device that are far away from the fibers as they are thiner and more homogeneous. By increasing the voltage, we increase preferentially the emission from those parts which do not contain any F8BT. On the other hand, devices made with the annealed fibers display a nice and constant emission of the F8BT even at a higher voltage (15V). The emission that we see in this case comes from the fiber as no F8BT is dispersed in the PVK film which is only used as a hole transporting material. The photoluminescence spectra of the active layers of the device display much lower relative emission intensity from the F8BT (with respect to the emission from the PVK) than the electroluminescence. Therefore, the emission from the F8BT that is seen in the electroluminescence spectra is mainly due to charge recombination directly on F8BT and not to energy transfer from PVK. The fact that increasing the voltage increases the relative electroluminescence from F8BT with respect to the electroluminescence from PVK also confirms the last point.

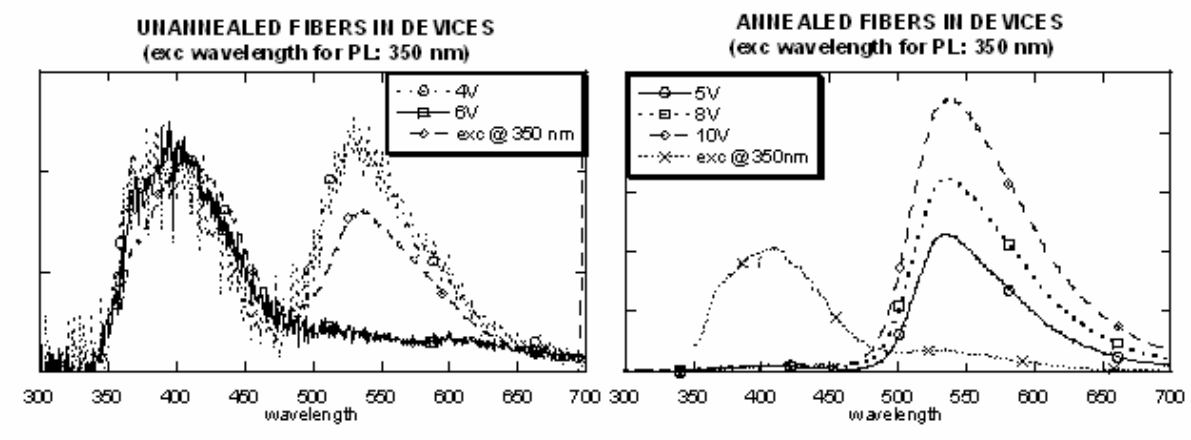

Figure IV-12: electroluminescence and photoluminescence spectra of (left) unannealed and (right) annealed fibers of F8BT-PEO in devices

Electrospun nanofibers can therefore be used as active material in OLED which means that they can be addressed both optically and electronically. This opens the path to a new

challenge: build a nano OLED based on a single electrospun nanofiber of electroluminescent polymer as the active material.

Conclusions:

The work here presented corresponds to the first steps towards the creation of very innovative devices and nano devices based on hybrid materials and host/guest sytems. More specifically, we have demonstrated that the enhanced photoluminescent properties of the inclusion compounds obtained by inserting an organic dye into the zeolite L framework have the potential to work in a functional device obtained by low cost fabrication methods. In fact, some of the major challenges concerning opto electronic devices based on organic dye molecules are to protect the dye from the environment (avoiding changes or quenching of the emission) and to obtain some peculiar luminescence properties from these molecules. Once included in the zeolite channels, the molecules are not only protected but they also exhibit polarized emission and this first level of organisation provides a perfect medium for fast energy transport.

To be able to connect these nano hybrid assemblies to the macroworld, conjugated polymers with electroluminescent properties were used. Conjugated polymers present one major advantage with respect to inorganic materials: they are easily processable with low cost fabrication techniques such as electrospinning or breath figure formation which can also provide a second level of organisation of the zeolite L crystals into the conjugated polymer. As we learn from nature, a higher level of organisation could lead to enhanced properties. Organising the zeolite L crystals into micro or nanostructured conjugated polymer thin films provides the optimal active layer for a zeolite L based Light Emitting Device as the aggregation of zeolite crystals is avoided even though their concentration is high. By adding dye loaded zeolites into oriented nanofibers, a two step energy transfer can be observed from

the polymer to the dye included in the nanochannels. Tuning the system, one can, on one hand, obtain a fiber which is optimised for the energy transfer (all dipole moments from the different molecules are aligned) or, one the other hand, aim for an equivalent contribution from the three molecules involved leading to multichromic or even white light emitting nanofibers.

In order to achieve the third level of organisation by building a functional device, both the fibers of electroluminescent polymer and the zeolite L crystals have to be contacted electrically. Simple devices embedding dye loaded zeolites or conjugated polymer fibers into their active layer display electroluminescence from the embedded species. The devices obtained during this work, although not as efficient as the state of the art of OLED, display remarkable properties. Zeolite L crystals could be included into the nanofibers which have shown electroluminescent in OLED or one could even think about a device architecture to fabricate nano light emitting devices based on conjugated polymer nanofibers embedding zeolite L crystals. Such devices could be used not only for lighting and display technologies but also in the field of biotechnologies where it is important to confine an excitation for example in a very narrow spatial range. On the other hand, hybrid light emitting devices based on conjugated polymers embedding dye loaded zeolite L crystals keep the mechanical properties of the conjugated polymer including the potential roll-to-roll fabrication and the device flexibility providing at the same time the enhanced electroluminescence properties from the inclusion compounds.

In the coming years, the proof of principles which is provided throughout this doctoral thesis could therefore be very useful to fabricate the future generations of materials for displays, lighting, sensing and nano excitation devices.

References:

Chapter I:

[1] Maxwell, James Clerk, "A Dynamical Theory of the Electromagnetic Field". **1865**.

[2] Maxwell, James Clerk, A Treatise on Electricity and Magnetism, 3rd ed., 2 vol. (**1892**, reissued **1954**).

[3] Newton, I. (**1952**) [1730]. *Opticks* (4th ed.). Dover (NY): Dover Publications. Book II, Part III, Propositions XII–XX; Queries 25–29.

[4] Einstein, A., *Annalen der Physik*, **1905**, *17*, 132–148.

[5] S. Bandyopadhyay, *Phys. Letters A*, **2000**, *276*, 233-239.

[6] J. B. Birks, "Photophysics of Aromatic Molecules", Wiley, London, **1970.**

[7] J. B. Birks in "Organic Molecular Photophysics", Vol. **2**, Ed., Wiley, London, **1975,** Chapter **9.**

[8] A. Jablonski, *Nature*, **1933**,*131*, 839.

[9] Lakowicz, J.R. 1983. Principles of Fluorescence Spectroscopy, Plenum Press, New York.

[10] Guilbault, G.G. 1990. Practical Fluorescence, Second Edition, Marcel Dekker, Inc., New York.

[11] Stokes, George Gabriel, Sir, On light : in three courses delivered at Aberdeen in November, 1883, December, 1884, and November, 1885.

[12] Memoir and scientific correspondence of the late Sir George Gabriel Stokes, selected and arranged by Joseph Larmor (Volume 2).

[13] Beer Lambert: *Essai d'Optique sur la Gradation de la Lumiere* (Claude Jombert, Paris, 1729)

[14] J. D. J. Ingle and S. R. Crouch, *Spectrochemical Analysis*, Prentice Hall, New Jersey (1988)

[15] C. Botta, S. Destri, M. Pasini, P. Picouet, G. Bongiovanni, A. Mura, M. Uslenghi, G. Di Silvestro, R. Tubino, Synth. Met. 2003, 139, 791.

[16] J. C. de Mello, H. F. Wittmann, R. H. Friend, Adv. Mater. 1997, 9, 230.

[17] Marvin Minsky, "Memoir on Inventing the Confocal Scanning Microscope," Published in *Scanning*, vol.10 pp128-138, 1988

[18] US patent US3013467 (A) by Marvin Minsky (19/12/1961)

[19] Pawley JB (editor) (2006). *Handbook of Biological Confocal Microscopy* (3rd ed. ed.). Berlin: Springer.

[20] Rost, F., Fluorescence microscopy. Vol. II. Cambridge University Press, Cambridge, United Kingdom (1995).

[21] Rost, F. and Oldfield, R., Fluorescence microscopy., Photography with a Microscope, Cambridge University Press, Cambridge, United Kingdom (2000).

[22] Bradbury, S. and Evennett, P., Fluorescence microscopy., Contrast Techniques in Light Microscopy., BIOS Scientific Publishers, Ltd., Oxford, United Kingdom (1996).

Chapter II :

[23] C. Sanchez, *J. Mat. Chem.*, 2005, **15**, 3557.

[24] D. T. Reilly, A. H. Burstein, *J Bone Joint Surg Am,*. 1974, **56**, 1001

[25] chem phys chem

[26] T.D. Clark, J. Tien, D.C. Duffy, K.E. Paul, G.M. Whitesides, *J. Am. Chem. Soc.*, **2001**, *123*, 7677.

[27] S.J. Hurst, E.K. Payne, L.D. Qin, C.A. Mirkin, *Angew. Chem. Int. Ed.* **2006**, *45*, 2672.

[28] V. Balzani, M. Venturi, A. Credi, *Molecular Devices and Machines*, Wiley-VCH, **2003**, Weinheim.

[29] Z. Popovic, M. Otter, S. Huber, G. Calzaferri, L. De Cola, *submitted for publication.*

[30] P.J. Holloway, *In Air Pollution and the Leaf Cuticle*, Ed.: K.E. Percy, J.N. Cape, R. Jagels, C.J. Simpson, Springer **1994**, Berlin, 1-13.

[31] E.A. Baker, *In the Plant Cuticle*, Ed.: D.F. Cutler, K.L. Alvin, C.E. Price, Academic Press **1982**, London, 139-166.

[32] R.N. Wenzel, *Ind. Eng. Chem.* **1936**, *28*, 988.

[33] Z.-Z. Gu, H. Uetsuka, K. Takahashi, R. Nakajima, H. Onishi, A. Fujishima, O. Sato, *Angew. Chem. Int. Ed*. **2003**, *42*, 894.

[34] Y. Wang, H. Li, L. Gu, Q. Gan, Y. Li and G. Calzaferri, *Microporous and Mesoporous Materials*, **2009**, *121*, 1-6.

[35] B. Bussemer, D. Munsel, H. Wünscher, G. J. Mohr, U.-W. Grummt**,** *J. Phys. Chem. B*, **2007**, *111*, 8–15.

[36] W. Müller, *Liebigs Ann. Chem.,* **1974**, 334.

[37] S. Megelski, A. Lieb, M. Pauchard, A. Drechsler, S. Glaus, C. Debus, A. J. Meixner, G. Calzaferri, *J. Phys. Chem.* B, **2001**, *105*, 25-35.

[38] G. Calzaferri, N. Gfeller, *J. Phys. Chem* **1992**, *96*, 3428.

[39] G. Calzaferri, H. Maas, M. Pauchard, M. Pfenniger, S. Megelski, A. Devaux, *Adv. Photochem*. **2002**, *27*, 1.

[40] G. Calzaferri, M. Pauchard, H. Maas, S. Huber, A. Khatyr, T. Schaafsma, *J. Mater. Chem*. **2002**, *12*, 1.

[41] Förster T., *Ann. Physik*, **1948**, *437*, 55.

[42] T. Förster, *Fluoreszenz Organischer Verbindungen*, Vandenhoek & Ruprecht, **1951**, Göttingen.

[43] T. Förster, in *Modern Quantum Chemistry*, Academic Press **1965**, New York, 93-137.

[44] D. L. Andrews, *Chem. Phys.* **1989**, *135*, 195-201.

[45] D. L. Andrews and D. S. Bradshaw, *Eur. J. Phys*,. **2004**, *25*, 845-858.

[46] N. Gfeller, G. Calzaferri, *J. Phys. Chem.*, **1997,** *101*, 1396.

[47] S. Huber, G. Calzaferri, *Angew. Chem.*, **2004**, *43*, 6738-6742.

[48] H. Maas, G. Calzaferri, *Angew. Chem. Int. Ed*. **2002**, *41*, 2284.

[49] W. Sun, J. Ji, J. Shen, *Langmuir*, **2008,** *24*, 11338-41.

[50] Michael Busby, Hannes Kerschbaumer, Gion Calzaferri, and Luisa De Cola, *Adv. Mater.*, 2008, *20*, 1614–1618.

Chapter III:

[51] György Inzelt “Conducting Polymers” Springer, 2008, Berlin, Heidelberg.

[52] Herbert Naarmann “Polymers, Electrically Conducting” in Ullmann's Encyclopedia of Industrial Chemistry 2002 Wiley-VCH, Weinheim.

[53] Semiconducting Polymers; Vol. , edited by G. Hadziioannou and P.F.v. Hutten (WILEY-VCH, Weinheim, 2007).

[54] J. H. Burroughes, D. D. C. Bradley, A. R. Brown, R. N. Marks, K. Mackay, R. H. Friend, P. L. Burns, and A. B. Holmes, *Nature*, **1990**, *347*, 539-541.

[55] Handbook of Conducting Polymers; Vol.1,2 , edited by T.A. Skotheim, R.L. Elsenbaumer, and J.R. Reynolds (Marcel Dekker, Inc., New York, 1998)

[56] Ito, T.; Shirakawa, H.; Ikeda, S., *J. Polym. Sci. Chem. Ed.,* **1974,** *12,* 11.

[57] Chiang, C.K.; Druy, M.A.; Gau, S.C.; Heeger, A.J.; Louis, E.J.; MacDiarmid, A.G.; Park, Y.W.; Shirakawa, H., *J. Am. Chem. Soc.,* **1978,** *100,* 1013.

[58] MacDiarmid, A.G.; Chiang, J.-C.; Richter, A.F.; Epstein, A.J., *Synth. Met.,* **1987,** *18,* 285.

[59] Kaner, R.B.; MacDiarmid, A.G., *Scientific American,* **1988,** *February,* 106.

[60] MacDiarmid, A.G.; Epstein, A.J., *Macromol. Chem.,* **1991,** *51,* 11.

[61] MacDiarmid, A.G.; Epstein, A.J., "Science and Technology of Conducting Polymers," in Frontiers of Polymer Research, P.N. Prasad and J.K. Nigam, Eds., Plenum Press, New York, **1991,** p. 259.

[62] Wang, Z.H.; Li, C.; Scherr, E.M.; MacDiarmid, A.G.; Epstein, A.J., *Phys. Rev. Lett.,* **1991,** *66,* 1745.

[63] MacDiarmid, A.J.; Epstein, A.J., *Synth. Met.,* **1994,** *65,* 1

[64] United States Patent 7562433 by S. Hong, W. G. Marancik, J. Parrell, M. Field, K. Marken, Y. Zhang, **2005**.

[65] R. Ramakrishnan, S. Subramanian, J. Rajan, *J. Appl. Phys.*, **2007**, *102*, 111101.

[66] D. Li, Y. Xia., *Adv. Mat.*, **2004**, *16*, 1151-1170.

[67] J. Zeleny, *Physical Review*, **1914**, *3*, 69-91

[68] FILATOV, Y. BUDYKA, A. KIRICHENKO, V. (Trans. D. LETTERMAN) *Electrospinning of micro- and nanofibers: fundamentals and applications in separation and filtration processes,* Begell House Inc, New York, USA, **2007**.

[69] TAYLOR, G. (**1964**) Disintegration of Water Drops in an Electric Field. Proceedings of the Royal Society of London A: Mathematical, Physical & Engineering Sciences, 280, 383-397

[70] TAYLOR, G. (**1965**) The force exerted by an electric field on a long cylindrical conductor. Proceedings of the Royal Society of London A: Mathematical, Physical & Engineering Sciences, 291, 145-158

[71] TAYLOR, G. (**1969**) Electrically Driven Jets. Proceedings of the Royal Society of London A: Mathematical, Physical & Engineering Sciences, 313, 453-475

[72] MELCHER, J. R. & TAYLOR, G. (**1969**) Electrohydrodynamics: A Review of the Role of Interfacial Shear Stresses. Annual Review of Fluid Mechanics, 1, 111-146

[73] DOSHI, J. & RENEKER, D. H. (**1995**) Electrospinning Process and Applications of Electrospun Fibers. Journal of Electrostatics, 35, 151-160

[74] REZNIK, S. N., YARIN, A. L., THERON, A. & ZUSSMAN, E. (**2004**) Transient and steady shapes of droplets attached to a surface in a strong electric field. Journal of Fluid Mechanics, 516, 349-377

[75] HOHMAN, M. M., SHIN, M., RUTLEDGE, G. & BRENNER, M. P. (**2001**) Electrospinning and electrically forced jets. I. Stability theory. Physics of Fluids, 13, 2201-2220

[76] Thandavamoorthy Subbiah, G. S. Bhat, R. W. Tock, S. Parameswaran, S. S. Ramkumar. Electrospinning of Nanofibers. Journal of Applied Polymer Science. June **2004**. Volume 96, Issue 2 (p 557-569)

[77] S. Lee, S.K. Obendorf. Use of Electrospun Nanofiber Web for Protective Textile Materials as Barriers to Liquid Penetration. Textile Research Journal. Sep **2007**.

[78] Formhals, *A., US* Patent, *1975504 (1934).*

[79] Formhals, *A., US* Patent, *2160962 (1939).*

[80] Formhals, *A., US* Patent, *2187, 306 (1940).*

[81] K. M. Sawicka, P. Gouma, *J. Nanoparticle Research*, **2006**, *8*, 769-781.

[82] J. H. Yu, S. V. Fridrikh, G. C. Rutledge, *Adv. Mat.*, **2004**, *16*, 1562-1566.

[83] D. Li , A. Babel, S. A. Jenekhe, Y. Xia, *Adv. Mat.*, **2004**, *16*, 2062-2066.

[84] A. K. Moghe, B. S. Gupta, *Polymer Reviews*, 2008, 48, 353 – 377.

[85] E. Zussman, A. L. Yarin, A. V. Bazilevsky, R. Avrahami, M. Feldman, *Adv. Mat.*, **2006**, *18*, 348-353.

[86] I. Cucchi, F. Spano, U. Giovanella, M. Catellani, A. Varesano, G. Calzaferri,C. Botta, *Small*, **2007**, *3*, 305 – 309

[87] V. Vohra, A. Devaux , L.-Q. Dieu, G. Scavia, M. Catellani, G. Calzaferri, C. Botta, *Adv. Mat.*, **2009**, *21*, 1146-1150.

[88] V. Vohra, M. Pasini, W. Porzio, S. Destri, G. Calzaferri, C. Botta, *submitted.*

[90] T. Jarusuwannapoom, W. Hongrojjanawiwat, S. Jitjaicham, L. Wannatong, M. Nithitanakul, C. Pattamaprom, P. Koombhongse, R. Rangkupan, P. Supaphol, *European Polymer Journal*, **2005** , *41* ,409–421.

[91] U. Giovanella, M. Pasini, S. Destri, W. Porzio, C. Botta, *Synth. Metals*, **2008**, *158*, 113-119.

[92] M. Pasini, U. Giovanella, P. Betti, A. Bolognesi, C. Botta, S. Destri, W. Porzio, B. Vercelli, G. Zotti, *Chem. Phys. Chem.*, in press.

[93] T. Olinga, S. Destri, W. Porzio, *Macromol. Chem. Phys.*, **1997**, *198*, 1091-1107.

[94] G. Zotti, A. Randi, S. Destri, W. Porzio, G. Schiavon, *Chem. Mater.*, **2002**, *14*, 4550-4557.

[95] N. Gfeller, S. Megelski, G. Calzaferri, *J. Phys. Chem. B*, 1998, **102**, 928.

[96] W. J. E. Beek, M. M. Wienk, R. A. J. Janssen, *Adv. Mat.*, 2004, **16**, 1009.

[97] S. Coe-Sullivan, W.-K. Woo, J. S. Steckel, M. Bawendi, V. Bulovic, *Organic Electronics*, 2003, **4**, 123.

[98] V. Vohra, S. Yunus, A. Attout, U. Giovanella, G. Scavia, R. Tubino, C. Botta, A. Bolognesi, *Soft Matter*, 2009, 5, 1656-1661.

[99] V. Vohra, A. Bolognesi, G. Calzaferri, C. Botta, *Langmuir*, **2009**, *25*, 12019-12023.

[100] E. Menard, M.A. Meitl, Y. Sun, J.-U. Park, D.J.-L. Shir, Y.-S. Nam, S.Jeon, J.A. Rogers, *Chem. Rev*., 2007, **107**, 1117.

[101] F.W. Kotch, R.T. Raines, *PNAS*, 2006, **103**, 3031.

[102] D. K. Goswami, B. Satpati, P. V. Satyam, B. N. Dev, *Current Science*, 2003, **84**, 903.

[103] T. Kawasaki, M. Tokuhiro, N. Kimizuka, T. Kunitake, *J. Am. Chem. Soc*,. 2001, **123**, 6792.

[104] V. Nicolosi, P. D. Nellist, S. Sanvito, E. C. Cosgriff, W J. Blau, S. Krishnamurthy,M. L. H. Green, D. Vengust, D. Dvorsek, D. Mihailovic, G. Compagnini, J. Sloan, V. Stolojan, J. D. Carey, S. J. Pennycook, J. N. Coleman, *Adv. Mat.*, 2007, **19**, 543.

[105] B. Erdogan, L. Song, J.N. Wilson, J.O. Park, M. Srinivasarao, U.H.F. Bunz, *J. Am. Chem. Soc*., 2004, **126**, 3678.

[106] L. Song, R.K. Bly, J.N. Wilson, S. Bakbak, J.O. Park, M. Srinivasarao, U.H.F. Bunz, *Adv. Mat*., 2004, **16**, 115.

[107] H. Yabu, M.Tanaka, K. Ijiro, M. Shimomura, *Langmuir*, 2003, **19**, 6297.

[108] A. Bolognesi, C. Botta, S.Yunus, *Thin Solid Films*, 2005, **492**, 307.

[109] F. Galeotti, I. Chiusa, L. Morello, S. Giani, D. Breviario, F. Damin, M. Chiari, A. Bolognesi, *European Polym. J.*, accepted.

[110] D. Zhao, T. M. Swager, *Org. Letters*, **2005**, *7*, 4357-4360.

[111] A.G. El-Shekeil, H. A. Al-Saady, F. A. Al-Yusufy, *Polymer International*, **1997**, *44*, 78-82.

[112] B. Xie, M. Bagui, R. Guo, K. Li, Q. Wang, Z. Peng, *J. Polym. Sci. Part A: Polym. Chem.*, **2007**, *45*, 5123-5135.

[113] V. Vohra, G. Calzaferri, A. Bolognesi, C. Botta, *in prep.*

[114] Gero Decher, *Science*, **1997**, *277*, 1232-1237.

[115] G.S. Lee Y.J.Lee K.B.Yoon, *J. Am. Chem. Soc.*, **2001**, *123*, 9769.

[116] N. Jessel, M. Oulad-Abdelghani, F. Meyer, P. Lavalle, Y. Haikel, P. Schaaf, and J.-C. Voegel, *PNAS,* **2006,** *103*, 8618-8621.

[117] O. Etienne, C. Picart, C. Taddei, P. Keller, E. Hubsch, P. Schaaf, J.C. Voegel, Y. Haikel, J.A. Ogier, and C. Egles, *Journal of Dental Research,* **2006**, *85*, 44-48

[118] C. Picart, J. Mutterer, L. Richert, Y. Luo, G. D. Prestwich, P. Schaaf, J.-C. Voegel, and P. Lavalle, *PNAS*, **2002**, *99*, 12531-12535.

[119] A. R. Esker, C. Mengel, and G. Wegner, *Science*, **1998**, *280*, 892-895.

Chapter IV:

[120] R. H. Friend, R. W. Gymer, A. B. Holmes, J. H. Burroughes, R. N. Marks, C. Taliani, D. D. C. Bradley, D. A. Dos Santos, J. L. Brédas, M. Lögdlund, W. R. Salaneck, *Nature*, **1999**, *397*, 121.

[121] R. H. Partridge, "Electroluminescence from polyvinylcarbazole films", 1, 2, 3 and 4, *Polymer* 1983 **24**, 733, 739, 748, 755

[122] C. W. Tang, S. A. VanSlyke, *Appl. Phys. Lett.*, **1987**, *51*, 913.

[123] J. H. Burroughes, D. D. C. Bradley, A. R. Brown, R. N. Marks, K. Mackay, R. H. Friend, P. L. Burn, A. B. Holmes, *Nature*, **1990**, *347*, 539–541.

[124] P. Chamorro-Posada, J. Martín-Gil, P. Martín-Ramos, L.M. Navas-Gracia, *Fundamentos de la Tecnología OLED* (*Fundamentals of OLED Technology*). University of Valladolid, Spain (2008).

[125] Shinar, Joseph (Ed.), *Organic Light-Emitting Devices: A Survey*. NY: Springer-Verlag (2004).

[126] Hari Singh Nalwa (Ed.), *Handbook of Luminescence, Display Materials and Devices*, Volume 1-3. American Scientific Publishers, Los Angeles (2003). Volume 1: Organic Light-Emitting Diodes

[127] Hari Singh Nalwa (Ed.), *Handbook of Organic Electronics and Photonics*, Volume 1-3. American Scientific Publishers, Los Angeles (2008).

[128] Müllen, Klaus (Ed.), *Organic Light Emitting Devices: Synthesis, Properties and Applications*. Wiley-VCH (2006).

[129] Yersin, Hartmut (Ed.), *Highly Efficient OLEDs with Phosphorescent Materials*. Wiley-VCH (2007).

[130] W.Graupner et al., "High Resolution Color Organic Light Emitting Diode Microdisplay Fabrication Method", SPIE Proceedings 4207, 11–19 (2000).

[131] T. R. Hebner, C. C. Wu, D. Marcy, M. H. Lu, J. C. Sturm, *Appl. Phys. Lett.*, **1998**, *72*, 519.

[132] J. Bharathan, Y. Yang, *Appl. Phys. Lett.*, **1998**, *72*, 2660.

[133] G. Gustafsson, Y. Cao, G. M. Treacy, F. Klavetter, N. Colaneri, A. J. Heeger, *Nature* **1992**, *357*, 477.

[134] C.M. Aguirre, S. Auvray, S. Pigeon, *Appl. Phys. Lett.*, **2006**, *88*, 183104.

[135] F. Zhang, A. Petr, U. Kirbach, L. Dunsch, J. Mat. Chem., 2003, 13, 265-267

[136] S. R. Forrest, D. D. C. Bradley, Adv. Mat., 2003, 15, 1043-1048.

[137] I.-N. Kang, Y.-B. Kim, S.-H. Lim, M.-C. Chung, S.-Y. Oh, S.-R. Kim, J.-H. Lee, *Polymers Bull. Korean Chem. Soc.*, **2008**, *29*, 135-138.

[138] G.-K. Ho, H.-F. Meng, S.-C. Lin, S.-F. Horng, C.-S. Hsu, L.-C. Chen, S.-M. Chang, *Appl. Phys. Lett.*, **2004**, *85*.

[139] D.-H. Hwang, M.-J. Park, S.-K. Kim, N.-H. Lee, C. Lee, Y.-B. Kim, H.-K. Shim, *J. Mater. Res.*, **2004**, *19*, 2081-2086.

[140] J.H. Lee, D. W. Kim, H. Jang, J. K. Choi, J. Geng, J. W. Jung, S. C. Yoon, H.-T. Jung, small, doi: 10.1002/smll.200900666